The Pennsylvania State University

The Graduate School

College of Engineering

LABORATORY AND FIELD-SCALE OBSERVATIONS OF FERROUS IRON OXIDATION AND FERRIC IRON PRECIPITATION AT AN ACID MINE DRAINAGE SITE

A Thesis in

Environmental Engineering

by

Juliana Faith Brown

Submitted in Partial Fulfillment
of the Requirements
for the Degree of

Master of Science

May 2010

The thesis of Juliana Faith Brown was reviewed and approved* by the following:

William D. Burgos
Professor of Environmental Engineering
Graduate Program Chair of Environmental Engineering
Thesis Advisor

John Regan
Associate Professor of Environmental Engineering

Peter J. Heaney
Professor of Mineral Sciences

*Signatures are on file in the Graduate School

ABSTRACT

The first study (Chapter 2) analyzed the aqueous chemistry, mineral precipitates, microbial communities, and Fe(II) oxidation rates at an acid mine drainage (AMD) site in the context of a depositional facies model. Both pool and terrace facies at upstream and downstream locations were studied. Fe(III) precipitates were determined to be schwertmannite with pin-cushion morphology at all locations, regardless of facie. Microbial community composition was studied with 16s rDNA cloning and fluorescence in situ hybridization (FISH) and found to transition from a Betaproteobacteria and *Euglena* dominated environment at the AMD spring to an *Acidithiobacillus* dominated environment downstream, as pH decreased. Microbial composition at adjacent pool and terraces was similar; thus, microbial community structure was more strongly a function of pH and other geochemical conditions rather than depositional facie. Intact pieces of terrace and pool sediments from upstream and downstream locations were used in laboratory reactors to measure rates of low-pH Fe(II) oxidation at variable residence times (2-10 h). Rates of Fe(II) oxidation were normalized to mass and surface-area. Mass-normalized oxidation rates ranged from 0.74 to 10.4 x 10^{-9} mol Fe L^{-1} s^{-1} g^{-1} and rates were faster for pool sediments compared to terrace sediments. Surface-area normalized rates ranged from 0.63 to 1.75 x 10^{-9} mol Fe L^{-1} s^{-1} cm^{-2} and the faster rates were also associated with pool sediments. Upstream sediments were also more efficient at Fe(II) oxidation than downstream sediments, regardless of facie, suggesting that Fe(II) oxidation rates were also dependent upon biogeochemical conditions, not solely the depositional facies environment. Sediments were irradiated with ^{60}Co and analyzed again to determine abiotic Fe(II) oxidation rates. No change in Fe(II) concentration was

observed for sterilized sediments, indicating that all Fe(II) oxidation was a result of biological activity. A depositional facies model explained some differences in Fe(II) oxidation kinetics, but this model could not explain differences in water chemistry, mineral composition, crystal morphology, or microbial community composition.

In the second study (Chapter 3), three low-pH coal mine drainage (CMD) sites in central Pennsylvania (Lower Red Eyes, Fridays-2, and Hughes Borehole) were studied to determine similarities in sediment composition, mineralogy, and morphology. Water from one site (Lower Red Eyes) was used in a discontinuous titration/neutralization experiment to produce Fe(III) minerals by abiotic neutralization/precipitation for comparison with the field precipitates that were produced by biological low-pH Fe(II) oxidation. Sediments were characterized using X-ray diffraction (XRD), extended X-ray absorption fine structure (EXAFS) spectroscopy, and scanning electron microscopy with energy dispersive spectroscopy (SEM-EDS). Even though the hydrology and chemistry of the CMD varied considerably between the three field sites, the mineralogy of the three iron mounds was found to be very similar. Schwertmannite was found to be the predominant mineral phase precipitated at low-pH with traces of goethite at some sampling locations. Schwertmannite particles occurred as micron sized spheroids with characteristic "pin-cushion" morphology at all sites. No trace metal incorporation was detected in sediments from the field, and no metals (other than Fe) were removed from the CMD at any of the field sites. Minerals formed by abiotic neutralization/precipitation (pH 5.18 – 8.34) were also found to consist primarily of schwertmannite. In contrast to low-pH precipitation, substantial trace metal removal occurred in the neutralized CMD, the subsequent precipitates were found to contain Al, and schwertmannite morphology

changed dramatically. While secondary minerals such as schwertmannite essentially store some of the emergent acidity from CMD sources, this mineral may be of industrial value because, at least when precipitated at low-pH, it does not contain trace metal contaminants.

TABLE OF CONTENTS

LIST OF FIGURES

LIST OF TABLES

ACKNOWLEDGMENTS

I would like to thank my Master's committee, especially my advisor Bill Burgos, for their direction and guidance throughout my education. I would also like to thank Jenn Macalady, Dan Jones, Trinh Desa, Dan Mills, Janna Lambson, Lyndsay Troyer, and Thomas Borch for their contributions to this study. I would like to acknowledge Brent Means and Malcolm Crittenden for leading me to the Lower Red Eyes field site. Lastly, I am grateful for the other students, my family, and Nathaniel for their support and encouragement along the way.

1. Introduction

This thesis contains two papers to be submitted for publication in relevant scientific journals. Chapter 2 contains a paper entitled "Application of a depositional facies model to an acid mine drainage site." The authors of this paper include Juliana F. Brown, Daniel Jones, Jennifer L. Macalady, and William D. Burgos. This paper introduces the idea of a depositional facies model and details the expansion of this model to an acid mine drainage (AMD) site. This paper also presents the results of flow-through laboratory reactor experiments, which allowed for the determination of Fe(II) oxidation rates at various locations along the AMD iron mound at Lower Red Eyes. Microbial analysis via fluorescence in situ hybridization was conducted by Jones and Macalady (Penn State, Department of Geosciences). Field chemistry, mineralogical characterizations, and laboratory reactor experiments were done by Brown (Penn State, Department of Civil and Environmental Engineering).

Chapter 3 contains a paper entitled "Schwertmannite formed by biological low-pH Fe(II) oxidation versus abiotic neutralization." The authors of this paper include Juliana F. Brown, Lyndsay D. Troyer, Thomas Borch, Janna Lambson and William D. Burgos. This paper combines field observations and analytical measurements at three different AMD sites in Central Pennsylvania. The Fe(III) precipitates formed at these sites were also compared to those formed abiotically in the laboratory. Fridays-2 samples were collected by Troyer and Borch (Colorado State University, Department of Chemistry). Fe EXAFS analysis was also done by Troyer at the Stanford Synchrotron Radiation Lightsource (SSRL). Abiotic precipitates were formed and imaged with electron microscopy by Lambson (Washington University in St. Louis). Aqueous chemistry

measurements of Fridays-2 and Hughes Borehole were determined by Melanie Lucas and Trinh DeSa, respectively (Penn State, Department of Civil and Environmental Engineering). Aqueous chemistry measurements at Lower Red Eyes and all other mineralogical characterizations were done by Brown.

2. Application of a Depositional Facies Model to an Acid Mine Drainage Site

2.1. Abstract

This study analyzed the aqueous chemistry, mineral precipitates, microbial communities, and Fe(II) oxidation rates at an acid mine drainage (AMD) site in the context of a depositional facies model. Both pool and terrace facies at upstream and downstream locations were studied. Fe(III) precipitates were determined to be schwertmannite with pin-cushion morphology at all locations, regardless of facie. Microbial community composition was studied with 16s rDNA cloning and fluorescence in situ hybridization (FISH) and found to transition from a Betaproteobacteria and *Euglena* dominated environment at the AMD spring to an *Acidithiobacillus* dominated environment downstream, as pH decreased. Microbial composition at adjacent pool and terraces was similar; thus, microbial community structure was more strongly a function of pH and other geochemical conditions rather than depositional facie. Intact pieces of terrace and pool sediments from upstream and downstream locations were used in laboratory reactors to measure rates of low-pH Fe(II) oxidation at variable residence times (2-10 h). Rates of Fe(II) oxidation were normalized to mass and surface-area. Mass-normalized oxidation rates ranged from 0.74 to 10.4 x 10^{-9} mol Fe L^{-1} s^{-1} g^{-1} and rates were faster for pool sediments compared to terrace sediments. Surface-area normalized rates ranged from 0.63 to 1.75 x 10^{-9} mol Fe L^{-1} s^{-1} cm^{-2} and the faster rates were also associated with pool sediments. Upstream sediments were also more efficient at Fe(II) oxidation than downstream sediments, regardless of facie, suggesting that Fe(II) oxidation rates were also dependent upon biogeochemical conditions, not solely the depositional facies environment. Sediments were irradiated with ^{60}Co and analyzed again

to determine abiotic Fe(II) oxidation rates. No change in Fe(II) concentration was observed for sterilized sediments, indicating that all Fe(II) oxidation was a result of biological activity. A depositional facies model explained some differences in Fe(II) oxidation kinetics, but this model could not explain differences in water chemistry, mineral composition, crystal morphology, or microbial community composition.

2.2. Introduction

Pennsylvania is currently the fourth largest coal producing state in the United States and has produced more than 25% of the total coal mined in the US during the past 200 years (USGS, 2008). Coal mining operations have left their mark on the environment and acid mine drainage (AMD), marked by high concentrations of acidity and metals, is a severe environmental impact to much of the Appalachian region of the United States. More than 10,000 km of streams in the Appalachian region are contaminated by AMD, with greater than 1,000 km of those in Pennsylvania (Herlihy et al., 1990). The cost of reclamation of AMD-contaminated watersheds in Pennsylvania alone is estimated to be between $5 and $15 billion (USGS, 2008); thus, cost-effective treatment systems are needed.

Passive treatment, presumably the most cost-effective form of treatment, is currently the most widely used treatment process for AMD contaminated streams. These systems usually consist of a series of ponds and wetlands designed to neutralize the AMD and precipitate iron and trace metals out of solution. Fe(III) precipitation is dependent upon the abiotic oxidation of Fe(II), which happens rapidly after neutralization. Often, Fe(III) precipitates form prior to the settling pond, resulting in “armoring” of the limestone and, more importantly, clogging of the limestone bed (Cravotta, 2008).

Armoring and clogging decrease the neutralization capacity of limestone; thus, the oxidation of Fe(II) and subsequent removal of Fe(III) must occur prior to neutralization treatment. At low pH, abiotic oxidation is kinetically limited; however, biologically catalyzed Fe(II) oxidation may be employed to enhance oxidation and Fe removal rates (Kirby et al., 1999). Biological oxidation rates can be 10^5 to 10^6 times faster than abiotic oxidation rates at low pH (Singer and Stumm, 1970; Nordstrom, 1985). The relationships between aqueous geochemistry, microbial communities, and Fe(III) precipitates are still not well understood; thus, further research is necessary to use biological Fe(II) oxidation to enhance the efficacy of passive AMD treatment.

In order to study smaller environments within a larger context, geoscientists have developed a depositional facies model which correlates aqueous chemistry, hydrologic conditions, mineral composition and morphology, and living organisms at specific locations (Walker and James, 1992). This facies model has been applied mostly to ancient sediment systems, including ancient river deltas, glacier systems, and coral reefs (Reading, 1996). Although the importance of microorganisms on sediment formation has been previously acknowledged, a study at Angel Terrace, Mammoth Hot Springs, Yellowstone National Park was the first to characterize microbial communities at distinct facies and focus on younger sedimentary systems (Fouke et al., 2003).

The study at Angel Terrace identified unique microbial communities, mineral compositions, sediment structure (e.g., cm-scale), and crystal morphology (e.g., µm-scale) at each facies (Fouke et al., 2000; Fouke et al., 2003). Similar structures and mineral morphology as those at Angel Terrace are also found at the Lower Red Eyes AMD site (Figure 2-1 and Figure 2-2). Terrace structures, also referred to as terraced

iron formations (TIF), at AMD sites such as the Tintillo River in Huelva, Spain have also been compared to travertine deposits at hot springs (España et al., 2007).

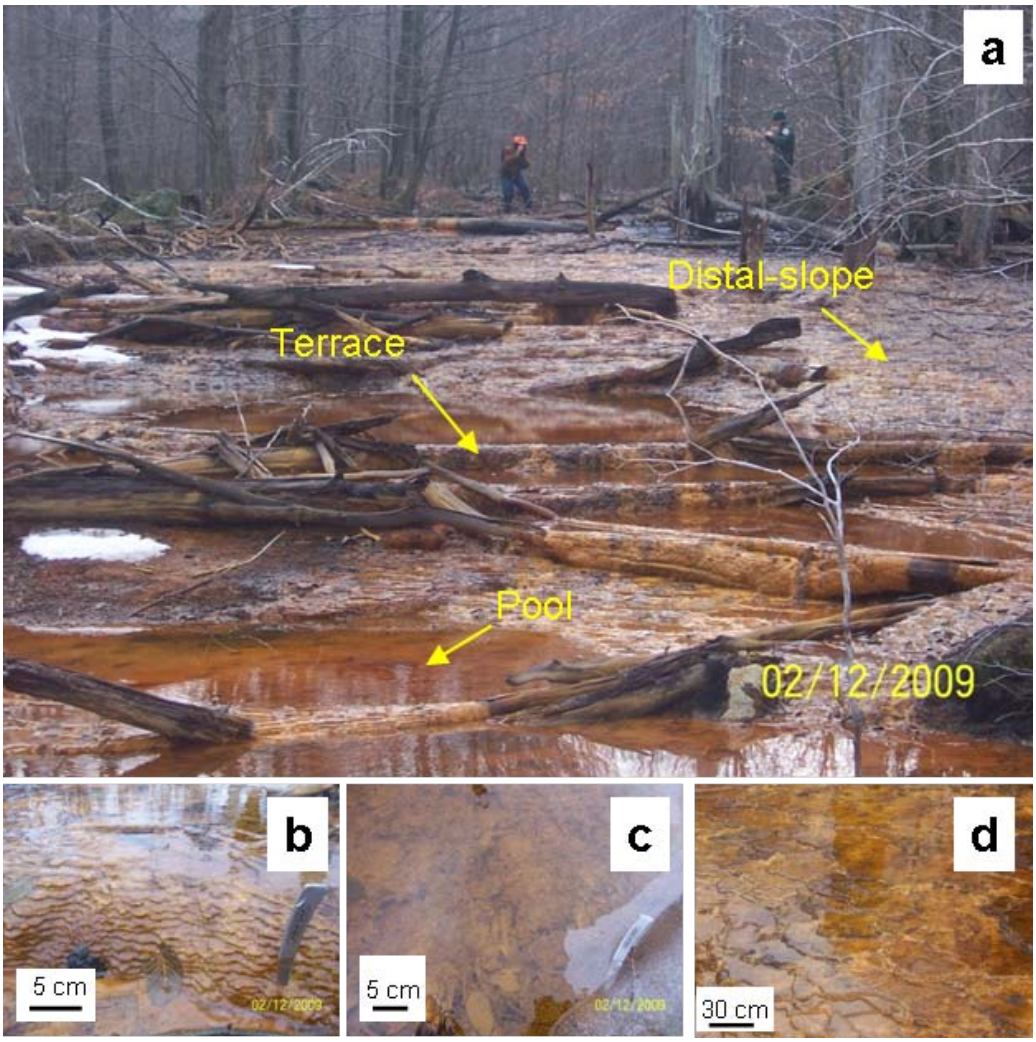

Figure 2-1: Specific facies at a) the upstream view of the upper portion of the Lower Red Eyes iron mound. Smaller photographs show a closer view of b) terrace facie, c) pool facie with cauliflower morphology sediments, and d) distal-slope facie, consisting of shallow pools and terraces less than 5 cm high.

Although the physical structures appear similar, the geochemical gradients at Angel Terrace and Lower Red Eyes are quite different. The temperature of the water at Angel Terrace was found to decrease from 73.2 ºC at the emergent spring to 28.0 ºC

within 5 m downstream (Fouke et al., 2000), while the emergent spring at Lower Red Eyes is an average 9.4 °C and increases to 13.5 °C to 28 °C 122 m downstream (due to seasonal variation). The pH at Angel Terrace was also found to increase from 6.0 to 8.0, as a result of CO_2 degassing (Fouke et al., 2000), while the pH decreases from 4.0 to 2.4 at Lower Red Eyes, as a result of Fe(III) hydrolysis and precipitation. At Angel Terrace, the depositional structures are also composed of carbonate precipitates while similar structures consist of Fe(III) precipitates at Lower Red Eyes.

Based on the physical similarities at Angel Terrace, the Tintillo River, and Lower Red Eyes, we hypothesized that a depositional facies model correlating microbial communities, mineral composition, and crystal morphology could also be extended to AMD sites. Changes in microbial community structure should affect Fe(II) oxidation efficiency; thus, the application of this model would imply that a specific depositional facies, such as a terrace or pool, would be most efficient at Fe(II) oxidation and Fe removal. An understanding of this model would provide the optimal conditions (microbial community structure, aqueous chemistry, and hydrodynamic characteristics) for low-pH Fe(II) oxidation to aid in AMD treatment.

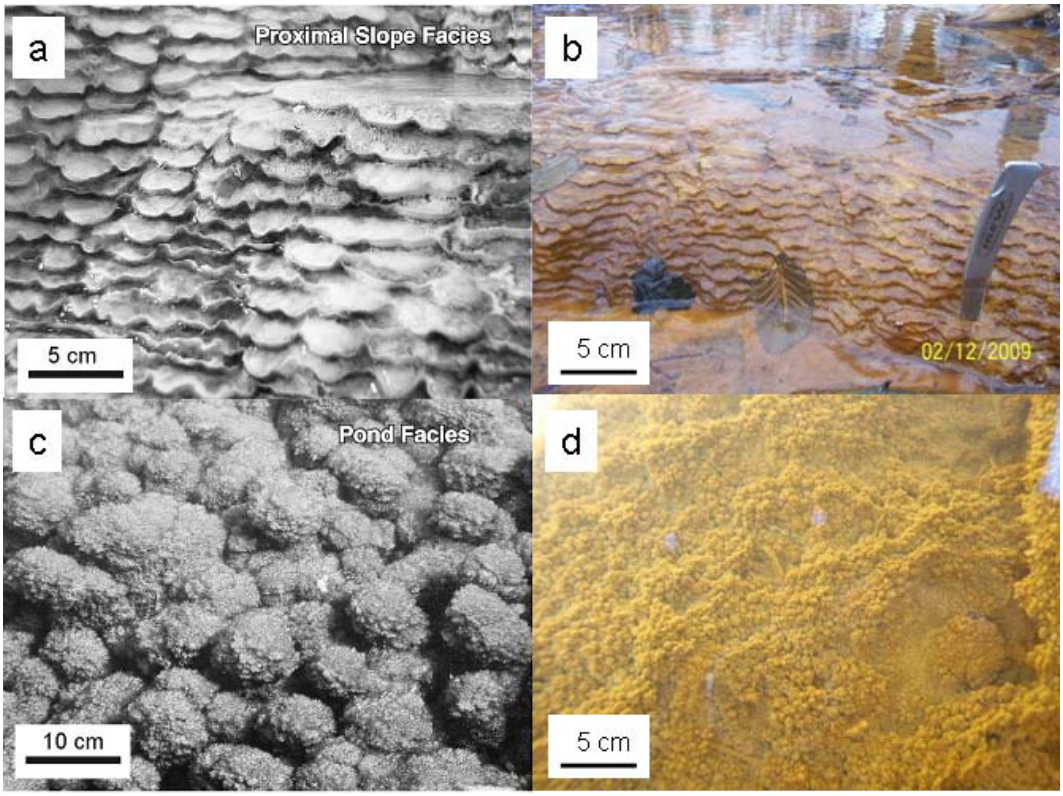

Figure 2-2: Similar terrace facies at a) Angel Terrace and b) Lower Red Eyes. Similar pool facies at c) Angel Terrace and d) Lower Red Eyes (Fouke et al., 2003).

2.3. Objectives

This study attempted to gain a better understanding of the biogeochemical relationships at AMD sites in order to promote low-pH Fe(II) oxidation for more efficient passive treatment systems. It was hypothesized that the depositional facies model developed for Angel Terrace (Fouke et al., 2000) can be applied to AMD sites. The purpose of this study was to determine the optimal conditions and depositional facies to promote low-pH Fe(II) oxidation.

2.4. Materials and Methods

2.4.1. Field Sampling

At Lower Red Eyes, 14 sampling sites were selected along a transect from the emergent AMD spring to 122 m downstream (Figure 2-4a). Sampling sites included both

small and large terrace and pool depositional facies. Of the 14 sampling sites, an upstream pool (UP), an upstream terrace (UT), a downstream pool (DP), and a downstream terrace (DT) were selected for mineralogical and microbial characterizations, and for laboratory reactor studies. The UP and UT locations were selected because they were the first large expanses of distinct depositional facies that allowed for the sampling and removal of several intact pieces of sediments (details below). The UP and UT locations were collected 27 m and 28 m from the AMD spring, respectively (Table 2-2). The DP and DT locations were selected because they were the last paired set of these depositional facies. The DP and DT sediments were collected 59 and 62 m from the AMD spring, respectively (Table 2-2).

Dissolved oxygen (DO) was measured in the field using an Oakton DO 300 Series field meter; temperature and pH were measured in the field with a Beckman Φ265 pH/Temp/mV meter; and, conductivity was measured using an Oakton CON 400 series field meter. Filtered (0.2 μm) water samples were preserved in the field with HCl (for dissolved Fe analysis) or HNO_3 (for dissolved metals analysis by ICP-AES). Samples for sulfate analysis and cell counts were neither filtered nor acidified. All water samples were transported on ice and stored at 4 ^{o}C until analysis.

Sediments for electron microscopy were collected from the top 2 cm and preserved with 2.5% glutaraldehyde. Sediments for X-ray diffraction (XRD) were not chemically preserved. Sediment and biofilm samples for microbial analyses were collected from the sediment surface using sterile transfer pipets. Samples for FISH were preserved immediately in 4% paraformaldehyde (PFA) as described in Macalady et al. (2007). Intact pieces of terrace sections and Fe(III) precipitate-covered leaves from the

pools were removed with a knife and collected in plastic storage containers to be used in flow-through reactors. All sediment samples were stored at 4 ^{o}C until analysis.

2.4.2. Mineralogical Characterizations

Unpreserved sediment samples were also analyzed for Al_2O_3, BaO, CaO, CoO, Cr_2O_3, Fe_2O_3, K_2O, MgO, MnO, Na_2O, NiO, P_2O_5, SiO_2, SrO, TiO_2, ZnO, ZrO_2, and ash content on a Perkin-Elmer Optima 5300 ICP-AES after lithium metaborate fusion. Samples were prepared for scanning electron microscopy (SEM) following a previously published procedure (Zhang et. al, 2007). Cell mineral suspensions were preserved in the field in 2.5% glutaraldehyde, followed by a series of ethanol dehydrations, after which samples were critical point dried using a BAL-TEC CP2030. Dried samples were imaged on an FEI Quanta 200 environmental SEM under low vacuum. Higher magnification images were also collected using a Jeol JSM-6700F field emission SEM with a working distance of 3 mm. XRD patterns were collected using a Rigaku D/Max Rapid II XRD with a Mo X-ray tube and a 0.3 mm collimator. Intensities were measured with the omega axis fixed at 0^{o} and phi axis oscillation between -20^{o} and 20^{o} with a 10 minute exposure time.

2.4.3. Microbial Characterizations

Acridine orange direct counting (AODC) was used to enumerate cells using both sediment and water samples. Cell counts from sediments were performed by extracting 1 gram of wet sediment with 9.5 mL of 0.1% sodium pyrophosphate adjusted to pH 3.5 with sulfuric acid. The samples were extracted for 45 minutes on a rotary shaker and then centrifuged on a Sorvall Evolution RC at 1,000 rpm for 20 min prior to AODC (Hurst, 2002).

Fluorescence in situ hybridization analyses were performed as described by Hugenholtz et al. (2001). Briefly, samples were placed in 10 well Teflon slides and, after drying, were dehydrated with 50%, 80%, and 90% ethanol for 3 min each. Hybridization buffer contained 0.9 M NaCl, 20 mM Tris/HCl at pH 7.4, 0.01% sodium dodecyl sulfate (SDS), 25 ng of fluorescently-labeled probe (Table 2-1), and formamide (concentration varied with probe). After incubation for 2 h at 46 °C, slides were incubated in wash buffer (20 mM Tris/HCl at pH 7.4, 0.01% SDS and NaCl based on Lathe 1985) for 15 min at 48 °C. Slides were then rinsed with deionized water and stained with 4',6'-diamidino-2-phenylindole (DAPI).

Table 2-1: Details of FISH probes used in this study.

Probe name	Sequence (5'-3')	% formamide	specificity	label	source
EUB338	GCT GCC TCC CGT AGG AGT	0-50%	most Bacteria	FITC	Amann et al., 1990
EUB338-II	GCA GCC ACC CGT AGG TGT	0-50%	Planctomycetales	FITC	Daims et al., 1999
EUB338-III	GCT GCC ACC CGT AGG TGT	0-50%	Verrucomicrobiales	FITC	Daims et al., 1999
ARCH915	GTG CTC CCC CGC CAA TTC CT	20%	most Archaea	CY3	Stahl and Amann, 1991
THIO1	GCG CTT TCT GGG GTC TGC	35%	Acidithiobacillus spp.	CY3, CY5	Gonzalez-Toril et al. 2003
BET42a	GCC TTC CCA CTT CGT TT	35%	most Betaproteobacteria, some Gammaproteobacteria	CY3	Manz et al., 1992
GAM42a	GCC TTC CCA CAT CGT TT	35%	most Gammaproteobacteria	CY3	Manz et al., 1992
cGAM42a	GCC TTC CCA CTT CGT TT	35%	competitor	none	Manz et al., 1992

EUBMIX is a mixture of EUB338, EUB338-II, and EUB338-III.
GAMBET is a mixture of GAM42a and BET42a.
GAM42a and BET42a target the 23S rRNA sequence. All other probes target the 16S rRNA sequence.

FISH probes used in this study (details in Table 2-1) target domain as well as broad phylum level bacterial divisions that are common in AMD environments. We also specifically targeted the genus *Acidithiobacillus* that includes the model iron-oxidizing bacterium *At. ferrooxidans.* Betaproteobacteria-specific probe Bet42a is known to target multiple Gammaproteobacteria (Yeates et al., 2003; Haaijer et al., 2006). We used the

PROBE-MATCH tool in ARB (Ludwig et al., 2004) to compare Bet42a against a publicly available database of 23S rRNA sequences (Pruesse et al., 2007 http://www.arb-silva.de), and found that Bet42a targeted >25% of gammaproteobacterial sequences. In order to effectively differentiate among beta- and gammaproteobacteria using these probes, we first determined total gamma-and betaproteobacteria by hybridizing a mixture of cy3-labeled Gam42a and Bet42a (GAMBET), to each sample (Table 2-1). Then, we determined total gammaproteobacteria by hybridizing a separate slide of the same sample with a mixture of cy3-labeled Gam42a and unlabeled competitor cGam42a (Table 2-1). The proportion of total betaproteobacteria was determined by subtracting total Gam42a-labeled cells from total GAMBET-labeled cells.

Slides were mounted with Vectashield and viewed with a Nikon Eclipse 80i epifluorescence microscope at 1000X. A monochrome Photometrics coolsnap ES^2CCD camera was used to obtain photomicrographs with NIS-Elements AS 3.0 software. Population data was generated by counting more than 500 DAPI-stained cells per probe combination. To adequately account for sample heterogeneity, count data for each probe combination was collected from at least eight photos (each representing a different microscope field) and from at least two slide wells.

2.4.4. Laboratory Reactors

Water for flow-through reactors was collected from the AMD emergence and stored in 13 L plastic carboys. The water was nitrogen flushed upon returning to the laboratory, stored at 4 °C and filtered (0.2 μm) prior to use in the reactors.

Flow-through reactors were constructed using intact pieces of natural sediments to measure Fe(II) oxidation kinetics under controlled conditions in the laboratory. The

surface area of the intact sediments was estimated by assuming that leaves were elliptical shaped and terrace pieces were trapezoidal. The length of each side was then measured and the area was computed. The reactors consisted of two plastic storage containers (13 cm x 8.2 cm x 6.4 cm) in series connected with Tygon L/S 14 tubing. Each reactor contained 175 mL of AMD, corresponding to a 0.6 cm water column height above the sediments. A peristaltic pump (Cole-Parmer Masterflex pump #7523-30 equipped with a Masterflex #7519-25 pump head) was used to pump water from a 19 L glass feed tank into the first container, from the first container into the second container, and from the second container into a waste jug at a constant flow rate (Figure 2-3). The reactor volume (a.k.a., pore volume) was defined as the total liquid volume in the two containers (350 mL). The hydraulic residence time was defined as the time required to convey one reactor volume through the two containers. Experiments were conducted sequentially at residence times of 10, 5, and 2 h, starting at the longest residence time and finishing at the shortest residence time. The flow rates for these residence times were 0.6, 1.2, and 2.9 mL/min, respectively. Reactors contained either terrace or pool sediments (8 - 113 g; 41 - 154 cm^2) conducted in duplicate and single replicate no-sediment controls were run at the same time. At the conclusion of experiments conducted with upper terrace and upper pool sediments, the intact sediment reactors were exposed to 50 kilogray of ^{60}Co radiation, and the whole experiment was repeated with these irradiated sediments serving as sterile controls.

Water samples were collected at the initial start (time = 0), and after 1, 2, 4, and 6 pore volumes of fluid had been pumped through the reactors. At the influent and effluent of each reactor, 1 mL of sample was collected and centrifuged at 13,400 rpm for 2 min to

separate any precipitates. Dissolved Fe and Fe(II) were measured from the sample. The pH of the remaining supernatant was measured with a Thermo Orion 550A benchtop pH meter and semi-micro Thermo Orion pH probe. Dissolved oxygen was also measured at each sampling point using an Extech ExStik II DO field meter. At pseudo-steady state for each residence time (described below), water samples were collected for AODC and ICP-AES and sediment samples were collected for FISH.

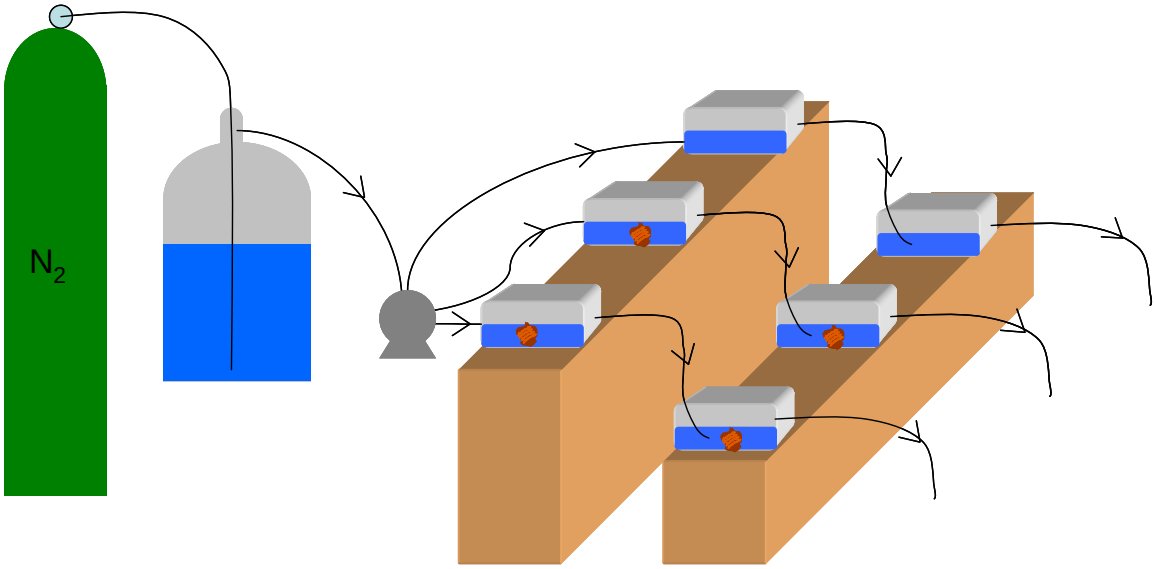

Figure 2-3: Schematic of laboratory reactor set-up, showing the feed tank (purged with nitrogen gas) pumping AMD water into three parallel reactors with two reactors in series. An intact sediment chunk is shown in the first two series of reactors.

2.4.5. Analytical Methods

Dissolved Fe(II) and Fe (after reduction by hydroxylamine-HCl) were determined using the ferrozine assay (Stookey, 1970). Ferrozine solution was prepared by adjusting 50 mM HEPES buffer to pH 6.8-7.0 with NaOH and adding 1 g/L of ferrozine iron reagent. The absorbance of all samples at 562 nm was measured using a Shimadzu UV-visible Spectrophotometer UV-1601. Dissolved Fe(III) concentrations were determined from the difference of Fe and Fe(II) measurements. Al, As, Ba, Ca, Co, Cr, Cu, Fe, K,

Mg, Mn, Na, Ni, Pb, Si, Sr, Ti, V, Zn, and Zr were analyzed on a Perkin-Elmer Optima 5300 ICP-AES (Table 2-1). Sulfate was measured on a HACH DR/2800 spectrophotometer using Hach Method 8051, SulfaVer 4.

2.5. Results

2.5.1. Site Description

Lower Red Eyes is a low flow (~0.44 L/s) AMD site located in Somerset County, PA, USA. The AMD discharge is the result of runoff that pools behind the low wall of a large former surface coal mine and then travels underground to emerge at a previously drilled exploratory borehole within the Prince Gallitzin State Forest (40° 14’ 25.25" N; 78° 44’ 49.2" W). The AMD source drains two coal mines, with a combined area of more than 250 acres, along the Clarion, Brookville, and Kittanning coal seams. Both sites were mined in the 1970s and operations continued into the 2000s. The anoxic AMD emerges into an algae-filled pool and flows downstream through a series of terraces formed on fallen trees and small and large pools (Figure 2-1a). After flowing through the forest for nearly 150 m, the discharge seeps back into the ground. This site is unique to the majority of low-pH Fe(II)-oxidizing AMD sites we have found in Pennsylvania, which typically flow into a nearby stream causing the geochemical gradient to be disrupted. As a result, at Lower Red Eyes the entire Fe(II) oxidation and Fe(III) precipitation process can be studied.

The emergent discharge has an average pH of 4.0, dissolved oxygen (DO) of 0.0 mg/L and dissolved concentrations of iron, manganese, aluminum, and sulfate of 9.7, 2.1, 1.6, and 31.3 mM, respectively (Table 2-2). The pH decreases with distance from the source to below 2.5, indicative of Fe(III) hydrolysis and precipitation (Figure 2-4b). DO

and temperature increase across the transect until DO is nearly saturated and temperature varies due to seasonal changes (Figure 2-4c-d). Dissolved Fe (sum of Fe(II) and Fe(III)) decreases along the transect as a result of Fe(II) oxidation and Fe(III) precipitation (Figure 2-5a). While dissolved Fe decreases across the iron mound, the fraction of Fe(III) increases dramatically due to Fe(II) oxidation (Figure 2-5b).

Table 2-2: Water chemistry at the emergent AMD spring (E), upstream pool (UP), upstream terrace (UT), downstream pool (DP), and downstream terrace (DT).

Site	pH	Dissolved oxygen (µM)	Dissolved Fe(II) (µM)	Total dissolved Fe (µM)	SO_4^{2-} (mM)	Mn (µM)	Al (µM)	Zn (µM)	Ca (µM)	AODC* (x 10^7 cells/ g sediment)
E	3.96 ± 0.25 N = 7	0.00 ± 0 N = 2	9724 ± 326 N = 5	9617 ± 387 N = 5	31.3 ± 4.0 N = 12	2057 ± 53 N = 3	1594 ± 44 N = 3	199 ± 23 N = 3	5539 ± 191 N = 3	--
UP	2.97 ± 0.05 N = 5	181 ± 4 N = 2	6160 ± 700 N = 2	8435 ± 263 N = 2	34.2 ± 10.5 N = 10	2093 ± 0.00 N = 2	1631 ± 26 N = 2	214 ± 11 N = 2	5614 ± 176 N = 2	--
UT	2.94 ± 0.03 N = 5	215 ± 37 N = 2	6357 ± 485 N = 2	8022 ± 143 N = 2	27.7 ± 2.6 N = 7	2148 ± 64 N = 2	1631 ± 52 N = 2	214 ± 21 N = 2	5814 ± 264 N = 2	0.44 ± 0.17
DP	2.64 ± 0.07 N = 7	188 ± 34 N = 4	3760 ± 308 N = 3	6429 ± 304 N = 3	32.9 ± 9.8 N = 11	2057 ± 64 N = 2	1631 ± 25 N = 2	214 ± 21 N = 2	5489 ± 0 N = 2	3.8 ± 2.6
DT	2.65 ± 0.09 N = 4	213 ± 39 N = 2	3797 N = 1	5444 N = 1	24.2 ± 4.5 N = 5	2093 N = 1	1594 N = 1	184 N = 1	5489 N = 1	2.2 ± 2.5

*Cell counts were done on sediment pieces used in laboratory reactor
As, Ba, Cu, Pb, Ti, Zr < 0.01 mg/L

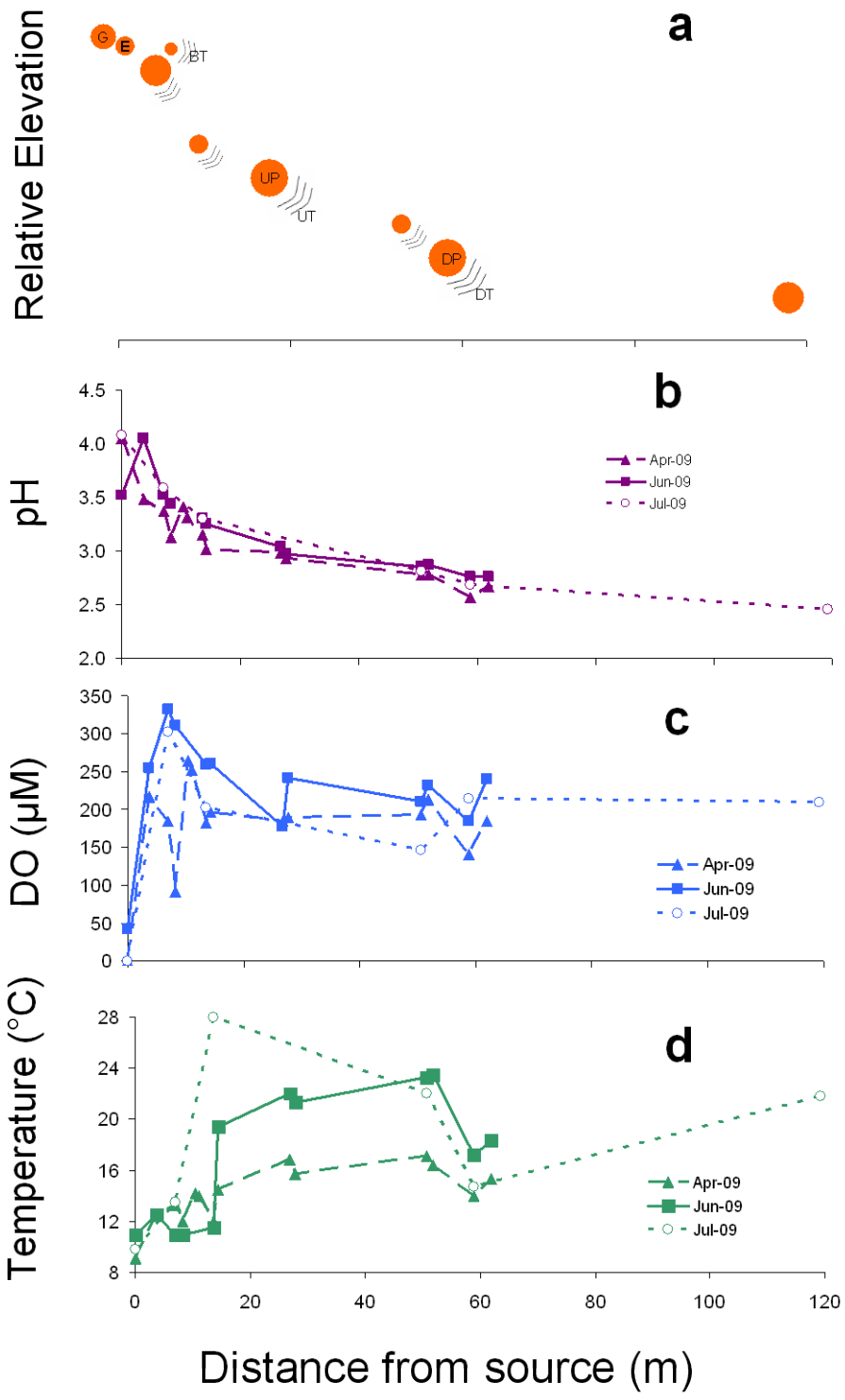

Figure 2-4: Site schematic and geochemical gradients at Lower Red Eyes. Orange circles represent pools and series of lines represent terraces. "E" is the AMD emergent spring, "G" is the algae pond upstream of the source, "BT" represents a terrace along the transect, and "UP", "UT", "DP", and "DT" represent the upstream pool, upstream terrace, downstream pool, and downstream terrace, respectively.

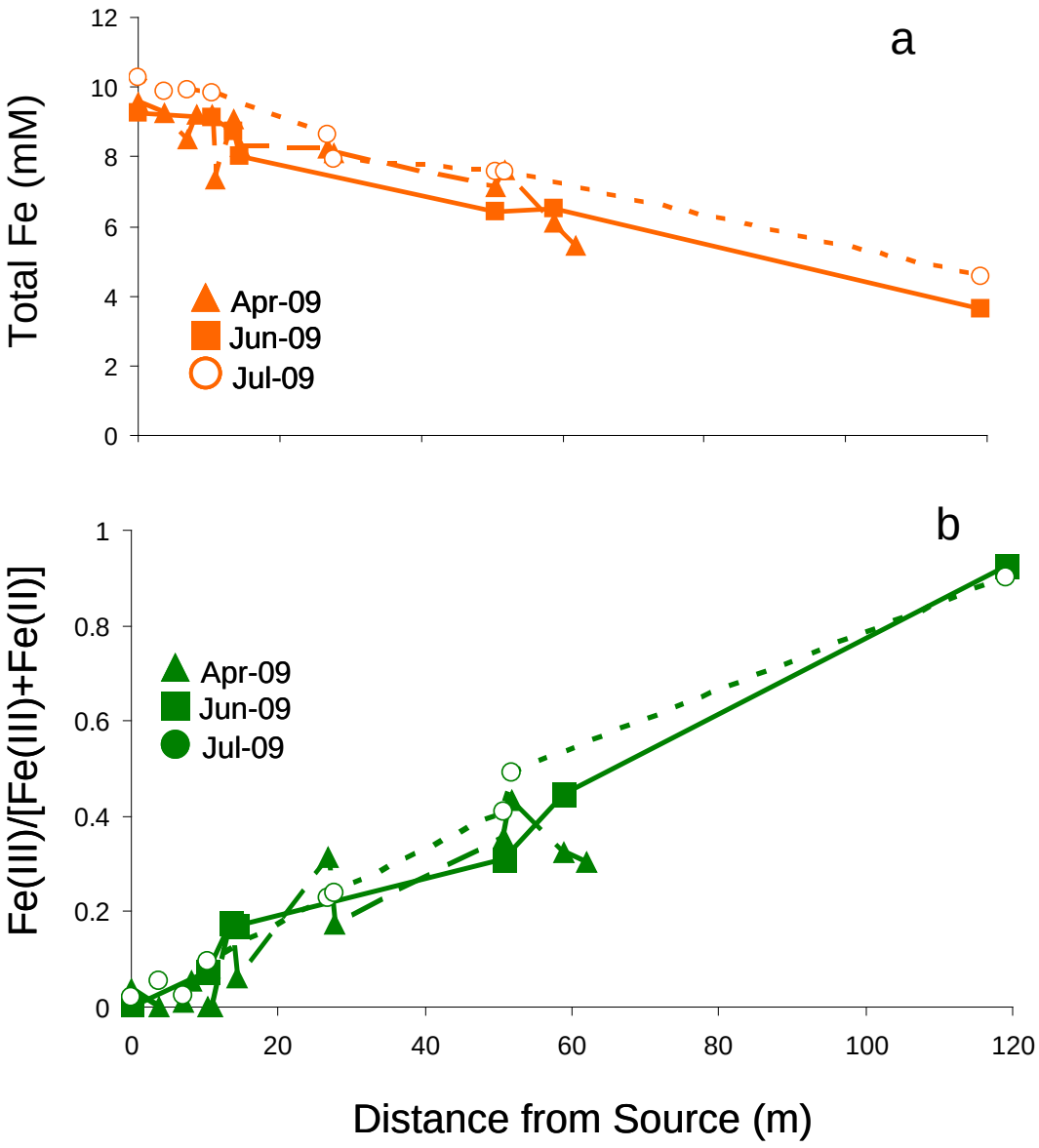

Figure 2-5: a) Total Fe and b) ratio of Fe(III) to total dissolved Fe (Fe(II) + Fe(III)) as a function of distance from the AMD source at Lower Red Eyes.

At the anoxic emergence, photosynthetic Eukarya were the predominant microorganisms. Elongated cells with rust colored granules were commonly observed under microscope, suggesting Fe sequestration. These cells appeared similar to *Euglena mutabilis*, which has been identified at AMD sites in Indiana, USA (Brake et al., 2001) and Spain (Espana et al., 2007). As the water became oxygenated and the pH dropped,

the predominant microorganisms transitioned from Euglena to acidophilic iron-oxidizing bacteria. Using a general Archaea FISH probe, we found less than 1% of cells downstream of the spring were identified as Archaea.

We identified three distinct depositional facies at Lower Red Eyes: terraces consisting of a vertical drop greater than 5 cm (Figure 2-1b); pools of quiescent water with a diameter of 1-2 m (Figure 2-1c); and, proximal-slope facie consisting of vertical drops less than 2 cm with shallow ponds behind those drops (Figure 2-1d). These facies were defined because each had distinct flow rate, water depth, and oxygen mixing, which affected the biology and subsequent Fe(II) oxidation rate at that specific facie. Pools were filled with quiescent, calm water that flowed smoothly from the pool to the adjacent terrace facie. Water along the terraces cascaded turbulently over the terrace face into the adjacent pool. Pools were estimated to have a diameter of 1.5 - 1.8 m and a water depth of 0.3 - 0.8 m, which yielded a residence time of 21 to 75 minutes in each pool. Terraces were approximately 10 cm high and 2.5 – 3 m wide with a water depth of 2.5 cm. This volume resulted in a residence time between 12 and 16 s for each terrace.

In pool facies, precipitates at both Lower Red Eyes and Angel Terrace displayed a stalked “cauliflower-like” morphology (Figure 2-2); however, these structures at Angel Terrace were much larger than Lower Red Eyes. These sediment stalks were somewhat “fluffy” and commonly deposited directly onto leaves and plant debris settled onto the pool bottoms. By contrast, the precipitates on the terraces and vertical lips of the proximal slopes were strongly cemented. These cemented sediments were composed of compacted leaves and organic matter.

2.5.2. Field Chemistry

Dissolved Fe(II) and Fe were measured downstream of the Lower Red Eyes AMD spring. The trends over time were similar for all sampling events and no seasonal variation was detected (Figure 2-4). At the spring, no Fe(III) was present and the concentration of Fe(II) averaged 9.7 mM (Table 2-2). The concentration of dissolved Fe(III) increased downstream while the concentration of dissolved Fe(II) decreased as a result of Fe(II) oxidation. Greater than 95% of the dissolved Fe(II) was oxidized to Fe(III) within 122 m of the spring. The concentration of dissolved Fe(III) increased from approximately 0 mM to more than 3 mM within 122 m of the spring. The concentration of Fe decreased with distance from the spring as a result of Fe(III) precipitation. Within 122 m of the spring, approximately 60% of dissolved Fe was removed. A corresponding decrease in pH was also detected along the transect, indicative of Fe(III) hydrolysis (Figure 2-4b). Although significant removal of dissolved Fe was observed, no change in trace metal cation concentrations was detected along the transect (Figure 2-6). Concentrations of Si and Zn appeared to increase at some sampling sites and As, Ba, Cu, Pb, Ti, and Zr were all below the ICP-AES detection limit.

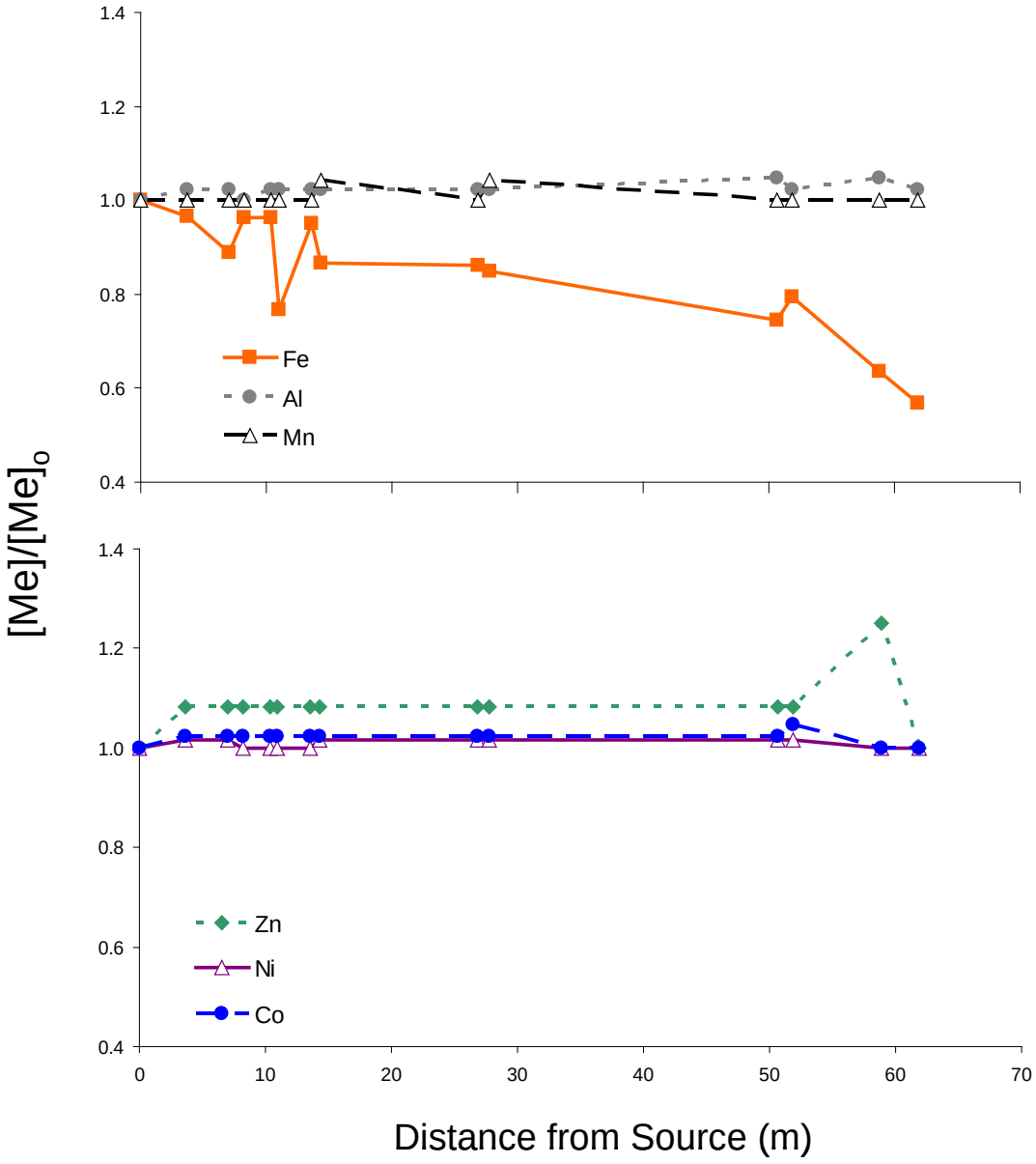

Figure 2-6: Normalized dissolved metal cation concentrations along the Lower Red Eyes transect.

2.5.3. Mineralogical Characterizations

Metal oxide composition of sediments was determined at four sampling locations within 61 m of the AMD spring. All samples indicated a composition of predominantly Fe_2O_3 (≥50%) and organic matter that was lost on ignition (30-40%) (Table 2-3). These results were consistent with the field observations of plant matter cemented into the

terraces and settled onto the pool bottoms. These results also indicated little or no selective uptake of trace metal cations or anions into the Fe(III) precipitates.

XRD indicated that the predominant mineral phase at all sampling sites along the Lower Red Eyes transect was poorly crystalline schwertmannite (Figure 2-7). Minor amounts of goethite were detected at a few sampling points, including the upper terrace and downstream pool locations. From SEM images, we found that sediment minerals from all locations contained spheres, ranging from 1-2 μm in diameter, with pin-cushion morphology (Figure 2-8) typical of schwertmannite (Bigham, 1990). EDS analysis confirmed a composition of Fe, S, and O. The high signal for S was consistent with XRD and SEM data indicating schwertmannite as the predominant phase. No trace metals were detected in the EDS analysis.

Table 2-3: Metal oxide percent composition of sediments collected at Lower Red Eyes. E is AMD source, G is algae-filled pool upstream of source, BT is a terrace along transect and DP is downstream pool. (Sch = schwertmannite and Gt = goethite)

	E	G	BT	DP
Distance from Source (m)	0	3.7	11	59
Al_2O_3 (%)	3.75	0.47	0.38	0.38
BaO (%)	< .01	< .01	< .01	< .01
CaO (%)	0.26	0.07	0.06	0.17
CoO (%)	< .01	< .01	< .01	< .01
Cr_2O_3 (%)	< .01	< .01	< .01	< .01
Fe_2O_3 (%)	49.7	65.6	62.6	58.6
K_2O (%)	< .05	< .05	< .05	< .05
MgO (%)	0.65	0.23	0.21	0.48
MnO (%)	0.1	<.01	< .01	0.06
Na_2O (%)	< .05	< .05	< .05	< .05
NiO (%)	< .01	< .01	< .01	< .01
P_2O_5 (%)	1.57	0.14	0.18	0.11
SiO_2 (%)	< .05	< .05	< .05	< .05
SrO (%)	<.01	< .01	< .01	<.01
TiO_2 (%)	0.13	0.07	0.07	0.08
ZnO (%)	0.02	<.01	<.01	0.01
ZrO_2 (%)	<.01	<.01	<.01	<.01
Loss on ignition (%)	43.8	33.4	36.5	40.1
Minerals	Sch + Gt	Sch	Sch	Sch + Gt

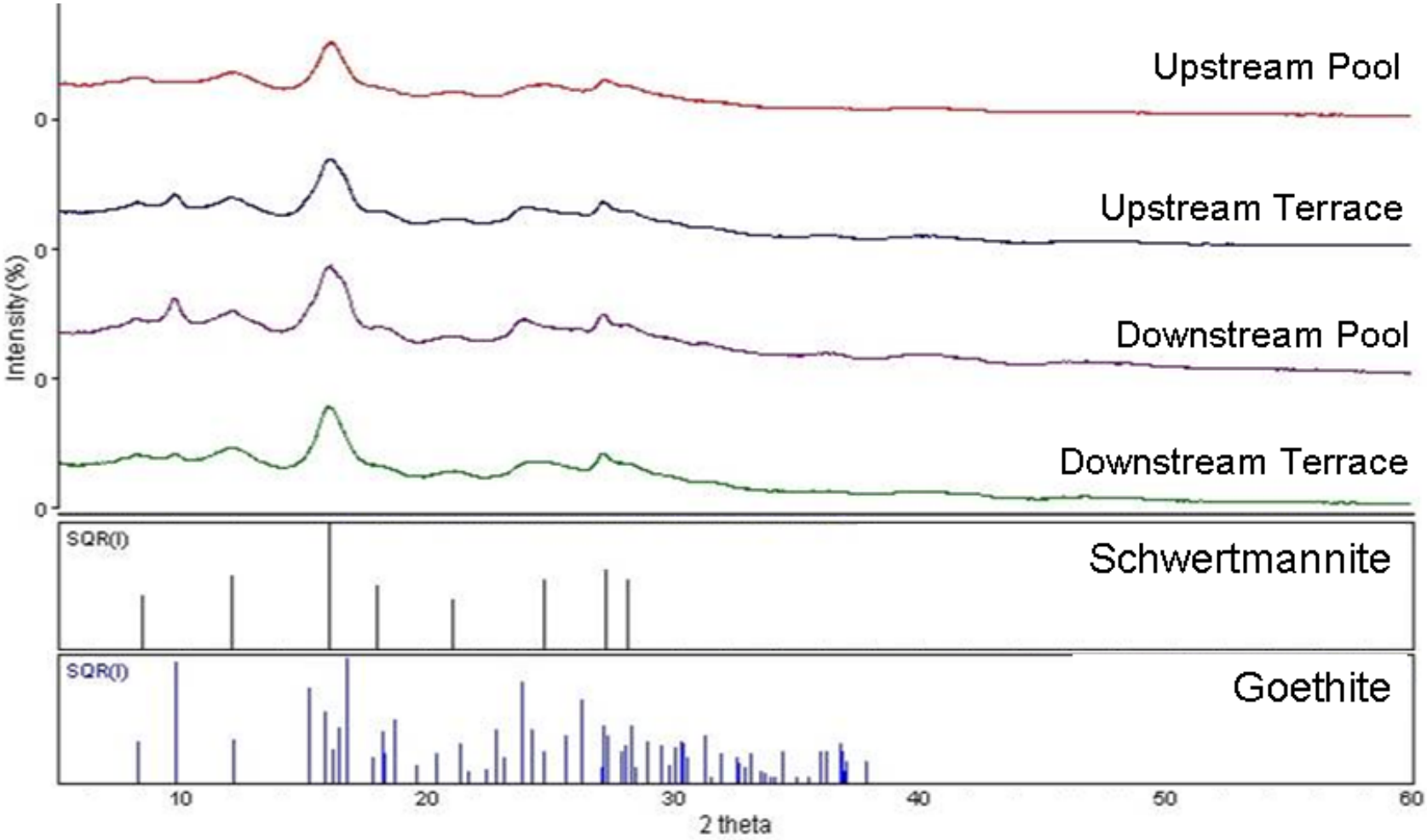

Figure 2-7: XRD patterns from samples at Lower Red Eyes compared to schwertmannite and goethite powder diffraction files from Jade 7.

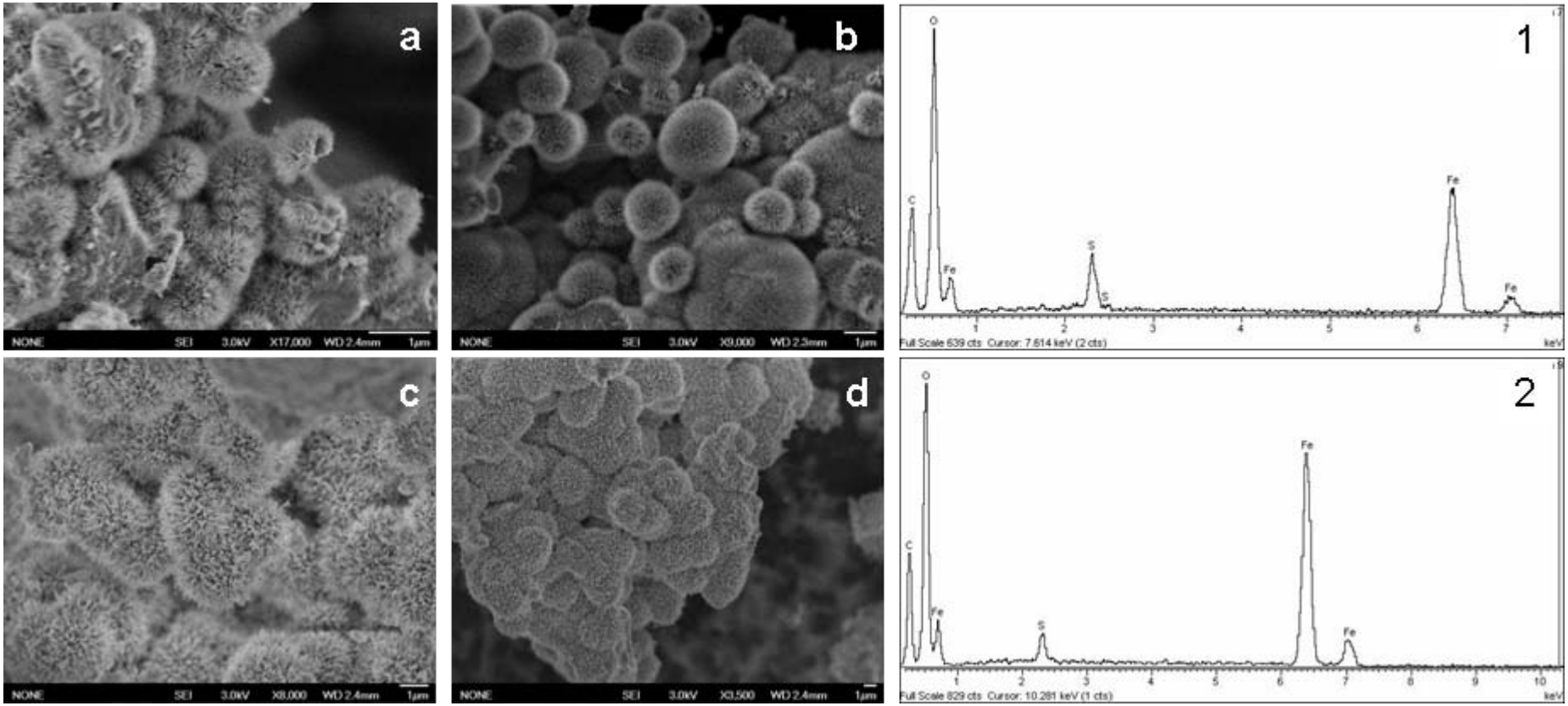

Figure 2-8: Schwertmannite pin-cushion morphology at a) the upstream terrace, b) the upstream pool, c) the downstream terrace, and d) the downstream pool. EDS of 1) an upstream pool and 2) a downstream pool.

2.5.4. Microbial Characterizations

AODC was used to determine sediment cell counts rather than aqueous counts due to the low concentration of cells in the AMD water. Cell counts were found to range from 10^6 to 10^7 cells/g at all sampling sites. Assuming that all biomass was extracted and counted, and that all cells have a density of 2.8×10^{-13} g/cell (Kirby et al., 1999), then the biomass concentration equaled 10^{-7}-10^{-6} g biomass/g sediment. This was much less than the percent of organic material that was lost on ignition (0.33-0.43 g organic matter/g sediment) as measured by lithium metaborate fusion (Table 2-3), suggesting that most of the ash content was plant matter such as leaves.

FISH was used to determine the microbial community composition of sediments at varying distance from the AMD spring (Figure 2-9). We used domain-specific probes to target the archaea and bacteria, as well as broad phylum-level probes to target the gamma- and betaproteobacteria divisions. Both of these divisions contain multiple iron-oxidizing acidophiles that are common to AMD environments (Johnson and Hallberg, 2003), and at all sites except the emergence, the combination of gamma- and betaproteobacterial probes labeled more than 80% of all DAPI-stained cells. We also specifically targeted the genus *Acidithiobacillus* (Gammaproteobacteria), which is common in low-pH AMD environments.

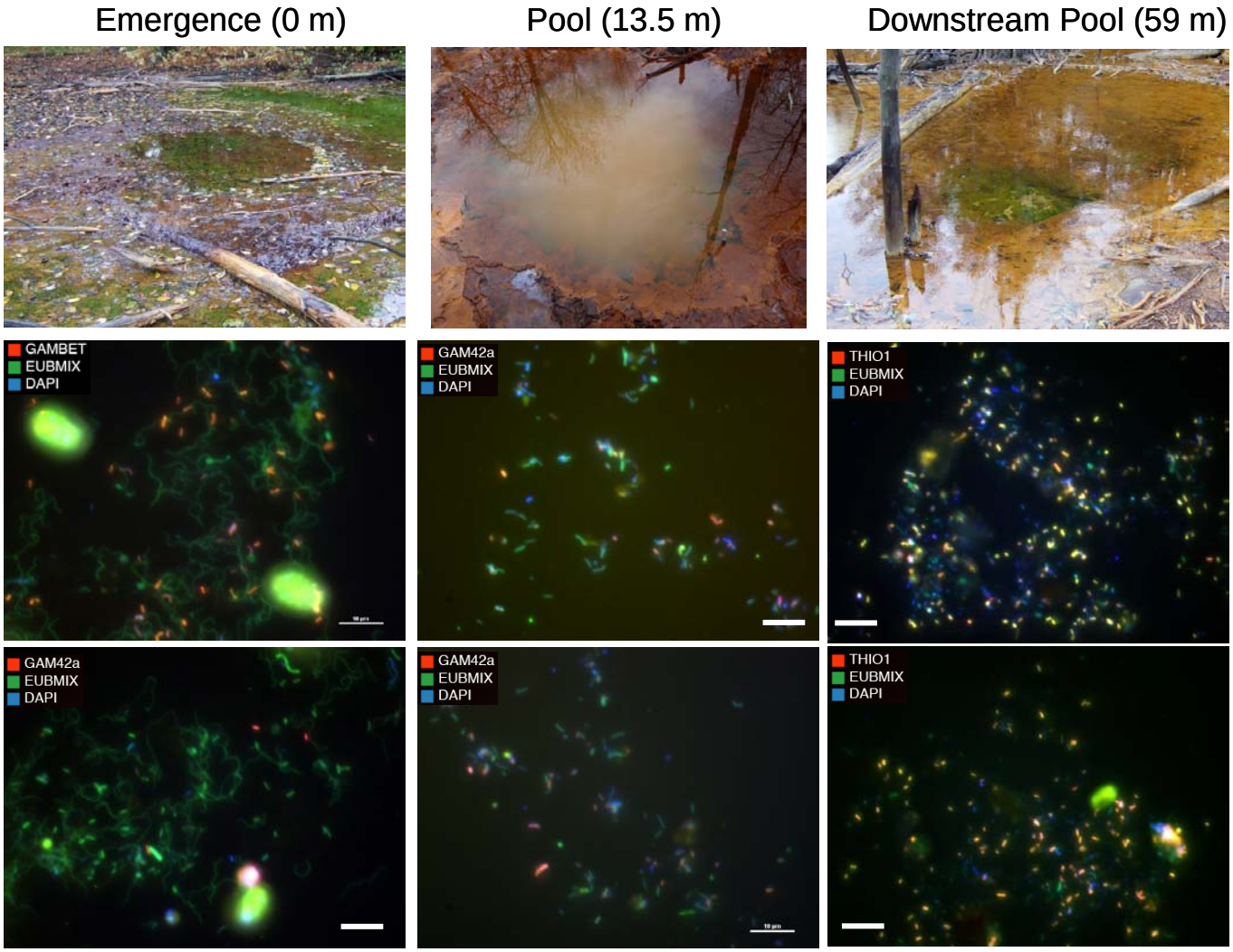

Figure 2-9: FISH images from samples collected at the emergence, a pool 13.5 m downstream, and a pool 59 m downstream show a transition from Betaproteobacteria to Gammaproteobacteria (not *Acidithiobacillus*) to *Acidithiobacillus.* Note that colors were superimposed and yellow/orange fluorescence indicates red and green probes were both targeted. (Scale bar is 10 μm)

At the emergence, *Euglena* were abundant, and bacterial communities were dominanted by bacteria with characteristic spirochete-morphology (Figure 2-6). Rod-shaped Betaproteobacteria made up 32% of the community (Figure 2-7). At 10 m from the spring, Betaproteobacteria increased in abundance to 70% of the community. The presence of Betaproteobacteria in the upstream communities was verified by cloning 16S rDNA sequences from a site 10 m downstream from the emergence. Greater than 60% of bacterial 16S rDNA phylotypes from this site were Betaproteobacteria (results not shown). Further downstream, Betaproteobacteria decreased and Gammaproteobacteria increased. At 59 m from the spring, *Acidithiobacillus* were the dominant microorganisms. More than 50% of all cells were identified as *Acidithiobacillus* and only 1% were identified as Archaea at this location. No *Acidithiobacillus* were observed less than 28 m from the source.

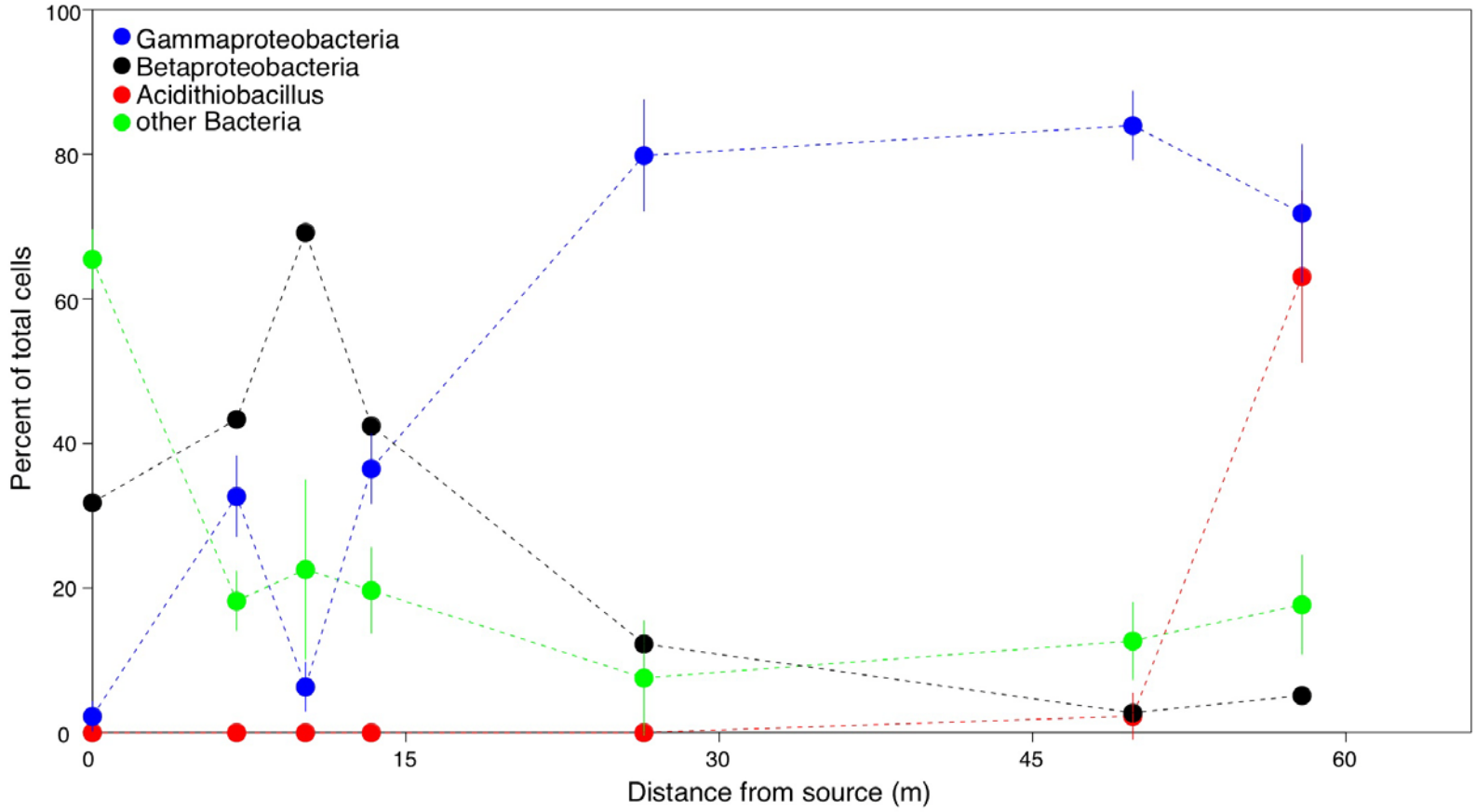

Figure 2-10: FISH analysis indicated that Betaproteobacteria decreased with distance from AMD source, while Gammaproteobacteria increased with distance from source as the pH dropped. Percent of total cells exceeds 100 because *Acidithiobacillus* are included in Gammaproteobacteria.

Microbial communities were also compared on the basis of facies (Figure 2-11). Overall, microbial communities from adjacent pools and terraces were similar (Appendix C, Table C-4). Changes in microbial community composition were more dependent upon distance from the emergence (Figure 2-10) than depositional facie. However, this conclusion is based on FISH analyses targeting only broad microbial divisions, and a different technique such as 16S rDNA cloning might resolve differences in community composition that we did not detect here. Furthermore, we did detect some differences between pool and terrace microbial communities (Table C-4). An upstream pool and terrace pair indicated a greater abundance of Betaproteobacteria and a lesser abundance of Gammaproteobacteria in the terrace as compared to the pool. Both the upper pool and terrace sediments contained minor amounts of Gammaproteobacteria but no *Acidithobacillus* while the downstream pool and terrace sediments contained primarily *Acidithiobacillus*.

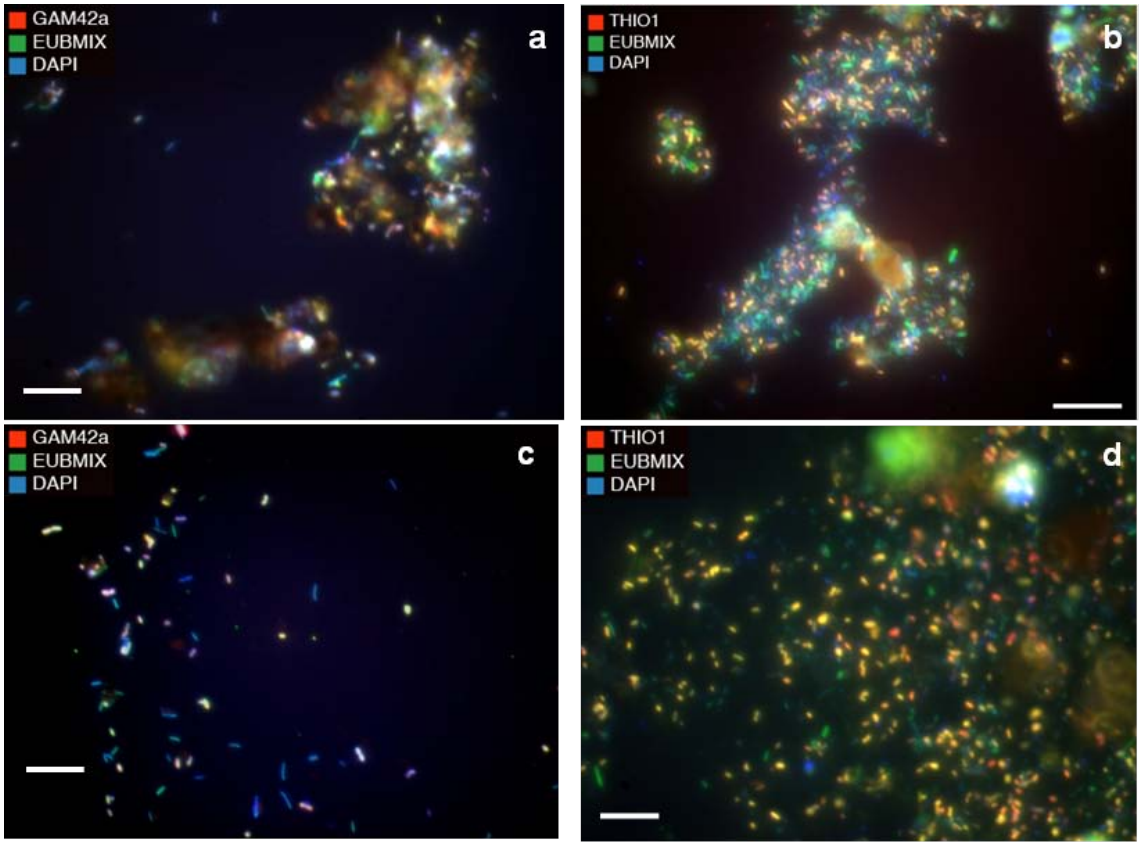

Figure 2-11: Similar microbial communities were observed at adjacent pool and terrace sites and *Acidithiobacillus* increased from upstream to downstream locations. a) upstream pool, b) downstream pool, c) upstream terrace, and d) downstream terrace (Scale bar is 10 μm)

The microbial communities changed significantly across the Lower Red Eyes iron mound with *Acidithiobacillus* increasing with distance from the spring and Betaproteobacteria decreasing with distance (Figure 2-10). Distinct microbial compositions did not appear at each facies, but appeared to be more dependent upon the pH of the water at any particular site. FISH analysis of reactor sediments also reflected the community composition of field sediments, such that Gammaproteobacteria (but not *Acidithiobacillus*) dominated in upstream sediments and *Acidithiobacillus* dominated in downstream sediments.

2.5.5. Kinetics of Low-pH Ferrous Iron Oxidation in Laboratory Reactors

Fe(II) oxidation rates were measured to determine if biogeochemical kinetics change as a function of depositional facies. The influent and effluent pH, DO, Fe(II) concentration, and Fe concentration were measured as a function of the number of pore volumes pumped through the reactors. Results for the upstream terrace sediments operated at a 10 h residence time are presented in Figure 2-12. We found that these sediments reached a pseudo-steady state condition with respect to the effluent Fe(II) concentration within two pore volumes, where the Fe(II) concentration decreased from 9.8 to nearly 4.5 mM. The concentration of dissolved Fe also decreased from 9.8 to below 8 mM, indicative of Fe(III) precipitation. The pH dropped rapidly over time, from pH 4.5 to pH 2.7. The effluent DO in the "live" sediment was significantly less than the effluent DO in the sterilized sediment reactors, as well as the no-sediment control reactors. The consumption of Fe(II) and DO, and the drop in pH and Fe, and the contrasting results compared to the control reactors, are all consistent with biological Fe(II) oxidation followed by hydrolysis and precipitation of Fe(III). These geochemical changes were also consistent with gradients observed downstream from the Lower Red Eyes spring.

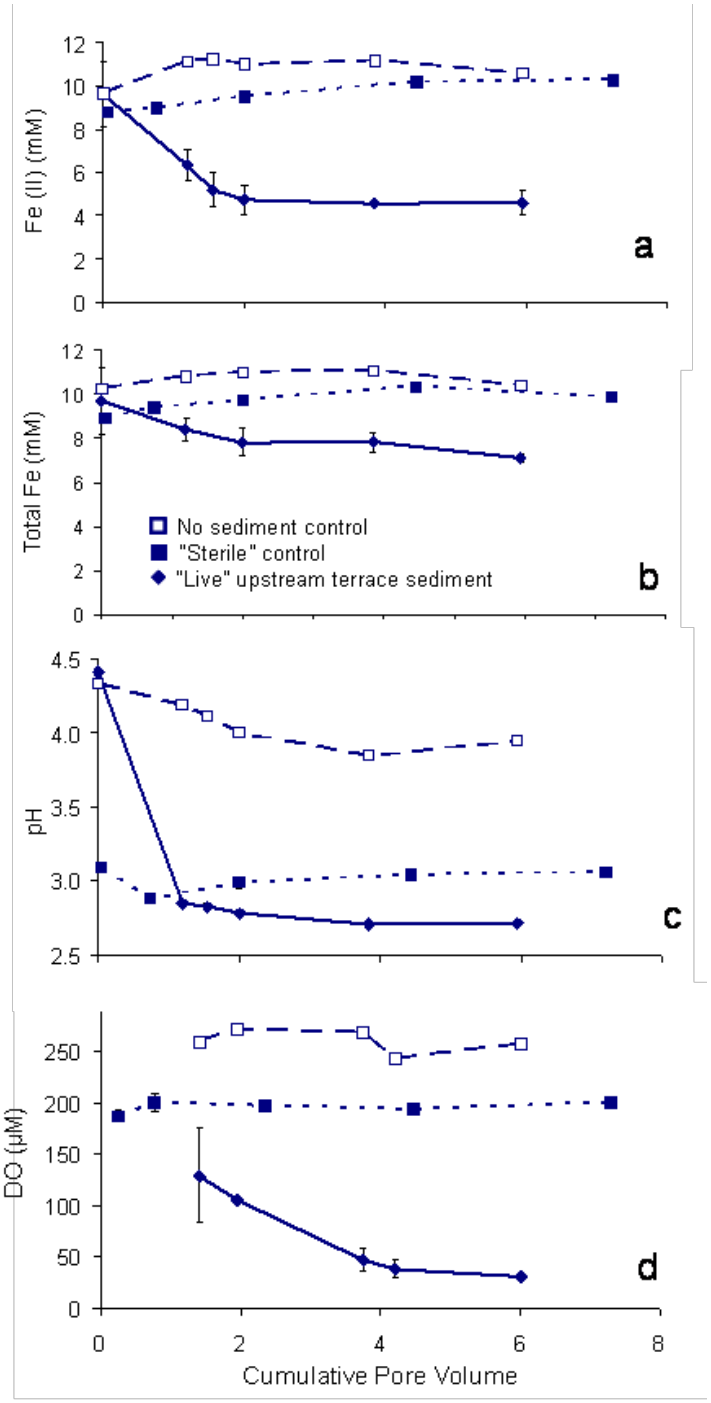

Figure 2-12: Geochemical changes with increasing pore volume at the 10 h residence time. a) Greater than 50% of dissolved Fe(II) was rapidly oxidized within 2 pore volumes. b) Nearly 25% of total dissolved Fe was removed from the AMD water. c) The pH decreased rapidly from ca. 4.5 to ca. 2.7. d) DO decreased from ca. 125 µM to less than 31µM. No changes were detected for either control reactor (no sediment and sterilized sediments); the initial pH of the sterile control was low due to storage, but no further decrease was observed.

The reactor influent was filtered (0.2-μm) and maintained under a N_2 atmosphere during these experiments, however, Fe(II) concentrations still dropped over storage times of up to 30 d, and varied slightly due to different collection dates. Therefore, to compare results over these continuous experiments where we incrementally decreased the hydraulic residence time, and to compare results between the different sediments, we present normalized concentration ratios of $[Fe(II)]_{out}/[Fe(II)]_{in}$ to account for these variances (Figure 2-13). The exact range of values for $[Fe(II)]_{in}$ in each experiment are included in the caption for Figure 2-13. With the upper terrace sediments, the $[Fe(II)]_{out}/[Fe(II)]_{in}$ ratio at pseudo-steady state was 0.45 at the 10 h residence time, indicating that 55% of the influent Fe(II) was oxidized (Figure 2-13a). With the upper terrace sediments, and all other sediments tested, the $[Fe(II)]_{out}/[Fe(II)]_{in}$ ratios increased as the hydraulic residence time decreased. These data suggest that the hydraulic residence across a natural or engineered iron mound utilized for low-pH Fe(II) oxidation will exert significant control on treatment performance.

Compared to sediments collected from the upstream locations, the sediments collected from the downstream locations achieved higher $[Fe(II)]_{out}/[Fe(II)]_{in}$ ratios, i.e., lower treatment performance. For example, with the downstream terrace sediments at the 10 h residence time, the $[Fe(II)]_{out}/[Fe(II)]_{in}$ ratio at pseudo-steady state was 0.72 (Figure 2-13b). These experiments were all conducted with nearly identical influent water chemistry, and abiotic oxidation of Fe(II) was negligible. Therefore, we speculate that these differences are caused by differences in the microbial communities found at these locations.

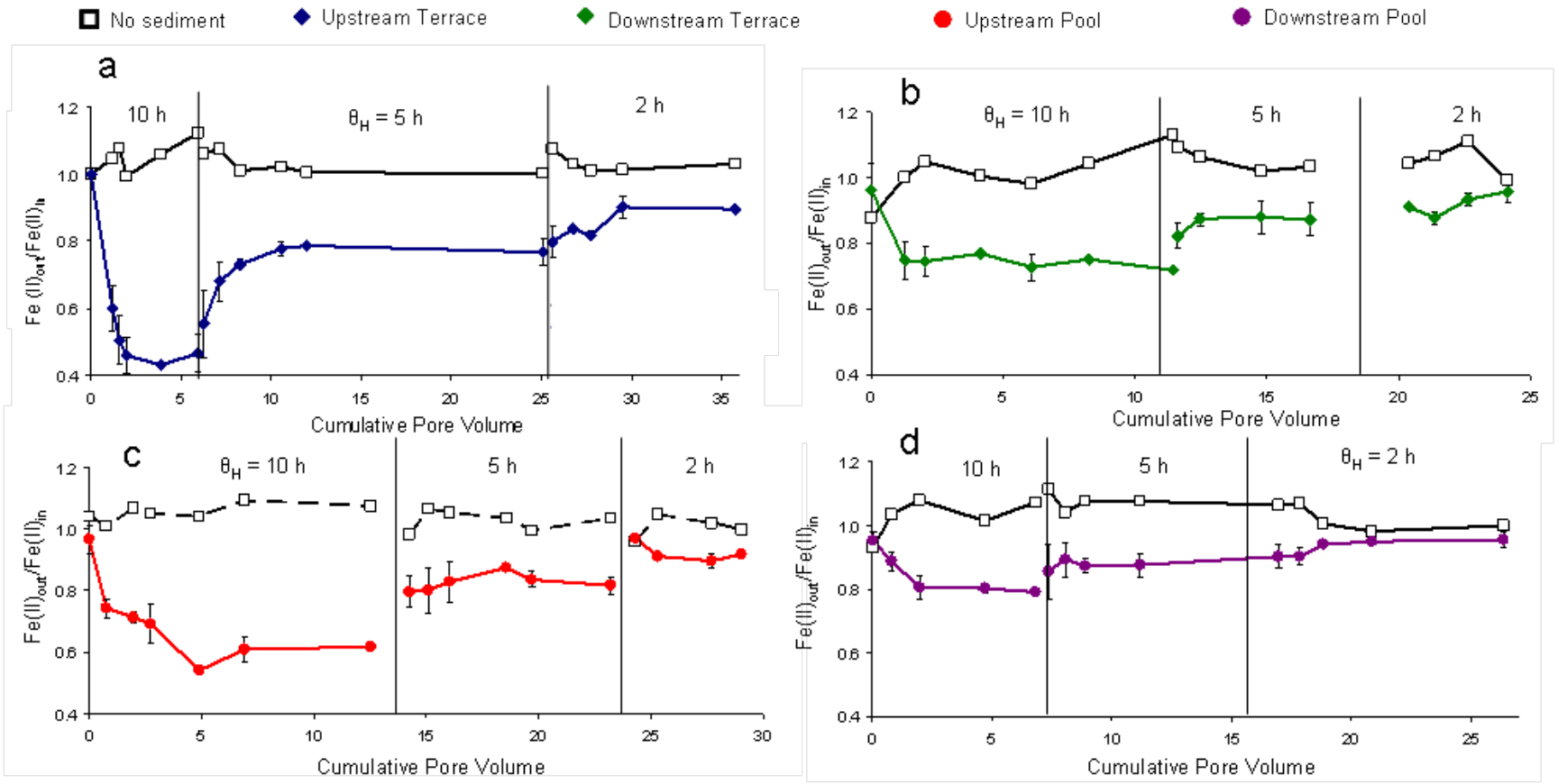

Figure 2-13: Normalized effluent Fe(II) concentrations for a) upstream terrace ($[Fe(II)]_{in}$ = 9.7–10.9 mM and pH_{in} = 3.6 – 4.1), b) downstream terrace ($[Fe(II)]_{in}$ = 9.4-10.3 mM and pH_{in} = 3.7 – 4.0) , c) upstream pool ($[Fe(II)]_{in}$ = 9.5 – 10.4 mM and pH_{in} = 3.2 – 3.6), and d) downstream pool ($[Fe(II)]_{in}$ = 9.5 - 10 mg/L and pH_{in} = 3.6 - 4.0).

The same sediments from UT and UP that were studied live were also studied as sterilized sediments to maintain a constant mass and surface area. The control reactors showed no decrease in dissolved Fe(II) or dissolved Fe concentration (Figure 2-12 and 2-14) at all studied residence times. The initial pH in the sterile control reactor was near 3 since the water had been stored for several weeks and Fe(III) precipitation occurred; however, no further decrease in pH was detected. A slight increase in dissolved Fe concentration was observed, which was determined to be due to dissolution of the Fe(III) minerals in the reactors. The increase in Fe concentration was most pronounced at the 10 h residence time, which was consistent with dissolution. It should be noted that $[Fe(II)]_{out}/[Fe(II)]_{in}$ ratios do not directly represent the kinetics of Fe(II) oxidation, nor do these ratios account for differences in the mass, surface area, and microbial biomass of the sediment pieces tested.

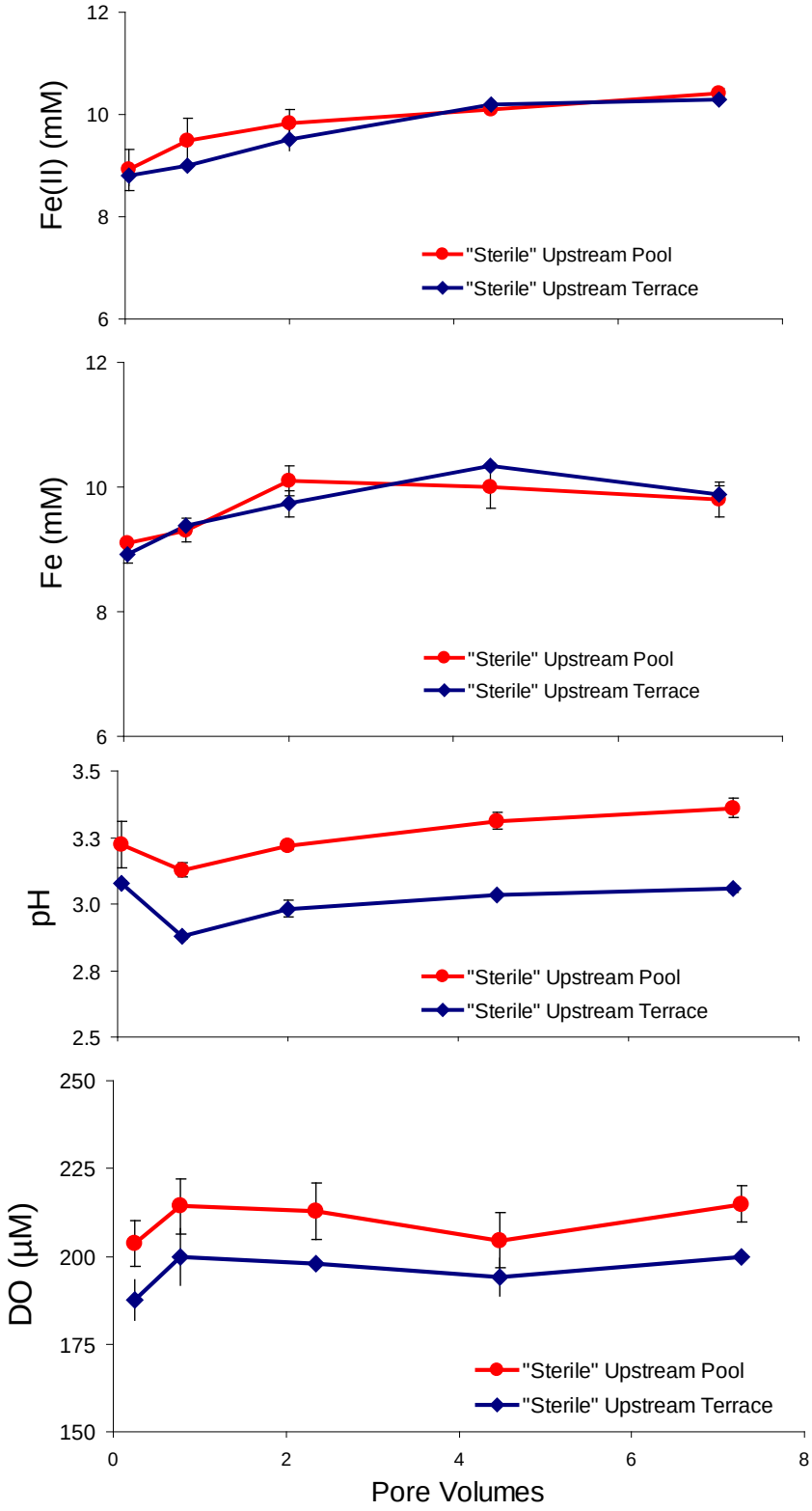

Figure 2-14: Geochemical gradients as a function of cumulative pore volume for "sterile" sediment reactors at a 10 h residence time.

The rate of Fe(II) oxidation was calculated for each individual container in the form of,

$$R_{Fe(II)} = \frac{[Fe(II)]_{in} - [Fe(II)]_{out}}{\theta_H} \quad (1)$$

where $R_{Fe(II)}$ is the rate of Fe(II) oxidation (mol Fe L^{-1} s^{-1}), $[Fe(II)]_{in}$ is the influent Fe(II) concentration at pseudo-steady state (mol L^{-1}), $[Fe(II)]_{out}$ is the effluent Fe(II) concentration at pseudo-steady state (mol L^{-1}), and θ_H is the hydraulic residence time (s^{-1}). Fe(II) oxidation rates were then normalized to the mass of the sediments (mol L^{-1} g^{-1} s^{-1}) and the surface area of the sediments (mol L^{-1} cm^{-2} s^{-1}) since terrace sediment pieces were larger than those from pools (Table 2-4). The rate of oxidation without normalization at the 10 h total residence time (5 h in each reactor) ranged from 0.57 to 1.58 x 10^{-7} mol L^{-1} s^{-1} for all sediments. The rate of oxidation for the upstream terrace was greater than that for the upstream pool ($P > 0.25$) and the rate at the downstream terrace was greater than that at the downstream pool ($P < 0.25$). Upstream sediments also resulted in greater oxidation rates than downstream sediments ($P > 0.15$). When normalized per gram of sediment, rates of Fe(II) oxidation ranged from 0.74 to 10.4 x 10^{-9} mol L^{-1} s^{-1} g^{-1}. The rate of oxidation was greater with upstream pool sediments than upstream terrace and downstream pool sediments than downstream terrace sediments ($P > 0.0005$) on a mass-normalized basis. Upstream pool and terrace sediments still produced greater oxidation rates than the downstream sediments ($P < 0.25$ and $P > 0.1$, respectively). When normalized per surface area, rates of Fe(II) oxidation ranged from 0.63 to 1.75 x 10^{-9} mol L^{-1} s^{-1} cm^{-2}. For surface area normalized rates, upstream sediments resulted in greater oxidation rates than downstream sediments ($P > 0.20$). The rate of oxidation was greater for upstream pool sediments than upstream terrace sediments ($P > 0.25$) and was also

greater for downstream pool sediments than downstream terrace sediments (P>0.10). All calculated rates, regardless of normalization, were within one order of magnitude of the range determined by Kirby and Brady (1998). Nordstrom (1985) found biologically catalyzed Fe(II) oxidation rates in the field to be nearly 7 x 10^{-7} mol L^{-1} s^{-1}, which was greater than all rates found in these reactors.

Pesic et al. (1989) proposed a rate law for biological low-pH Fe(II) oxidation in batch reactors in the general form of:

$$d[Fe(II)]/dt = -k_{bio}*C_{bact}*[Fe(II)]*DO*[H^+] \quad (2)$$

where k_{bio} is a 4th-order biotic rate constant (mol^{-2} L^3 mg cells^{-1} s^{-1}), C_{bact} is the concentration of Fe(II)-oxidizing bacteria in solution (mg cells L^{-1}), and [Fe(II)], DO and $[H^+]$ are the concentrations in the reactor (all in mol L^{-1}). To evaluate the dependency of the rates of Fe(II) oxidation measured in our experiments ($R_{Fe(II)}$), we plotted $R_{Fe(II)}$ (mol L^{-1} s^{-1}) against C_{bact} (R^2 = 0.1), [Fe(II)] (R^2 = 0.1), DO (R^2 = 0.3), and $[H^+]$ (R^2 = 0.1) established at the corresponding pseudo-steady state condition and found essentially no correlations (R^2 values noted). Correlations were not improved when variables were plotted against mass-normalized (mol L^{-1} g^{-1} s^{-1}) or surface-area normalized (mol L^{-1} cm^{-2} s^{-1}) rate expressions (Appendix B). Importantly, the rates of Fe(II) oxidation (regardless of units) were not correlated to the hydraulic residence time which demonstrates that hydrodynamic conditions in the reactors did not change significantly enough to alter the Fe(II) oxidation rate (e.g., by promoting gas transfer of O_2 and/or CO_2).

Weak correlations between reactant concentrations and the rate of Fe(II) oxidation were likely partially caused by how these reactors were operated. Chemostatic conditions were not maintained in the reactors, but instead pseudo-steady state conditions

reflected the reaction extent achievable in response to the hydraulic residence time. For example, the extent of Fe(II) oxidation was greatest at the longest residence time and, in turn, led to greater consumption of DO and a lower pH. This then produced a weak, negative correlation between $R_{Fe(II)}$ and DO. Upstream terrace reactors were also studied at greater volumes, which provided greater water column heights above the sediments, to determine the optimal water column height. The volume was increased to 325 mL (water column = 2 cm) and 475 mL (water column = 3 cm), resulting in Fe(II) oxidation rates of 0.69 and 0.50 x 10^{-7} mol L^{-1} s^{-1}, respectively. The effluent Fe(II) concentration at pseudo-steady state increased with increasing water volume; thus, the effluent DO at pseudo-steady state also increased with volume (Figure 2-15). The slower rate of Fe(II) oxidation indicated that sheet-flow conditions were necessary to optimize oxygen transfer and oxidation rates. So while our kinetic data may not reveal a mechanistic rate law, the measured rates of Fe(II) oxidation can still be used for treatment system design purposes.

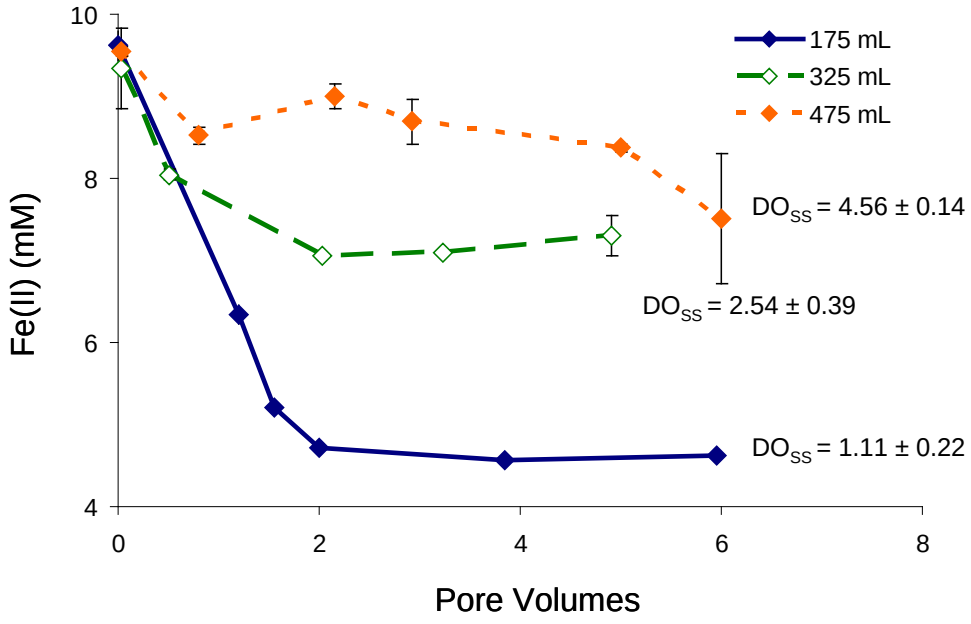

Figure 2-15: Fe(II) gradient as a function of time for varied water volumes in laboratory reactors. DO at pseudo-steady state (DO_{SS}) is noted for each reactor.

Surface-area normalized rates (mol L^{-1} cm^{-2} s^{-1}) are likely best for rate comparisons in this pool-and-terrace, iron-depositing system because the majority of Fe(II) oxidation likely occurs at the sediment-water interface, whether along the terrace faces or submerged at the bottom of the pools. Furthermore, surface-area normalized rates are also commonly used in the design of AMD treatment systems. Treatment performance in terms of grams of metal removed per day per square meter (gdm) is used for sizing ponds and wetlands. We found values of 5.2 ± 0.44, 5.9 ± 0.22, 3.4 ± 1.88, and 6.3 ± 3.80 (g Fe d^{-1} m^{-2}) for UT, UP, DT, DP, respectively. Pool sediments resulted in greater gdm values than terrace sediments. No correlation between gdm and residence time was observed. In comparison, design guidelines for iron removal from net-acid coal mine drainage using aerobic wetlands range from 2 to 5 (g Fe d^{-1} m^{-2}) (Hedin and Nairn, 1992).

Table 2-4: Reactor data for 10 h residence time.

	Upstream Terrace	*Upstream Pool*	*Downstream Terrace*	*Downstream Pool*
Average mass of sediments (g)	103 ± 9.30	13.0 ± 9.70	100 ± 3.20	11.8 ± 2.58
Average surface area of sediments (cm^2)	130 ± 17.0	59.8 ± 11.2	119 ± 17.9	56.5 ± 17.5
Average net $Fe(II)_{out}/Fe(II)_{in}$	0.45 ± 0.04	0.61 ± 0.02	0.73 ± 0.02	0.80 ± 0.01
Average net Fe_{out}/Fe_{in}	0.73 ± 0.02	0.79 ± 0.09	0.86 ± 0.04	0.88 ± 0.02
$R_{Fe(II)}$ ($x10^{-7}$ mol L^{-1} s^{-1})	1.58 ± 0.53	1.03 ± 0.31	0.75 ± 0.25	0.57 ± 0.23
$R_{Fe(II)}$ ($x10^{-9}$ mol L^{-1} s^{-1} g^{-1})	1.60 ± 0.41	10.4 ± 6.58	0.74 ± 0.24	4.79 ± 1.58
$R_{Fe(II)}$ ($x10^{-9}$ mol L^{-1} s^{-1} cm^{-2})	1.25 ± 0.49	1.75 ± 0.56	0.63 ± 0.17	1.08 ± 0.52

2.6. Conclusions

All studied sediments increased the oxidation of dissolved Fe(II) and removal of dissolved Fe when compared to control reactors. GDM values of 3.4 to 6.3 g d^{-1} m^{-2} suggested that existing iron mounds downstream of AMD sites provide a cost effective treatment for AMD. GDM values found in this study were greater than those from a similar study at an AMD site with a lower concentration of dissolved Fe (DeSa et al., 2010). This indicated that greater GDM values can be achieved with higher initial Fe concentrations, however, this does not correlate to greater removal efficiency. Sterilized controls showed no decrease in dissolved Fe or Fe(II), indicating that all observed Fe(II) oxidation in sediment reactors was the result of microbial activity. Fe(II) oxidation was greater than dissolved Fe removal for all samples and oxidation and removal efficiency increased with increasing residence time. Upstream sediments were more effective at Fe(II) oxidation and Fe removal than downstream sediments, regardless of facie. When normalized to mass and surface area, pool sediments resulted in greater Fe(II) oxidation rates than terrace sediments at both upstream and downstream locations; however, this difference in oxidation and removal rates was minor compared to the difference between upstream and downstream samples. This suggested that the Fe(II) oxidation rate was dependent upon geochemical conditions, especially pH. The microbial communities were also found to change as a result of pH changes and Fe(II) oxidation was fastest at higher pH conditions, where Betaproteobactoeria dominated and *Acidithiobacillus* were sparse.

A depositional facies model, such as that applied to Angel Terrace, did explain some differences in Fe(II) oxidation kinetics; however, water chemistry, mineralogy,

crystal morphology and microbial communities could not be correlated with depositional facies. Similar to Angel Terrace, the physical structure of sediments at pool and terrace facies at Lower Red Eyes were distinct on a centimeter scale. Terraces were composed of cemented sediments, while pool bottoms were coated with cauliflower-like, loose sediments. In addition, both sites exhibited drastic changes in pH, DO, microbial community structure and temperature across the transect. There were also significant differences in Fe(II) oxidation rates across the Fe mound.

Unlike the thermal travertine-depositing system of Angel Terrace, many variables were not correlated with facies at the cold-spring schwertmannite depositing system of Lower Red Eyes. Microbial communities were not distinct at adjacent pool and terrace facies, but did change with evolving geochemical conditions. The method of microbial analysis, FISH, in this study was not as comprehensive as the 16S rRNA clone library created for Angel Terrace (Fouke et al., 2003); thus, a more in depth microbial study of Lower Red Eyes may result in distinct microbial community structures at each facie. The predominant mineralogy of Fe(III) precipitates was found to be schwertmannite along the entire mound, regardless of facie. The crystal morphology was also found to be pin-cushion spheres, indicative of schwertmannite, at all sampling locations. These results indicated that the facies model could not explain all trends in biogeochemical conditions at this AMD site and the geochemical gradient of pH and aqueous Fe concentration was the major controlling factor for Fe(II) oxidation and removal efficiency.

3. Schwertmannite Formed by Biological Low-pH Ferrous Iron Oxidation versus Abiotic Neutralization

3.1. Abstract

In this study, three low-pH coal mine drainage (CMD) sites in central Pennsylvania (Lower Red Eyes, Fridays-2, and Hughes Borehole) were studied to determine similarities in sediment composition, mineralogy, and morphology. Water from one site (Lower Red Eyes) was used in a discontinuous titration/neutralization experiment to produce Fe(III) minerals by abiotic neutralization/precipitation for comparison with the field precipitates that were produced by biological low-pH Fe(II) oxidation. Sediments were characterized using X-ray diffraction (XRD), extended X-ray absorption fine structure (EXAFS) spectroscopy, and scanning electron microscopy with energy dispersive spectroscopy (SEM-EDS). Even though the hydrology and chemistry of the CMD varied considerably between the three field sites, the mineralogy of the three iron mounds was found to be very similar. Schwertmannite was found to be the predominant mineral phase precipitated at low-pH with traces of goethite at some sampling locations. Schwertmannite particles occurred as micron sized spheroids with characteristic "pin-cushion" morphology at all sites. No trace metal incorporation was detected in sediments from the field, and no metals (other than Fe) were removed from the CMD at any of the field sites. Minerals formed by abiotic neutralization/precipitation (pH 5.18 – 8.34) were also found to consist primarily of schwertmannite. In contrast to low-pH precipitation, substantial trace metal removal occurred in the neutralized CMD, the subsequent precipitates were found to contain Al, and schwertmannite morphology changed dramatically. While secondary minerals such as schwertmannite essentially store some of the emergent acidity from CMD sources, this mineral may be of industrial

value because, at least when precipitated at low-pH, it does not contain trace metal contaminants.

3.2. Introduction

Pennsylvania is currently the fourth largest coal producing state and has produced more than 25% of the total coal mined in the United States during the past 200 years of mining operations (USGS, 2008). These practices, though, have left their mark on the environment. Coal mine drainage (CMD) is a severe environmental threat to much of the Appalachian region of the United States. CMD marked by low pH, and high concentrations of Fe and acidity is commonly referred to as acid mine drainage (AMD). More than 10,000 km of streams in the Appalachian region are contaminated by CMD, with greater than 1,000 km of those in Pennsylvania (Herlihy et al., 1990). The cost of reclamation of contaminated watersheds in Pennsylvania, alone, is estimated between $5 and $15 billion (USGS, 2008).

Fe(III)-containing precipitates, often referred to as “yellowboy”, are found at AMD sites, coating rocks and streambeds. In certain settings where AMD springs emerge with elevated concentrations of Fe(II), biological low-pH Fe(II) oxidation produces terraced mounds of Fe(III) minerals that can be several feet thick. Most of these phases are amorphous and hard to identify; however, a recently identified mineral, schwertmannite ($Fe_8O_8(OH)_{4.5}(SO_4)_{1.75}$), appears to be the predominant phase for low-pH water with high concentrations of sulfate, while goethite is also present in minor amounts (Bigham, 1996; Acero et. al, 2006). Schwertmannite is metastable with respect to goethite; thus, schwertmannite is often found on the surface of AMD sites while goethite

is found to increase with depth and in the summer months (Acero et al., 2006; Kumpulainen et al., 2007; Peretyazhko et al. 2009).

In order to offset the high costs associated with AMD treatment, it may be possible to collect the large amounts of Fe(III) precipitates at AMD sites for industrial reuse. Hedin (2003) showed that Fe(III) precipitates collected at an AMD site are similar to those mined for use as a pigment. Since these pigments may be used in products such as cosmetics and ceramic serving ware, the incorporation of trace metals in the Fe(III) mineral is a concern. Due to the kinetic limitation of abiotic Fe(II) oxidation at low pH, it is widely believed that acidophilic Fe(II) oxidizing microorganisms, such as *Ferrimicrobium acidiphilum*, of the Acidimicrobiales subclass, (Lane et al., 1992; Senko et al., 2008) and *Acidithiobacillus ferrooxidans* (Johnson et al., 2005) are responsible for oxidation of Fe(II), and subsequent precipitation of Fe(III) at AMD sites. It is possible that the elemental composition of biogenic precipitates formed at low-pH AMD sites differ from those formed as a result of abiotic precipitation after neutralization of AMD water. The objectives of this study were to identify the mineral phases present and to determine the trace metal incorporation of Fe(III) precipitates at three AMD sites in western Pennsylvania. For comparison purposes, this study also identified the structure and trace metal incorporation of minerals formed via abiotic neutralization/precipitation at pH 5.18-8.34.

3.3. Site Descriptions

Three AMD sites in western Pennsylvania were included in this project: Lower Red Eyes in Somerset County, PA, USA; Fridays-2 in Clearfield County, PA, USA; and,

Hughes Borehole in Cambria County, PA, USA (Figure 3-1). Physical characteristics and water chemistry for each site are provided in Table 3-1.

Figure 3-1: Site photos of the AMD field sites. Photographs at Lower Red Eyes were taken in February 2009 and include: a) an upstream and b) terrace features that formed on a log; c) The iron mound with terrace features at Fridays-2 was photographed in May 2007 (a ledge/terrace can be seen in the bottom left corner); d) the 0.6 ha iron mound at Hughes Borehole was also photographed in May 2007.

Lower Red Eyes. Lower Red Eyes is a low flow (~0.44 L/s) AMD artesian spring that emerges within the Prince Gallitzin State Forest near Winder, PA (40° 14’ 25" N; 78° 44’ 49" W). The AMD is believed to originate from a nearby surface mine operated from the 1970s into the 2000s, and located along the Clarion, Brookville, and Kittanning coal seams. The AMD flows downstream across a spectacular iron mound of terraces and pools (Figure 3-1) before eventually seeping back into the ground (150 m downstream of the spring). This site is unique to the other two field sites, in that the AMD is never

hydrologically captured by a larger receiving stream, such that a more extensive geochemical gradient is established. The AMD at this site is characterized by higher acidity, metals, and sulfate as compared to the other two field sites (Table 3-1).

Fridays-2. Fridays-2 is the smaller of two AMD discharges (2.3 L/s) that drain the underground Fridays Mine complex. Fridays Mine was located in Hollywood, PA (41° 14’ 34" N; 78° 32’ 28" W) along the Kittanning coal seam and was first mined in the late 1800s (PA DEP, 2006). Fridays-2 emerges as an artesian spring at a collapsed mine entry, and flows 5 – 15 m over an iron mound before discharging to an unnamed tributary of Bennett Branch. The AMD flows over the mound as shallow (ca. 1 cm) sheet flow, and drops over a ca. 1 m high ledge (bottom let corner of Figure 3c) before immediately joining the tributary. The ledge of the iron mound contains dramatic stalactite-like Fe precipitates. Because of the higher flow rate and shorter path length across the iron mound, the extent of Fe(II) oxidation at Fridays-2 is much less compared to Lower Red Eyes (Figure 3-2).

Hughes Borehole. Hughes Borehole is a high flow (63 L/s) artesian spring that was purposefully drilled to drain a very large underground mine complex (2,900 ha) near Portage, PA (40° 24′ 31" N; 78° 39′ 17" W) (GAI Consultants, 2007; DeSa et al., 2010). The AMD emerges near, and later flows into, the Little Conemaugh River. The AMD emergence is surrounded by a 0.61 ha iron mound that is up to 2 m deep. The AMD flows across the iron mound through relatively deep channels (ca. 0.5 m; captures most of the flow from the borehole) and as shallow sheet flow (ca. 1 cm) before discharging off the iron mound ca. 60 m downstream of the borehole.

Table 3-1: Water chemistry measurements for Lower Red Eyes, Fridays-2, and Hughes Borehole at the AMD source

	Lower Red Eyes	**Fridays-2**	**Hughes Borehole**
Flow (L/s)	0.4	2.3	20-125
Temp (°C)	9.4 ± 0.7 N = 7	9.8 ± 0.1 N=4	12.7 ± 0.6 N = 30
DO (µM)	0 ± 0 N = 2	11.3 ± 13.4 N=4	34.4 ± 25.0 N = 21
Conductivity (mS/cm)	4.36 ± 0.16 N =7	0.772 ± 0.001 N=2	1.08 ± 0.1 N = 23
pH	4.04 ± 0.25 N = 7	4.1 ± 0.2 N=4	3.96 ± 0.25 N = 29
Dissolved Fe (µM)	9620 ± 387 N = 5	809 ± 61 N=6	1590 ± 6 N = 7
Dissolved Fe(II) (µM)	9720 ± 326 N = 5	--	1790 ± 312 N = 25
Al (µM)	1590 ± 43 N = 3	741 ± 89 N=6	304 ± 14 N = 7
Mn (µM)	2060 ± 53 N = 3	24 ± 2 N=6	44 ± 0.4 N = 7
SO_4^{2-} (µM)	31,170 ± 3833 N = 12	3300 ± 941 N=2	5970 ± 656 N = 5
Zn (µM)	199 ± 23 N = 3	--	4.1 ± 0.2 N = 7
Acidity (mM $CaCO_3$/L)	14.2`	2.0	2.3 ± 0.05 N = 7

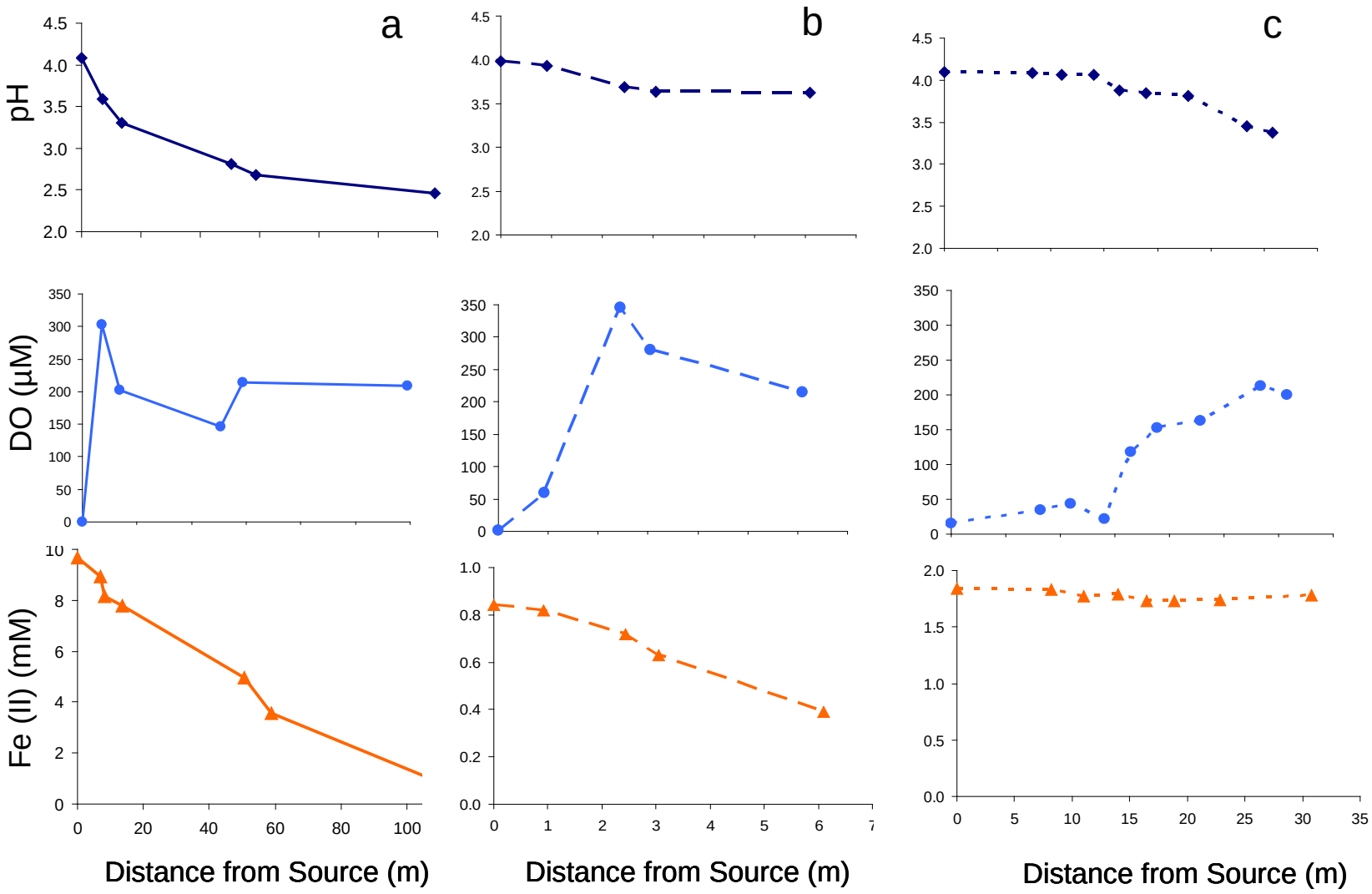

Figure 3-2: Water chemistry trends for a) Lower Red Eyes (July 2009), b) Fridays-2 (July 2006), and c) Hughes Borehole (August 2007).

3.4. Materials and Methods

3.4.1. Field Sampling

Sediments were collected from several locations on each iron mound, while results from select samples are presented herein. Sediments were collected from the top 2 cm of the iron mounds for mineralogical characterizations. These samples were stored at 4 ^{o}C until analysis. Sediments were also anoxically collected horizontally into the face of the iron mound ledge in 2 locations (H-1, H-4) at Fridays-2 as a function of depth. The soil cores collected were approximately 6 cm in total depth. The cores were stored at 4 °C and then transferred to an anaerobic chamber (5% H_2 and 95% N_2) where they were divided into 3 sections of approximately 2 cm each and dried for analysis. Dissolved oxygen (DO) was measured in the field using an Oakton DO 300 Series field meter; temperature and pH were measured in the field with a Beckman Φ265 pH/Temp/mV meter; and conductivity was measured using an Oakton CON 400 series field meter. Filtered (0.2 μm) water samples were preserved in the field with HCl (for dissolved Fe analysis) or HNO_3 (for dissolved metals analysis by inductively coupled plasma-atomic emission spectrometry, ICP-AES). Samples for sulfate analysis were neither filtered nor acidified. All water samples were transported on ice and stored at 4 ^{o}C until analysis.

3.4.2. Abiotic Neutralization/Precipitation

AMD from the Lower Red Eyes spring was used in a discontinuous titration/neutralization experiment to produce Fe(III) precipitates via abiotic reactions at a number of different pH values. The theoretical total acidity of the Lower Red Eyes AMD was calculated based on pH and measured concentrations of dissolved Fe(II), Fe(III), Mn, and Al according to Kirby and Cravotta (2005), and found to equal 28.3 meq/L. Four

acid-washed plastic bottles were filled with 250 mL of Lower Red Eyes AMD. NaOH was titrated into Lower Red Eyes AMD in aliquots equivalent to ¼ of the theoretical total acidity of the water, until the pH of the system reached pH 8.3. This amounted to first adding 17.8 mL of 0.10 N NaOH to each bottle of Lower Red Eyes AMD (i.e., to complete 25% of the neutralization). The bottles were stirred to maintain a small vortex and purged continuously with compressed air for one hour, and then refrigerated (4 ^{o}C) overnight. The following day, the bottles were removed from the refrigerator to come to room temperature, the pH was measured in the overlying water in all four bottles, and one bottle was returned to the refrigerator (pH 5.18). For the remaining three bottles, another 17.8 mL of 0.10 N NaOH was added to each bottle and identical procedures were followed over the next three days to produce suspensions equivalent to 50% (pH 5.36), 75% (pH 6.21), and 100% neutralization (pH 8.34) of the theoretical total acidity. One day after the 100% neutralization suspension was produced, all of the suspensions were transferred to centrifuge tubes and centrifuged at 8,000 rpm for 10 min. Supernatant samples were collected and preserved with HNO_3 for dissolved metals analysis by inductively coupled plasma atomic emission spectroscopy (ICP-AES). Pelletized precipitates were air-dried for SEM analysis, or dried under nitrogen for XRD analysis.

3.4.3. Analytical Methods

Dissolved trace metal concentrations in preserved water samples were analyzed on a Perkin-Elmer Optima 5300 ICP-AES. The composition of metal oxides was determined for unpreserved sediment samples via ICP-AES, after lithium metaborate fusion.

Sediment samples were prepared for scanning electron microscopy (SEM) following a previously published procedure (Zhang et. al, 2007). Samples were preserved in the field with 2.5% glutaraldehyde. Samples were then prepared for imaging with a series of ethanol dehydrations followed by critical point drying using a BAL-TEC CP2030 instrument. Dried samples were mounted onto carbon SEM stubs and imaged on an FEI Quanta 200 environmental SEM under low vacuum. Higher magnification images were also collected using a Jeol JSM-6700F field emission SEM with a working distance of 3 mm.

Powder X-ray diffraction patterns were collected using a Rigaku D/Max Rapid II X-ray diffractometer (XRD) with a Mo X-ray tube and a 0.3 mm collimator. Intensities were measured with the omega axis fixed at 0^o and phi axis oscillation between -20^o and $+20^o$ with a 10 min exposure time. Data was integrated from $0\text{-}360^o$ with a step size of 0.02 using AreaMax software and all data analysis was performed using Jade 7 software.

Dry samples for X-ray absorption spectroscopic analyses were packed in Teflon sample holders and sealed with a Kapton polyimide film to prevent oxidation while minimizing X-ray absorption. The structural environment of Fe was determined using extended X-ray absorption fine structure (EXAFS) spectroscopy at the Stanford Synchrotron Radiation Lightsource (SSRL) on beamlines 10-2 (26-pole wiggler) running under dedicated conditions. The storage ring was operated at 3.0 GeV and at currents between 60 and 100 mA. The Fe EXAFS analytical procedures used here were similar to those described previously (Borch et al., 2007). Energy selection was accomplished with a Si (111) monochromator and spectra were recorded in X-ray transmission mode using ion chambers. A set of Fe reference compounds was used to perform linear combination

(LC) k^3-weightened EXAFS spectral fitting using the SIXPACK interface to IFEFIT (Webb, 2005). Linear combinations of the reference compounds were optimized and the only variable parameters were the fractions of each reference compounds. Detection limit for minor constituents is approximately 5% (Hansel et al. 2003). Reference compounds were chosen based on their likelihood of being present in the soil or a reaction product (including, for example, criteria such as elemental composition), and were included in the fit only if they contributed with a fraction of 0.05 or more. Reference compounds were also selected based on previous mineralogical characterization of Fridays-2 sediments which helped in constraining the LC-XAFS fitting (Peretyazhko et al., 2009).

3.5. Results and Discussion

3.5.1. Acid Mine Drainage Chemistry

The three field sites all contained iron mounds that formed via biological low-pH Fe(II) oxidation (Figure 3-1), yet the AMD water chemistry (Table 3-1 and Figure 3-2) and hydrodynamics across the iron mounds varied significantly. Lower Red Eyes AMD had the highest concentrations of metals, acidity, and sulfate, the lowest flow rate, and the longest residence time across its iron mound. The decrease in pH, Fe(II), and Fe are consistent with low-pH Fe(II) oxidation and Fe(III) hydrolysis (Figure 3-2). Fridays-2 AMD had the lowest concentration of Fe(II), acidity, and sulfate, an intermediate flow rate, and likely the shortest residence time across its iron mound. Hughes Borehole AMD had intermediate concentrations of Fe(II), acidity, and sulfate, an extremely high flow rate, and variable residence times across its iron mound because of a combination of flow along scoured channels or across shallow iron terraces. Even though Fe(II) and Fe

concentrations did not drop dramatically across the Fridays-2 and Hughes Borehole iron mounds, Fe precipitation over the past several decades has produced mound sediments 1 – 2 m deep.

3.5.2. Mineralogy of Natural Sediments

Iron precipitates varied across these sites with respect to their physical features and morphology. For example, at Lower Red Eyes, Fe precipitates were classified into unique depositional facies such as terraces, pools, and proximal slopes (Fouke et al., 2000; Brown et al., submitted). Terraces consisted of vertical drops greater than 5 cm, pools contained quiescent water with diameters of 1-2 m, and proximal-slopes consisted of vertical drops less than 5 cm. At Fridays-2, the predominant depositional facie was proximal slopes, but there was one high terrace (1 m) that the AMD ran over before entering the adjacent unnamed tributary. At Hughes Borehole, the predominant depositional facie was proximal slopes, however, the majority of the AMD was conveyed along deep (0.5 m), narrow (1 m wide), scoured channels. With sediments of widely varied colors (yellow, orange, red, brown) and distinct morphologies (e.g., cemented terrace faces, loose "flower stalks" on pool bottoms, highly porous channel edges), one might expect a variety of Fe minerals, or at least a variety of crystal morphologies of the predominant Fe mineral. Somewhat surprisingly, we recently reported that schwertmannite was the predominant mineral across the whole Lower Red Eyes iron mound, regardless of water chemistry/location on the mound or the depositional facie (Brown et al., submitted). Consistent with these previous results, we now report that schwertmannite was the predominant mineral at all three field sites based on XRD (Figure 3-3), SEM (Figure 3-4), and Fe EXAFS (Figure 3-6).

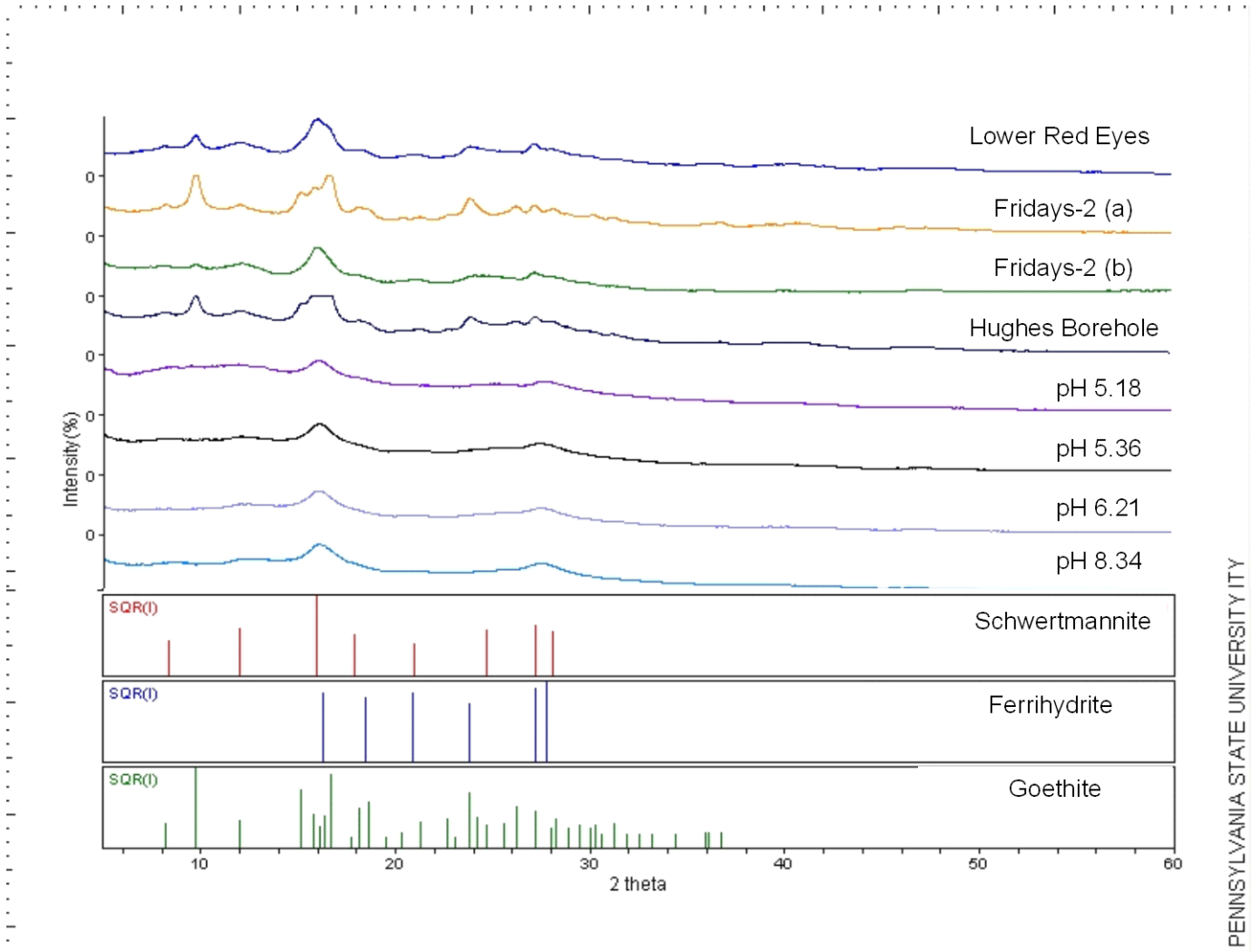

Figure 3-3: X-ray diffraction for samples collected from a downstream pool at Lower Red Eyes; Fridays-2 at a) H1-1 inner and b) H4-1 inner; Hughes Borehole at the main channel, and precipitates formed abiotically in the lab (pH 5.18-8.34).

Based on very similar XRD patterns from sediments collected from Fridays-2, Hughes Borehole, and Lower Red Eyes, all sediments consisted predominantly of schwertmannite with trace amounts of goethite (Figure 3-3). SEM analysis of all field samples also revealed a predominance of spherical particles (1 – 2 μm diameter) with a "pin-cushion" morphology characteristic of schwertmannite (Figure 3-4a-d). The intensity of goethite peaks varied between the three field sites, and varied across individual field sites. Surface sediments from Fridays-2 had the most intense goethite peaks, while several samples at Lower Red Eyes had no discernable goethite peaks. The Lower Red Eyes AMD contained the highest sulfate concentration which would favor the stabilization of schwertmannite, while the Fridays-2 AMD contained the lowest sulfate concentration which could favor the conversion of schwertmannite to goethite. Regardless of AMD site and distance from the source, schwertmannite was the predominant precipitate formed. No mineralogical phases other than schwertmannite and goethite were detected at any site. These findings were similar to those at other AMD sites in Pennsylvania (Peretyazhko et al., 2009; DeSa et al., 2010), Ohio (Gagliano et al., 2004), Austria (Schwertmann et al., 1995), Australia (Burton et al., 2008), Sweden (Jonsson et al., 2005), and Spain (Acero et al., 2006; España et al., 2007).

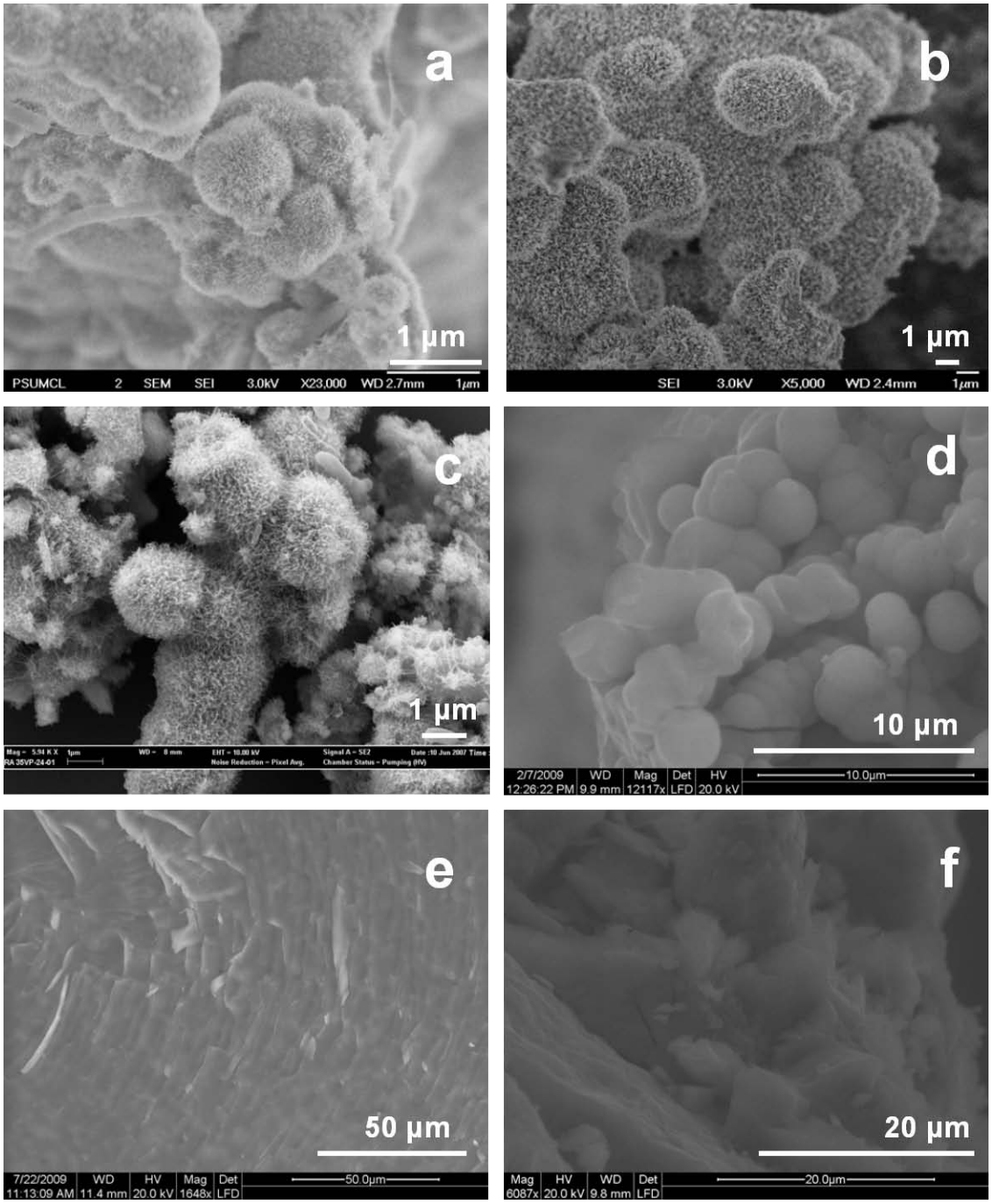

Figure 3-4: SEM images of representative samples from: a) Lower Red Eyes at the AMD source; b) Lower Red Eyes at a downstream pool; c) Fridays-2; d) Hughes Borehole; and abiotic precipitates formed in the lab at e) pH 5.18 and f) pH 8.34.

Based on Fe EXAFS analyses, goethite decreased with depth for samples H-1 and H-4 collected at Fridays-2(Figure 3-6). This finding is contrary to previous studies that have shown a greater extent of schwertmannite to goethite conversion occurred at greater

depths into the sediment column (Gagliano et al. 2004; Peretyazhko et al., 2009) and over extended incubation periods (ca. 350 – 550 d) (Bigham et al., 1996; Acero et al., 2006). Peretyazhko et al. (2009) characterized the iron mineralogy at Fridays-2, and another low-pH coal mine discharge in Pennsylvania known as Gum Boot Run. Schwertmannite to goethite conversion was observed at Gum Boot Run, where the AMD spring contains significantly less sulfate (1 mM) than Fridays-2 (4 mM), while no schwertmannite transformation occurred with surface sediments from Fridays-2. We speculate that the mineralogical transformation from schwertmannite to goethite on the surface of these iron mounds will differ in the field (when bathed in water with ~constant sulfate concentration and pH) as compared to no-flow, batch conditions used for aging experiments (when pH and dissolved constituents change over time).

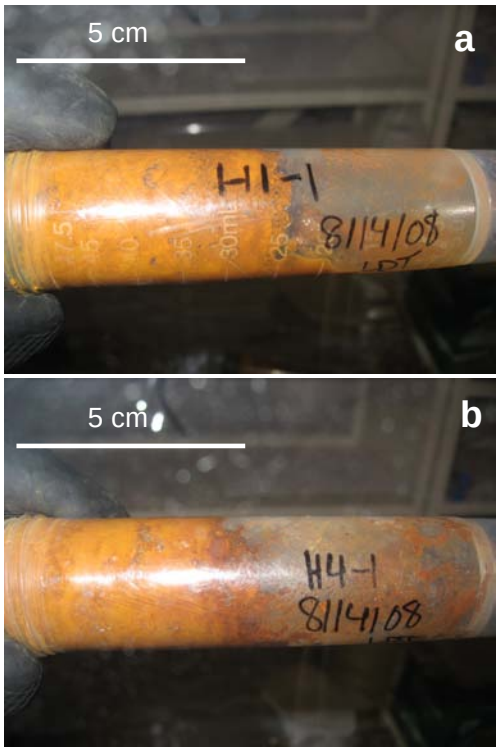

Figure 3-5: Core samples were collected at Fridays-2: a) H1-1, sampled horizontally into the iron terrace and b) H4-1, sampled horizontally into the iron terrace. Cores were 6 cm long and were divided into three 2 cm sections. The surface of the core is on the right hand side of the photo and the deepest part of the core is the left hand side.

EXAFS analysis was done on two samples collected at Fridays-2. Sample H-1 was determined to be predominantly schwertmannite with some goethite. Spectra for a surface and inner sample of H-1 (right hand and left hand side of Figure 3-5, respectively) can be viewed in Figure 3-6. The sample consisted of 60.7% schwertmannite at the surface, 37.3% goethite, and 2.1% pyrite (Figure 3-6a). The inner sample contained more schwertmannite (76.7%) and the remainder was identified as goethite (figure 3-6b). Sample H-4 was also determined to be predominantly schwertmannite. At the surface, the sample contained 82.9% schwertmannite and the remaining 17.1% was identified as goethite (Figure 3-6c). The inner sample consisted entirely of schwertmannite (Figure 3-6d). EXAFS data confirmed XRD and SEM conclusions that schwertmannite is the dominant mineral phase at the Fridays-2 site with lesser amounts of goethite.

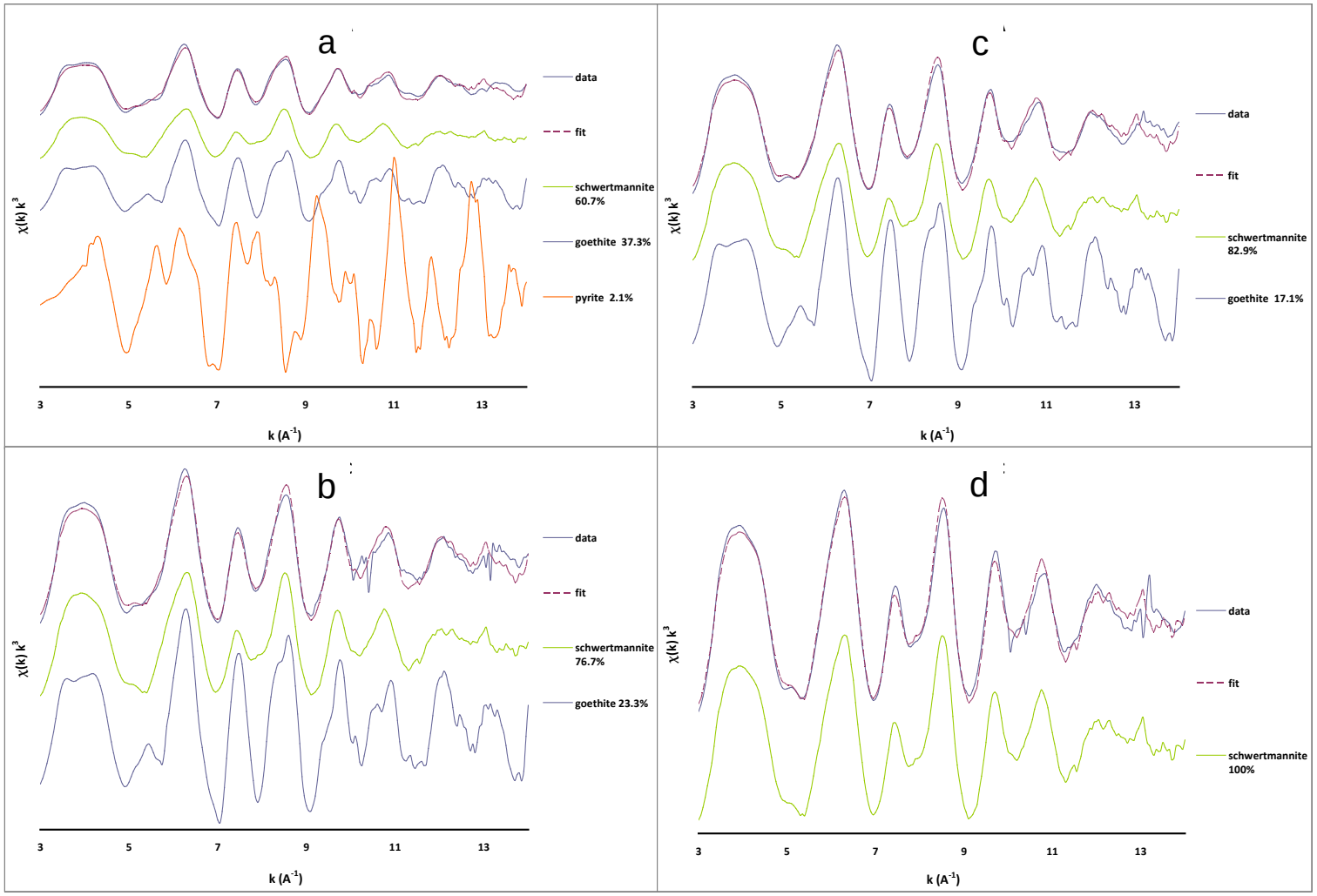

Figure 3-6: EXAFS of Fridays-2: a) H-1 surface, b) H-1 inner, c) H-4 surface, and d) H-4 inner. Schwertmannite was the predominant mineral phase in all samples and increased with depth. Goethite was present in lesser amounts in all samples except H-4 inner.

3.5.3. Mineralogy from Abiotic Neutralization/Precipitation

Our discontinuous titration process yielded precipitates that formed at pH values of 5.18, 5.36, 6.21, and 8.34. While solids were all collected by centrifugation after a total of four days, the solids formed at the different final pH values had aged for different times. For example, the solids formed at pH 5.18 had aged at 4^{o}C for 72 h beyond its initial overnight equilibration, while the solids formed at pH 8.34 had aged for only the overnight equilibration. We believe the different aging times exerted little effect because solids began to form in all the bottles at the same time (i.e., when pH was increased from 4.05 to 5.18). After the first neutralization (pH 5.18) an orange precipitate formed and its color remained unchanged for the whole aging period. After the second neutralization (pH 5.36) a dark green precipitate formed initially but then became orange after 1 h. After the third neutralization (pH 6.21) a green precipitate formed initially but then became orange-brown. After the fourth and final neutralization (pH 8.34) an orange precipitate formed and its color remained unchanged for the whole aging period. Images of the final precipitates can be viewed in Figure 3-7. Because of the decreasing solubility of Fe(III) with increasing pH, the mass of precipitate formed increased with increased neutralization.

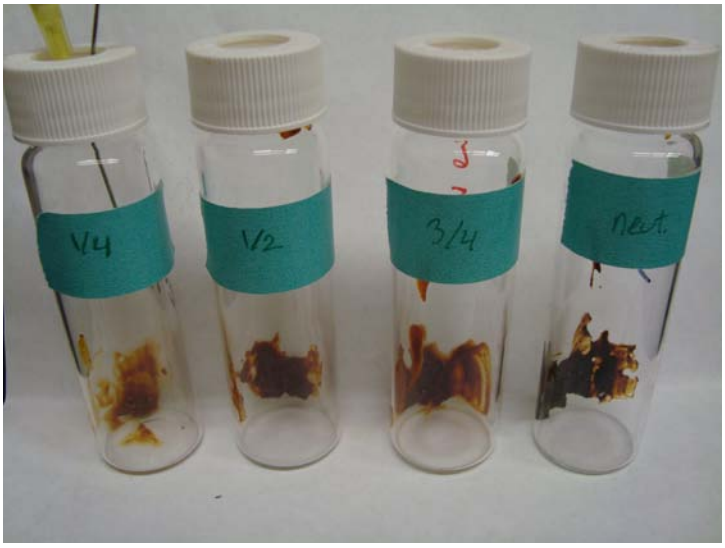

Figure 3-7: Precipitates were formed at pH 5.18, pH 5.36, pH 6.21, and pH 8.34 (from left to right). All precipitates were orange-brown colored after aging.

The XRD patterns for all precipitates formed via abiotic neutralization indicated poorly crystalline schwertmannite, but with no traces of goethite (Figure 3-3). The peaks also appeared similar to 6-line ferrihydrite; however, the reference pattern for 6-line ferrihydrite did not account for the small peaks at 12 and 25 º2θ. The intensities of the schwertmannite peaks were less than that of the schwertmannite peaks identified in precipitates collected from the field sites. This result was similar to a previous study that found poorly ordered schwertmannite to precipitate at a field site in Finland at a pH of 6.0 to 6.2 (Kumpulainen et al., 2007). SEM analysis of the neutralized precipitates revealed distinctly different particle morphologies (Figure 3-4e-f) as compared to field samples (Figure 3-4a-d). Instead of spheres with a pin-cushion texture, neutralized precipitates appeared as laths fused into much larger particles. Characteristic dimensions of these lathes (and other planar features) were difficult to generalize from these SEM micrographs; however, the lathes might range from 1-5 µm by 5-20 µm while the particles ranged from 0.2 – 1.0 mm. SEM-EDS analysis indicated the presence of Al,

suggesting that trace metals were incorporated into the neutralized precipitates while no Al was ever detected by SEM-EDS analysis of the field samples (Figure 3-8).

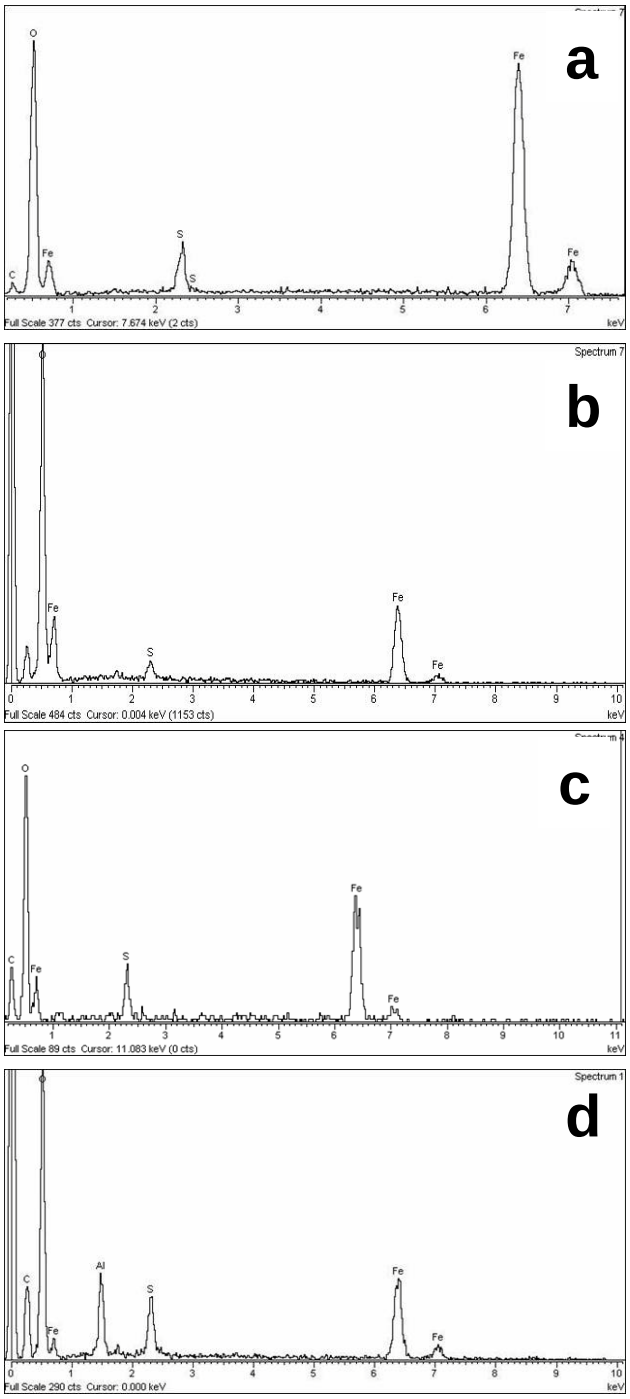

Figure 3-8: EDS of a) Lower Red Eyes b) Fridays-2, and c) Hughes Borehole indicated a composition of Fe, S, and O, indicative of schwertmannite with no trace metal incorporation. EDS of precipitates formed abiotically at d) pH 5.18 contained signals for Al.

The incorporation of Al and other trace metals into the neutralized precipitates was confirmed by measuring the loss from solution of these elements from the supernatant of the neutralized suspensions (Figure 3-9). Loss from solution provided a far better detection limit for trace metal incorporation as compared to SEM-EDS or elemental analysis of the solids (following lithium metaborate fusion). For comparative visualization purposes, dissolved metal concentrations remaining in the neutralized suspensions are presented as normalized to their initial concentrations in the Lower Red Eyes AMD spring (pH 4.05) and plotted against the final pH of the equilibrated suspension. In addition to iron, many other metals were removed via abiotic neutralization/precipitation (R-hand portion of Figure 3-9; Table 3-2). For example, dissolved Al decreased from 1,630 μM at pH 4.05 to <0.4 μM at pH 5.18 (i.e., >99% removal) while dissolved Mn decreased from 2,000 μM at pH 4.05 to 673 μM at pH 5.18 (66% removal). Important trace metals in Appalachian CMD include Zn, Ni, and Co. In a survey of 140 abandoned deep coal mine discharges in Pennsylvania, the most abundant trace metals, in order of median concentrations (in μM), were Zn (2.0), Ni (1.4), Co (1.0), Ti (0.10), Cu (0.03), Cr (0.02), Pb (0.001) and Cd (0.001) (Cravotta, 2008). The concentrations (also in μM) of Zn (199), Ni (100), and Co (71) in the Lower Red Eyes AMD spring were all exceptionally high and reflect important differences between surface coal mine and deep mine AMD chemistry, and the high metal content of the overburden in the surface mine adjacent to Lower Red Eyes. Dissolved Zn decreased from 199 μM at pH 4.05 to <0.15 μM at pH 5.18 (99% removal), while Ni decreased from 100 μM to 5 μM at pH 5.18 (95% removal), and Co decreased from 71 μM to 6.4

µM at pH 5.18 (91% removal), and these removal efficiencies remained essentially constant as the pH was further increased.

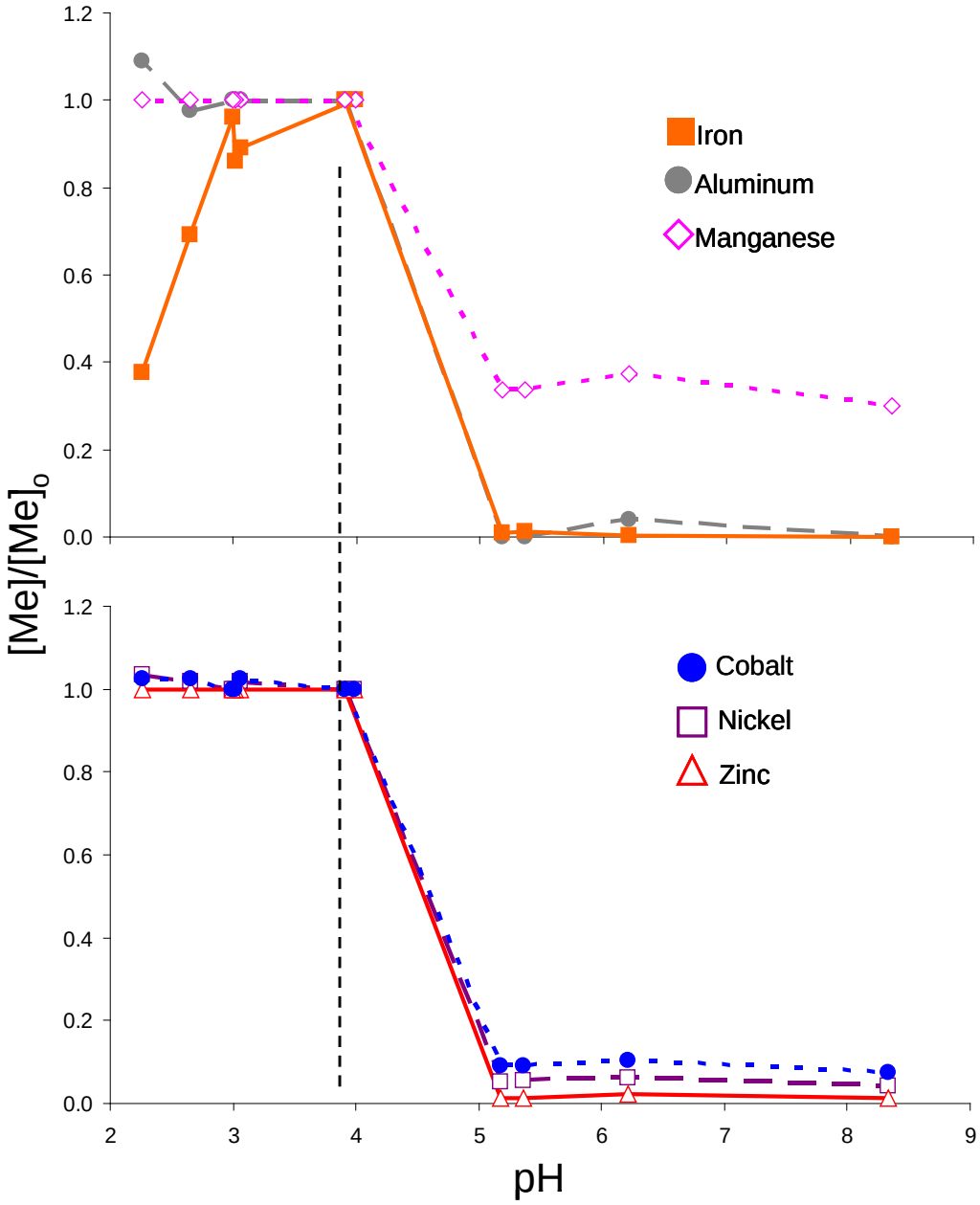

Figure 3-9: Metal concentration in AMD water normalized to initial concentration was measured as a function of pH. The dashed line indicates conditions at the Lower Red Eyes AMD source. Left of the dashed line corresponds to field conditions and right of the dashed line corresponds to abiotic neutralization/precipitation.

Table 3-2: Dissolved metal concentrations as a function of pH after precipitation of Fe(III). pH 4.04 corresponds to the emergence at Lower Red Eyes. All concentrations are in µM.

	pH 4.04	pH 5.18	pH 5.36	pH 6.21	pH 8.34
Al	1631	<0.4	1.85	63.0	1.48
As	<0.1	0.1	<0.1	<0.1	<0.1
Ba	0.07	0.22	0.22	0.29	0.22
Ca	5365	5864	5864	5614	5864
Co	71.3	6.4	6.4	7.3	5.3
Cr	0.58	0.19	0.38	0.38	0.19
Cu	<0.2	<0.2	<0.2	<0.2	<0.2
Fe	9044	91.3	109	16.7	<0.2
K	332	435	460	460	307
Mg	15840	4937	4937	4732	4320
Mn	2002	673	673	746	601
Na	283	1479	1305	313	252
Ni	101	5.11	5.45	6.30	4.26
Pb	0.14	<0.05	<0.05	<0.05	<0.05
Si	427	99.7	196	210	110
Sr	3.99	32	62.8	67.3	35.4
Ti	<0.2	31.3	29.2	5.01	4.39
V	0.59	<0.2	<0.2	<0.2	<0.2
Zn	199	<0.2	<0.2	<0.2	<0.2
Zr	0.11	1.75	1.75	3.29	1.64

The incorporation of trace metals into the iron mound sediments was never observed at any of the field sites. Based on dissolved metal concentrations as a function of distance from the AMD springs only iron was ever found to be lost from solution. Based on laboratory incubations with sterilized sediments and sediments maintained under a N_2 atmosphere as compared to "live" sediments, the precipitates from all field sites were produced via biological low-pH Fe(II) oxidation (Senko et al., 2008; DeSa et al., 2010; Brown et al., submitted). To compare trace metal chemistry associated with the precipitates formed by the abiotic neutralization of the Lower Red Eyes versus precipitates formed by biological oxidation, we have plotted normalized dissolved metal concentrations as a function of pH on the iron mound (L-hand portion of Figure 3-9). In

this combined plot, the dashed center line represents the emergent AMD spring, while points to the left represent sample sites further and further downstream of the AMD spring (where pH values continue to decline due to greater Fe(II) oxidation and Fe(III) hydrolysis). As shown in Figure 3-9, no trace metals were removed across the Lower Red Eyes iron mound. Increased metal concentrations (e.g. Al, Co) were likely caused by mound mineral dissolution at the lowest pH values. ICP-AES analysis of field sediments from Lower Red Eyes and Hughes Borehole confirmed that no trace metal incorporation occurred (Table 3-3). Iron oxide and organic material (presumed as mass loss on ignition) comprised 93.5 and 99.2% of the sediment composition at Lower Red Eyes and Hughes Borehole, respectively.

Table 3-3: Sediment composition was measured with ICP-AES for samples collected near the AMD spring at Lower Red Eyes and Hughes Borehole.

Metal Oxide (%)	Lower Red Eyes	Hughes Borehole
Al_2O_3	3.75	0.39
CaO	0.26	0.04
Fe_2O_3	49.7	66.7
MgO	0.65	0.18
MnO	0.1	< 0.01
P_2O_5	1.57	0.09
TiO_2	0.13	0.08
ZnO	0.02	< 0.01
BaO, CoO, Cr_2O_3, NiO	<0.01	
K_2O, Na_2O, SiO_2	<0.05	
Loss on Ignition (1000 ^oC)	43.8	32.5

3.5.4. Environmental Implications

The mineral composition and trace metal incorporation appeared to be similar at all studied low-pH Fe(II)-oxidizing AMD field sites. Schwertmannite was the predominant phase with minor amounts of goethite at all locations and no trace metal incorporation was detected. Schwertmannite was expected to be the predominant mineral at Lower Red Eyes based on pe/pH data (Figure 3-10). Fe(III) minerals formed via abiotic neutralization/precipitation also consisted of predominantly schwertmannite, but a significant amount of trace metals were incorporated into the mineral structure at pH greater than 5. The solubility of schwertmannite decreased from pH 2 to pH 8 (Figure 3-11), which was consistent with schwertmannite precipitation at pH 5.18-8.34. Low-pH precipitation appeared to be most effective for industrial reuse since negligible metal contamination occurred; however, schwertmannite conversion to goethite is an acid-producing reaction where 0.26-0.40 mol H^+ could be released per mole of Fe(III) (Bigham et al., 1996; Peine et al., 200; Kawano and Tomita, 2001; Peretyazhko et al. 2009). Thus, the precipitation of schwertmannite via biological low-pH Fe(II) oxidation produces a source of long-term acidity that could affect the properties of paints and ceramics that may contain ochre pigments. Abiotic neutralization/precipitation appeared to be necessary for remediation of metals other than Fe from AMD contaminated water.

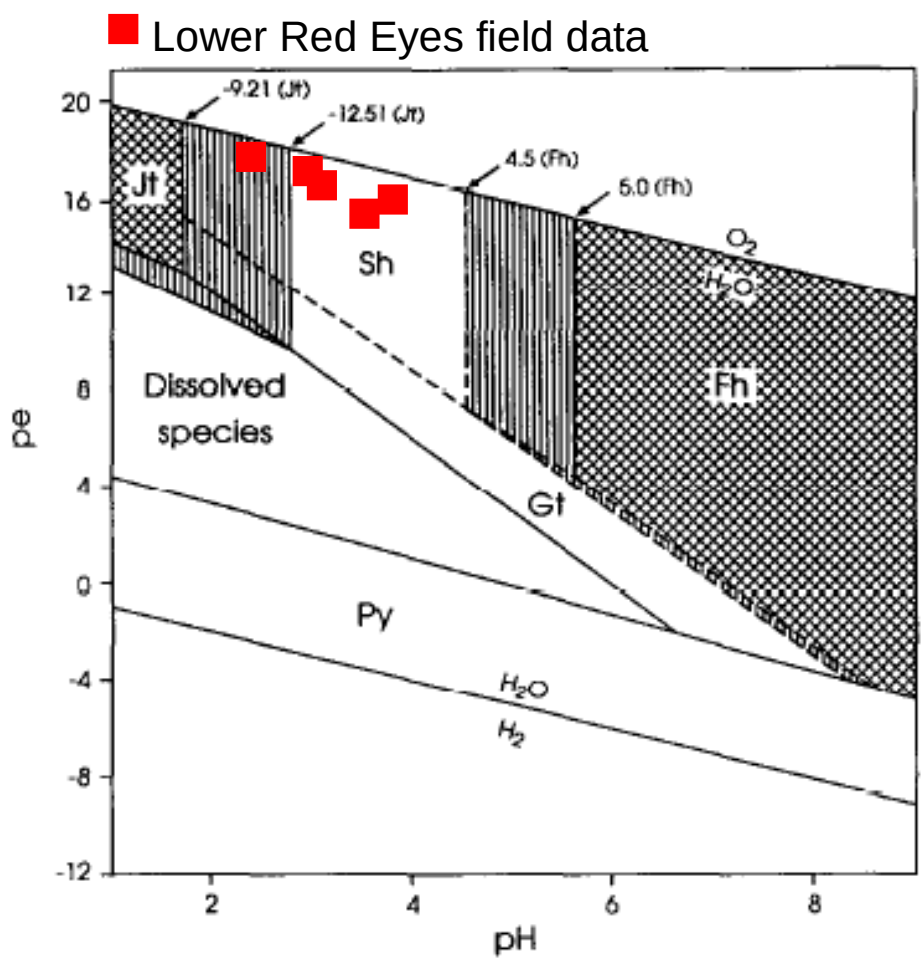

Figure 3-10: pe-pH diagram (from Bigham et al., 1996) with Lower Red Eyes data, supports schwertmannite precipitation at all sampling locations.

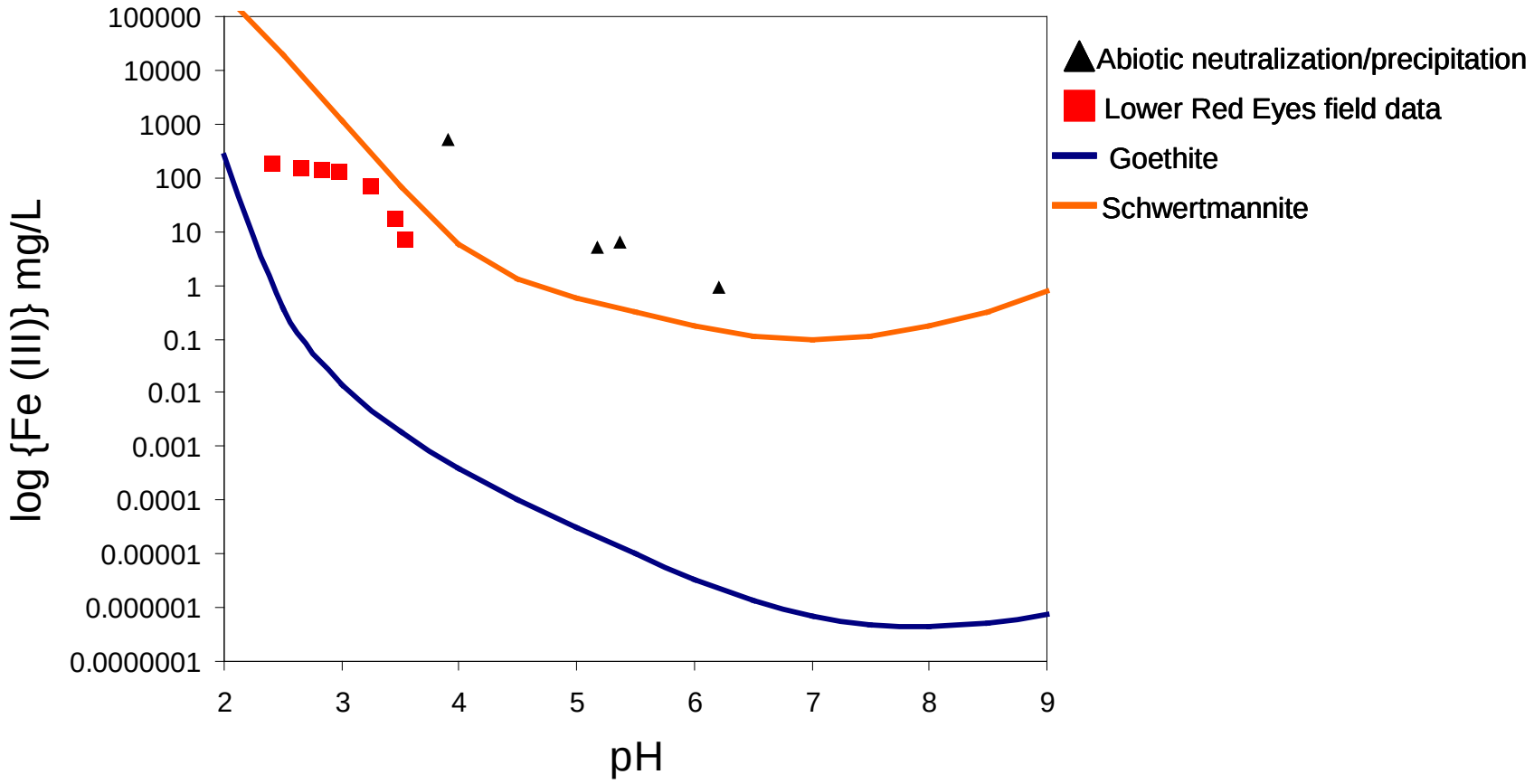

Figure 3-11: Schwertmannite and goethite solubility as a function of pH from pH 2-9 (the ranges of precipitation studied). Lower Red Eyes field data conditions predicted goethite precipitation, contrary to actual observations. Circum-neutral precipitation conditions were oversaturated with respect to schwertmannite. Schwertmannite was metastable with respect to goethite at all pH values. ($[SO_4^{2-}]$ = 30 mM and any decrease in sulfate during neutralization experiment was neglected; Circum-neutral precipitation data was plotted assuming all Fe(II) had been oxidized to Fe(III)).

4. Conclusions

The major conclusions from this study are as follows:

- Fe(III) precipitates collected from Lower Red Eyes enhanced Fe(II) oxidation, improving AMD treatment systems. All Fe(II) oxidation was the result of biological activity.
- A depositional facies model explained some differences in Fe(II) oxidation kinetics but did not account for mineralogy and microbial community differences, which were more dependent upon geochemical conditions, especially pH.
- Pool facies yielded faster mass and surface-area normalized Fe(II) oxidation rates and gdm removal when compared to terrace facies.
- Fe(II) oxidation rates were not strongly correlated to hydraulic residence time, $[H^+]$, DO, [Fe(II)], C_{bact}, sediment mass, or surface area.
- Fe(II) oxidation increased with increasing residence time and decreasing water volume (i.e. water column height).
- Schwertmannite with pin-cushion morphology was the predominant Fe(III) mineral at Lower Red Eyes, Hughes Borehole, and Fridays-2, regardless of depositonal facies and water chemistry.
- Biogenic precipitates formed at low-pH may be more suitable for industrial reuse because no trace metals were incorporated; however, the conversion of schwertmannite to goethite is a long-term source of acidity (Bigham et al., 1996; Peine et al., 200; Kawano and Tomita, 2001; Peretyazhko et al. 2009).
- Fe(III) minerals formed via abiotic neutralization/precipitation were all identified as schwertmannite.

- Schwertmannite formed via abiotic neutralization/precipitation contained trace metals; thus, abiotic neutralization/ precipitation was more efficient at remediation of AMD with high concentrations of metals.

BIBLIOGRAPHY

Acero, P., Ayora, C., Torrentó, C., Nieto, J.M. (2006) The behavior of trace elements during schwertmannite precipitation and subsequent transformation into goethite and jarosite. *Geochimica et Cosmochimica Acta,* **70:** 4130-4139.

Amann, R., Binder, B.J., Olson, R.J., Chisholm, S.W., Devereux, R., and Stahl, D.A. (1990) Combination of 16S rRNA-targeted oligonucleotide probes with flow cytometry for analyzing mixed microbial populations. *Applied and Environmental Microbiology,* **56**: 1919-1925.

Bigham, J.M., Schwertmann, U., Carlson, L., Murad, E. (1990) A poorly crystallized oxyhydroxysulfate of iron formed by bacterial oxidation of Fe(II) in acid mine waters. *Geochimica et Cosmochimica Acta,* **54:** 2743-2758.

Bigham, J.M., Schwertmann, U., Traina, S.J., Winland, R.L., Wolf, M. (1996) Schwertmannite and the chemical modeling of iron in acid sulfate waters. *Geochimica et Cosmochimica Acta,* **60:** 2111-2121.

Borch, T., Masue, Y., Kukkadapu, R.K., Fendorf, S. (2007) Phosphate imposed limitations on biological reduction and alteration of ferrihydrite. *Environmental Science & Technology,* **41:** 166-172.

Brake, S.S., Dannelly, H.K., Connors, K.A., Hasiotis, S.T. (2001) Influence of water chemistry on the distribution of an acidophilic protozoan in an acid mine drainage system at the abandoned Green Valley coal mine, Indiana, USA. *Applied Geochemistry,* **16:** 1641-1652.

Brown, J.F., Jones, D., Macalady, J.L., Burgos, W.D. (2010) To be submitted.

Burton, E.D., Bush, R.T., Sullivan, L.A., Mitchell, D.R.G. (2008) Schwertmannite transformation to goethite via the Fe(II) pathway: Reaction rates and implications for iron-sulfide transformation. *Geochimica et Cosmochimica Acta,* **72:** 4551-4564.

Cravotta, C.A. (2008) Laboratory and field evaluation of a flushable oxic limestone drain for treatment of net-acidic drainage from a flooded anthracite mine, Pennsylvania, USA. *Applied Geochemistry*, **23**: 3404-3422.

Cravotta, C.A. (2008b) Dissolved metals and associated constituents in abandoned coal-mine discharges, Pennsylvania, USA. Part 2: Geochemical controls on constituent concentrations. *Applied Geochemistry,* **23:** 203-226.

Daims, H., Brühl, A., Amann, R., Schleifer, K.-H., and Wagner, M. (1999) The domain-specific probe EUB338 is insufficient for the detection of all Bacteria: Development and evaluation of a more comprehensive probe set. *Systematic and Applied Microbiology,* **22**: 434-444.

DeSa, T.C., Brown, J.F., Burgos, W.D. (2010) Laboratory and field-scale evaluation of low-pH Fe(II) oxidation at Hughes Borehole, Portage, Pennsylvania. *Mine Water and the Environment* (In press).

España, J. S., Pastor, E. S., Pamo, E. L. (2007) Iron terraces in acid mine drainage systems: A discussion about the organic and inorganic factors involved in their formation through observations from the Tintillo acidic river (Riotinto mine, Huelva, Spain). *Geosphere*, **3:** 133-151.

Fouke, B.W., Farmer, J.D., Des Marais, D.J., Pratt, L., Sturchio, N.C., Burns, P.C., Discipulo, M.K. (2000) Depositional facies and aqueous-solid geochemistry of travertine-depositing hot springs (Angel Terrace, Mammoth Hot Springs, Yellowstone National Park, U.S.A.). *Journal of Sedimentary Research*, **70:** 565-585.

Fouke, B.W., Bonheyo, G.T., Sanzenbacher, B., Frias-Lopez, J. (2003) Partitioning of bacterial communities between travertine depositional facies at Mammoth Hot Springs, Yellowstone National Park, U.S.A. *Canandian Journal of Earth Science*, **40**: 1531-1548.

GAI Consultants (2007) Final Report: Phase I SRB Low Mine Storage and Treatment 363 Project Evaluation. Volume 1 of 2.

Gagliano, W.B., Brill, M.R., Bigham, J.M., Jones, F.S., Traina, S.J. (2004) Chemistry and mineralogy of ochreous sediments in a constructed mine drainage wetland. *Geochimica et Cosmochimica Acta*, **68:** 2119-2128.

Gonzalez-Toril, E., Llobet-Brossa, E., Casamayor, E.O., Amann, R., and Amils, R. (2003) Microbial ecology of an extreme acidic environment, the Tinto river. *Applied Environmental Microbiology*, **69:** 4853–4865.

Haaijer, S.C.M., Van der Welle., M.E.W., Schmid, M.C., Lamers, L.P.M., Jetten, M.S.M., and Op den Camp, H.J.M. (2006) Evidence for the involvement of betaproteobacterial *Thiobacilli* in the nitrate-dependant oxidation of iron sulfide minerals. *FEMS Microbiology Ecology*, **58**: 439-448.

Hansel, C.M., Benner, S.G., Neiss, J., Dohnalkova, A., Kukkadapu, R.K., Fendorf, S. (2003) Secondary mineralization pathways induced by dissimilatory iron reduction of ferrihydrite under advective flow. *Geochimica et Cosmochimica Acta*, **67**: 2977-2992.

Hedin R.S., Nairn R.W. (1992) Designing and sizing passive mine drainage treatment systems. Proceedings of the 13th Annual WV Surface Mine Drainage Task Force Symposium. http://wvmdtaskforce.com/proceedings/1992.cfm. Accessed January 18, 2010.

Hedin, R.S. (2003) Recovery of a marketable iron oxide from mine drainage in the USA. *Land Contamination & Reclamation*, **11:** 93-97.

Herlihy, A.T., Kaufmann, P.R., Mitch M.E. (1990) Regional estimates of acid mine drainage impact on streams in the Mid-Atlantic and Southeastern United States. *Water, Air and Soil Pollution,* **50**: 91-107.

Hugenholtz, P., Tyson, G.W., and Blackall, L.L. (2001) Design and evaluation of 16S rRNA-targeted oligonucleotide probes for fluorescent in situ hybridization. In Gene Probes: Principles and Protocols. Aquino de Muro, M., and Rapley, R. (eds). London: Humana Press, pp. 29-42.

Hurst, Christon, L et al., Manual of Environmental Microbiology, 2nd ed. ASM Press, Washington DC, 2002: pg 511.

Johnson, D.B., and Hallberg, K.B. (2003) The microbiology and acidic mine waters. *Research in Microbiology,* **154**:466-473.

Johnson, D.B., Okibe, N., Hallberg, K.B. (2005) Differentiation and identification of iron-oxidizing acidophilic bacteria using cultivation techniques and amplified ribosomal DNA restriction enzyme analysis. *Jounal of Microbiological Methods,* **60:** 299-313.

Jonsson, J., Persson, P., Sjoberg, S., Lovgren, L. (2005) Schwertmannite precipitated from AMD: phase transformation, sulphate release, and surface properties. *Applied Geochemistry,* **20:** 179-191.

Kirby, C.S, Elder Brady, J.A. (1998) Field determination of Fe^{2+} oxidation rates in acid mine drainage using a continuously-stirred tank reactor. *Applied Geochemistry,* **13:** 509-520.

Kirby, C.S., Thomas, H.M., Southam, G., Donald, R. (1999) Relative contributions of abiotic and biological factors in Fe(II) oxidation in mine drainage. *Applied Geochemistry,* **14**: 511-530.

Kirby C.S., Cravotta C.A. III (2005) Net alkalinity and net acidity 1: Theoretical considerations. *Applied Geochemistry,* **20**: 1920-1940.

Kumpulainen, S., Carlson, L., Räisänen, M.L. (2007) Seasonal variations of ochreous precipitates in mine effluents in Finland. *Applied Geochemistry*, **22:** 760-777.

Lathe, R. (1985) Synthetic oligonucleotide probes deduced from amino acid sequence data: theoretical and practical considerations. *Journal of Molecular Biology,* **183**: 1-12.

Ludwig, W., Strunk, O., Westram, R., Richter, L., Meier, H., Yadhukumar et al. (2004) ARB: a software environment for sequence data. *Nucleic Acids Research,* **32**: 1363-1371.

Macalady, J.L., Jones, D.S., and Lyon, E.H. (2007) Extremely acidic, pendulous microbial biofilms from the Frasassi cave system, Italy. *Environmental Microbiology,* **9**: 1402-1414.

Manz, W., R. I. Amann, W. Ludwig, M. Wagner, and K.-H. Schleifer. (1992) Phylogenetic oligodeoxynucleotide probes for the major subclasses of peoteobacteria: problems and solutions. *Systematic and Applied Microbiology,* **15**: 593-600.

Nordstrom, D.K. (1985) The rate of ferrous iron oxidation in a stream receiving acid mine effluent. *U.S. Geological Survey Water-Supply Paper,* **2270**: 113-119.

Pennsylania Department of Environmental Protection (2006) The Development of a Mine Drainage Restoration Plan for Bennett Branch, Sinnemahoning Creek: Clearfield, Elk, and Cameron Counties, Pennsylvania.

Peretyazhko, T., Zachara, J.M., Boily, J.-F., Xia, Y., Gassman, P.L., Arey, B.W., Burgos, W.D. (2009) Mineralogical transformations controlling acid mine drainage chemistry. *Chemical Geology,* **262:** 169-178.

Pesic, B., Oliver, D.J., Wichlacz, P. (1989) An electrochemical method of measuring the oxidation rate of ferrous to ferric iron with oxygen in the presence of *Thiobacillus ferrooxidans*. *Biotechnology and Bioengineering*, **33**: 428-439.

Pruesse, E., Quast, C., Knitttel, K., Fuchs, B.M., Ludwig, W., Peplies, J., and Glockner, F.O. (2007) SILVA: a comprehensive online resouce for quality checked and aligned ribosomal RNA sequence data compatible with ARB. *Nucleic Acids Research,* **35**: 7188-7196.

Reading, H.G. (1996) Sedimentary environments: processes, facies, and stratigraphy. Blackwell science, London, England.

Senko, J.M., Wanjugi, P., Lucas, M., Bruns, M.A., Burgos, W.D. (2008) Characterization of Fe(II) oxidizing bacterial activities and communities at two acidic Appalachian coalmine drainage-impacted sites. *The ISME Journal,* **0:**1-12.

Singer, P.C. and Stumm, W. (1970) Acidic mine drainage: the rate-determining step. *Science,* **167:** 1121-1123.

Stahl, D.A., and Amann, R. (1991) Development and application of nucleic acid probes. In *Nucleic acid techniques in bacterial systematics*. Stackebrandt, E., and Goodfellow, M. (eds). Chichester, England: John Wiley & Sons Ltd., pp. 205-248.

Stookey, L.L. (1970). Ferrozine – a new spectrophotometric reagent for iron. *Analytical Chemistry,* **42**: 779-781.

United States Geological Survey. (2008) Coal mine drainage projects in Pennsylvania. US Geological Survey. (http://pa.water.usgs.gov/projects/amd/). Accessed January 27, 2010.

Walker, R.G, James, N.P. (1992) Facies Models: response to sea level change. Geotext I, Geological Association of Canada.

Webb, S.M. (2005) SIXpack: a graphical user interface for XAS analysis using IFEFFIT. *Physica Scripta*, **T115**: 1011-1014.

Yeates, C., Saunders, A.M., Crocetti, G.R., and Blackall, L.L. (2003) Limitations of the widely used GAM42a and BET42a probes targeting bacteria in the *Gammaproteobacteria* radiation. *Microbiology*, **149**:1239-1247

Zhang, G., Dong H., Kim J., and Eberl D.D. (2007) Microbial reduction of structural Fe^{3+} in nontronite by a thermophilic bacterium and its role in promoting the smectite to illite reaction. *American Mineralogist*, **92**: 1411-1419.

Zink T., Wolfe A., Curley K. (2005) Restoring the Wealth of the Mountains: Cleaning up Appalachia's Abandoned Mines. Trout Unlimited.

Appendix A: Water chemistry measurements at Lower Red Eyes

Table A-1: Average field measurements for Lower Red Eyes are displayed with the standard deviation and the number of measurements (N).

Sample	Distance from source (ft)	pH	Temp (°C)	Dissolved oxygen (mg/L)	Conductivity (mS/cm)
E	0	4.04 ± 0.25 N = 7	9.4 ± 0.7 N = 7	0.59 ± 0.70 N = 5	4.36 ± 0.16 N =7
G	12	3.89 ± 0.35 N =3	11.5 ± 1.8 N = 3	7.56 ± 0.86 N = 2	4.40 ± 0.16 N = 3
P1	23	3.53 ± 0.10 N = 5	12.2 ± 1.3 N = 5	8.74 ± 2.49 N = 3	4.40 ± 0.16 N = 5
T1	27	3.28 ± 0.23 N = 2	11.5 ± 0.8 N = 2	6.45 ± 4.97 N = 2	4.64 ± 0.11 N = 2
BP	34	3.45 ± 0.28 N = 5	12.9 ± 2.0 N = 5	7.96 ± 0.70 N = 2	4.26 ± 0.21 N = 5
BT	36	3.45 ± 0.20 N = 2	15.4 ± 1.9 N = 2	8.08 N = 1	4.43 ± 0.19 N = 2
SPA	44.5	3.24 ± 0.11 N = 6	15.3 ± 6.5 N = 6	6.37 ± 1.45 N = 4	4.50 ± 0.16 N = 6
STA	47	3.09 ± 0.14 N = 3	17.4 ± 2.6 N = 3	7.42 ± 1.05 N = 3	4.35 ± 0.34 N = 3
LPA	88	2.98 ± 0.05 N = 5	19.3 ± 4.7 N = 5	5.79 ± 0.14 N = 2	4.39 ± 0.27 N = 5
LTA	91	2.94 ± 0.03 N = 5	18.4 ± 4.5 N = 5	6.88 ± 1.19 N = 2	4.36 ± 0.41 N = 5
SPB	166	2.82 ± 0.06 N = 5	20.6 ± 5.0 N = 5	5.86 ± 1.07 N = 3	4.30 ± 0.78 N = 5
STB	170	2.83 ± 0.06 N = 2	20.0 ± 5.0 N = 2	7.12 ± 0.42 N = 2	4.35 ± 0.36 N = 2
LPB	193	2.65 ± 0.07 N = 7	16.3 ± 2.2 N = 7	6.02 ± 1.09 N = 4	4.88 ± 0.23 N = 7
LTB	203	2.66 ± 0.09 N = 4	18.2 ± 3.8 N = 4	6.80 ± 1.24 N = 2	4.40 ± 0.61 N = 4
DS	391	2.40 ± 0.09 N = 5	18.8 ± 3.1 N = 5	6.61 ± 0.32 N = 3	5.38 ± 0.41 N = 5

Table A-2: Average metal concentrations for Lower Red Eyes with standard deviation and the number of measurements (N). All metals other than Fe were measured with ICP-AES.

Sample	Dissolved Fe(II) (mg/L)	Total dissolved Fe (mg/L)	Mn (mg/L)	Al (mg/L)	Zn (mg/L)	Co (mg/L)	Ca (mg/L)	Mg (mg/L)
E	543.03 ± 18.22 N = 5	537.24 ± 21.6 N = 5	113 ± 2.9 N = 3	43 ± 1.2 N = 3	13 ±1.5 N = 3	4.3 ± 0.17 N = 3	222 ± 7.64 N = 3	387 ± 7.6 N = 3
G	526.29 ± 6.75 N = 2	533.93 ± 25.16 N = 2	115 ± 0 N = 2	43 ± 0 N = 2	14 ± 0.7 N = 2	4.4 ± 0.07 N = 2	223 ± 3.54 N = 2	388 ± 10.6 N = 2
P1	503.13 ± 35.11 N = 3	510.88 ± 39.66 N = 3	115 ± 0 N = 3	43 ± 0 N = 2	14 ± 0.7 N = 2	4.4 ± 0.14 N = 2	225 ± 0.00 N = 2	390 ± 7.1 N = 2
T1	470.78 ± 21.60 N = 2	501.25 ± 19.47 N = 2	115 N = 1	42 N = 1	13 N = 1	4.3 N = 1	220 N = 1	385 N = 1
BP	505.61 ± 39.26 N = 3	523.95 ± 20.93 N = 3	113 ± 2.9 N = 3	43 ± 0.6 N = 3	13 ± 0.6 N = 3	4.3 ± 0.10 N = 3	223 ± 5.77 N = 3	387 ± 10.4 N = 3
BT	459.27 N = 1	410.00 N = 1	115 N = 1	44 ± 0.7 N = 1	13 N = 1	4.3 N = 1	220 N = 1	375 N = 1
SPA	419.09 ± 16.7 N = 3	493.62 ± 12.26 N = 3	113 ± 3.5 N = 2	44 ± 0.7 N = 2	13 ± 0 N = 2	4.3 ± 0.07 N = 2	220 ± 0 N = 2	385 ± 7.1 N = 2
STA	403.06 ± 44.84 N = 2	455.75 ± 10.18 N = 2	115 ± 7.1 N = 2	44 ± 0.7 N = 2	13 ± 0 N = 2	4.3 ± 0.07 N = 2	220 ± 7.07 N = 2	388 ± 3.5 N = 2
LPA	343.92 ± 39.13 N = 2	471.22 ± 14.69 N = 2	115 ± 0 N = 2	44 ± 0.7 N = 2	14 ± 0.7 N = 2	4.4 ± 0.07 N = 2	225 ± 7.07 N = 2	390 ± 14.1 N = 2
LTA	355.18 ± 27.13 N = 2	447.90 ± 8.01 N = 2	118 ± 3.5 N = 2	44 ± 1.4 N = 2	14 ± 1.4 N = 2	4.5 ± 0.21 N = 2	233 ± 10.61 N = 2	393 ± 10.6 N = 2
SPB	257.23 ± 13.18 N = 4	395.69 ± 27.38 N = 4	113 ± 2.9 N = 3	43 ± 0.6 N = 3	13 ± 0.6 N = 3	4.3 ± 0.10 N = 3	225 ± 10.00 N = 3	392 ± 7.6 N = 3
STB	227.55 ± 18.25 N = 2	423.13 ± 1.96 N = 2	115 ± 0 N = 2	44 ± 0.7 N = 2	14 ± 0.7 N = 2	4.5 ± 0.07 N = 2	230 ± 7.07 N = 2	395 ± 21.2 N = 2
LPB	210.33 ± 17.21 N = 3	358.77 ± 16.99 N = 3	113 ± 3.5 N = 2	44 ± 0.7 N = 2	14 ± 1.4 N = 2	4.3 ± 0.07 N = 2	220 ± 0 N = 2	385 ± 7.1 N = 2
LTB	211.97 N = 1	303.87 N = 1	115 N = 1	43 N = 1	12 N = 1	4.2 N = 1	220 N = 1	375 N = 1
DS	27.02 ± 13.55 N = 4	226.38 ± 29.44 N = 5	118 ± 10.6 N = 2	50 ± 2.8 N = 2	14 ± 0.7 N = 2	4.5 ± 0.28 N = 2	238 ± 24.75 N = 2	413 ± 24.7 N = 2

Table A-3: Water chemistry along Lower Red Eyes transect can be observed as the average ± standard deviation with number of replications (N). Total acidity was calculated based on the equation of Kirby & Cravotta (2005).

Sample	Sulfate (mg/L)	Total Acidity (mg $CaCO_3$/L)	Phosphate (mg/L)	Total Suspended Solids (mg/L)	Non-purgeable Organic Carbon (mg/L)	Total Nitrogen (mg/L)
E	2992 ± 368 N = 12	1418.9	0.50 ± 0.07 N = 3	7.5 ± 2.12 N = 2	1.113 ± 0.01 N = 5	0.568 ± 0 N = 4
G	2900 ± 300 N = 7	1412.9	0.12 ± 0.05 N = 3	370 ± 70.71 N = 2	0.951 ± 0.01 N = 5	0.489 ± 0.01 N = 4
P1	2980 ± 278 N = 10	1320.8	0.12 ± 0.06 N = 3	39.5 ± 0.71 N = 2	0.843 ± 0 N = 3	0.504 ± 0.01 N = 4
T1	3733 ± 973 N = 6	1425.8	0.22 ± 0.06 N = 3	--	1.767 ± 0.02 N = 3	0.542 ± 0.01 N = 4
BP	3220 ± 957 N = 10	1447.2	0.19 ± 0.02 N = 3	--	1.822 ± 0.03 N = 3	0.448 ± 0.01 N = 4
BT	2300 ± 100 N = 3	1292.6	0.10 ± 0.06 N = 3	--	0.926 ± 0.01 N = 3	0.382 ± 0 N = 4
SPA	2918 ± 608 N = 11	1467.0	0.32 ± 0.09 N = 3	73 ± 1.41 N = 2	4.676 ± 0.05 N = 4	0.214 ± 0.01 N = 5
STA	2567 ± 379 N = 3	1357.9	0.16 ± 0.04 N = 3	--	1.859 ± 0.02 N = 3	0.504 ± 0.01 N = 3
LPA	3280 ± 1012 N = 10	1452.4	0.09 ± 0.06 N = 3	43.5 ± 6.36 N = 2	1.782 ± 0.02 N = 3	0.559 ± 0.01 N = 3
LTA	2657 ± 251 N = 7	1396.5	0.13 ± 0.02 N = 3	--	0.921 ± 0.02 N = 5	0.439 ± 0.01 N = 4
SPB	2720 ± 691 N = 10	1374.4	0.17 ± 0.06 N = 3	--	1.175 ± 0.02 N = 4	0.469 ± 0.01 N = 4
STB	2940 ± 483 N = 5	1453.5	0.21 ± 0.04 N = 3	--	1.139 ± 0.02 N = 3	0.461 ± 0 N = 4
LPB	3155 ± 942 N = 11	1293.8	0.22 ± 0.04 N = 3	13.0 ± 2.83 N = 2	4.923 ± 0.09 N = 4	0.222 ± 0 N = 5
LTB	2320 ± 432 N = 5	1179.6	0.18 ± 0.07 N = 3	--	1.280 ± 0.01 N = 3	0.526 ± 0.01 N = 5
DS	3122 ± 452 N = 12	1418.9	--	--	--	--

Appendix B: Ferrous Iron Oxidation Rate Correlation Data

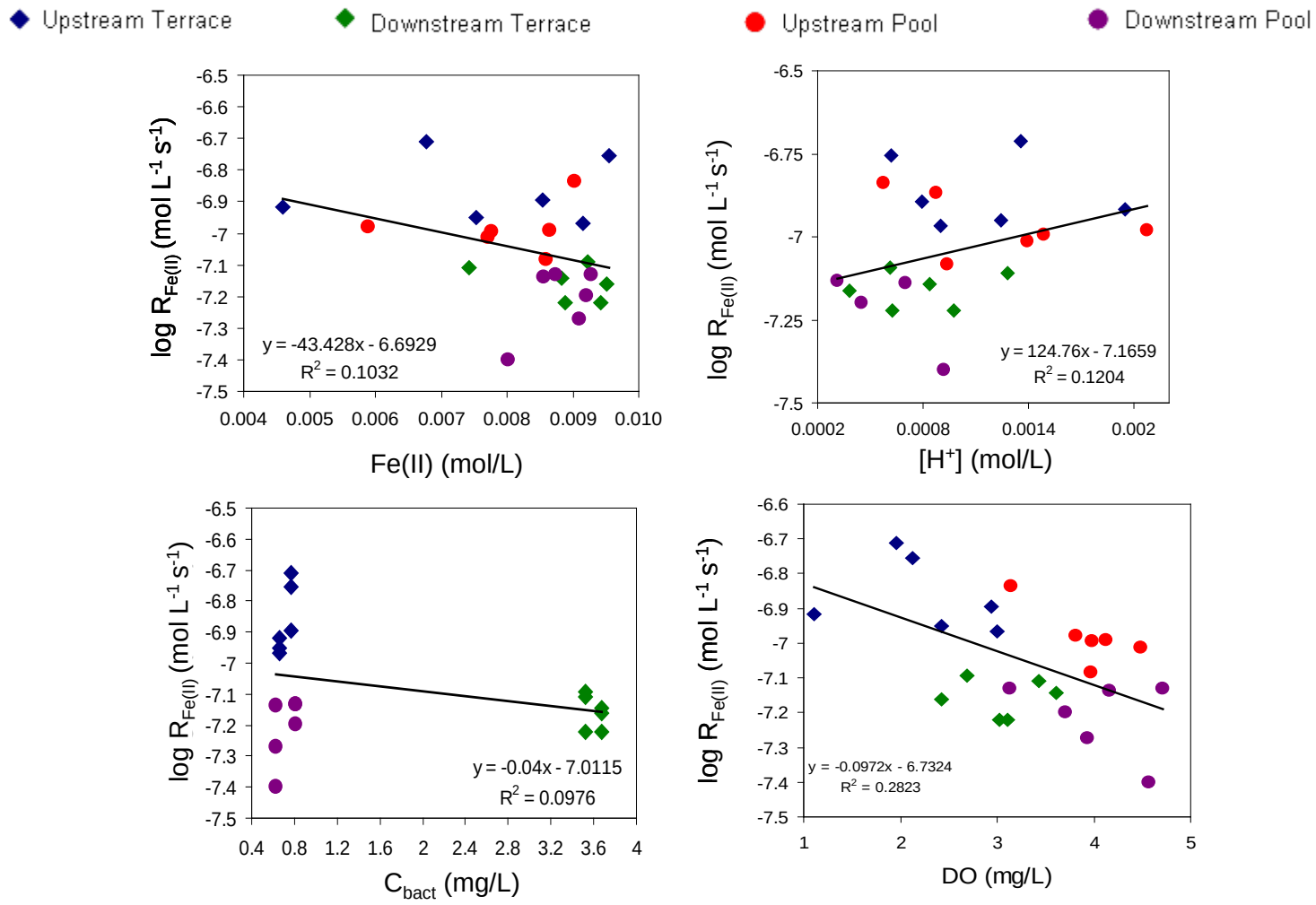

Figure B-1: Fe(II) oxidation rates (mol L^{-1} s^{-1}) were not correlated to [Fe(II)], [H^+], DO, or C_{bact} at steady state.

Table B-1: Data corresponding to Figure B-1 and B-2.

Sample	Rate (mol L^{-1} s^{-1})		Fe (II) (mol/L)		$[H^+]$ (mol/L)		C_{bact} (mg/L)	DO (mg/L)		Residence time in individual reactor (h)
	average	SD	average	SD	average	SD		Average	SD	
UT - A	1.94E-07	4.37E-08	0.0068	0.0007	1.36E-03	1.90E-04	0.77	1.96	0.79	5
UT- B	1.21E-07	3.37E-08	0.0046	0.0003	1.95E-03	6.15E-05	0.66	1.11	0.22	5
UP - A	1.01E-07	4.07E-08	0.0078	0.0006	1.49E-03	0.00E+00	--	3.98	0.99	5
UP - B	1.05E-07	2.26E-08	0.0059	0.0005	2.07E-03	1.57E-04	--	3.82	0.34	5
DT - A	7.19E-08	2.96E-08	0.0088	0.0002	8.40E-04	7.48E-05	3.67	3.61	0.63	5
DT - B	7.76E-08	2.25E-08	0.0074	0.0003	1.28E-03	3.76E-05	3.52	3.44	0.14	5
DP - A	7.38E-08	1.48E-08	0.0087	0.0002	6.67E-04	7.64E-05	0.81	4.71	0.74	5
DP - B	3.99E-08	1.38E-08	0.0080	0.0004	9.21E-04	6.02E-05	0.63	4.57	0.79	5
UT - A	1.27E-07	1.46E-08	0.0085	0.0005	7.94E-04	1.18E-04	0.77	2.94	0.48	2.5
UT- B	1.12E-07	1.98E-08	0.0075	0.0006	1.24E-03	1.09E-04	0.66	2.43	0.10	2.5
UP - A	8.27E-08	2.27E-09	0.0086	0.0000	9.40E-04	1.78E-04	--	3.97	1.27	2.5
UP - B	9.71E-08	2.40E-08	0.0077	0.0002	1.39E-03	8.16E-05	--	4.48	0.05	2.5
DT - A	6.02E-08	2.28E-08	0.0094	0.0001	6.25E-04	4.74E-05	3.67	3.11	0.42	2.5
DT - B	6.01E-08	2.23E-08	0.0089	0.0002	9.74E-04	6.13E-05	3.52	3.02	0.25	2.5
DP - A	6.33E-08	2.84E-08	0.0092	0.0002	4.48E-04	6.09E-05	0.81	3.71	0.25	2.5
DP - B	7.28E-08	1.27E-08	0.0086	0.0002	6.98E-04	7.71E-05	0.63	4.17	0.40	2.5
UT - A	1.76E-07	2.03E-08	0.0095	0.0002	6.21E-04	4.92E-05	0.77	2.13	0.54	1
UT- B	1.08E-07	6.59E-08	0.0092	0.0002	9.03E-04	6.03E-05	0.66	3.00	1.27	1
UP - A	1.46E-07	7.30E-08	0.0090	0.0003	5.73E-04	1.58E-04	--	3.15	1.14	1
UP - B	1.36E-07	1.04E-07	0.0087	0.0002	8.78E-04	1.01E-04	--	4.13	0.47	1
DT - A	6.90E-08	1.82E-08	0.0095	0.0002	3.84E-04	2.54E-05	3.67	2.43	0.09	1
DT - B	8.09E-08	7.81E-08	0.0092	0.0002	6.13E-04	5.00E-01	3.52	2.69	0.23	1
DP - A	7.39E-08	4.63E-08	0.0093	0.0001	3.15E-04	4.31E-05	0.81	3.13	0.44	1
DP - B	5.35E-08	5.46E-08	0.0091	0.0001	4.15E-04	5.22E-05	0.63	3.94	0.40	1

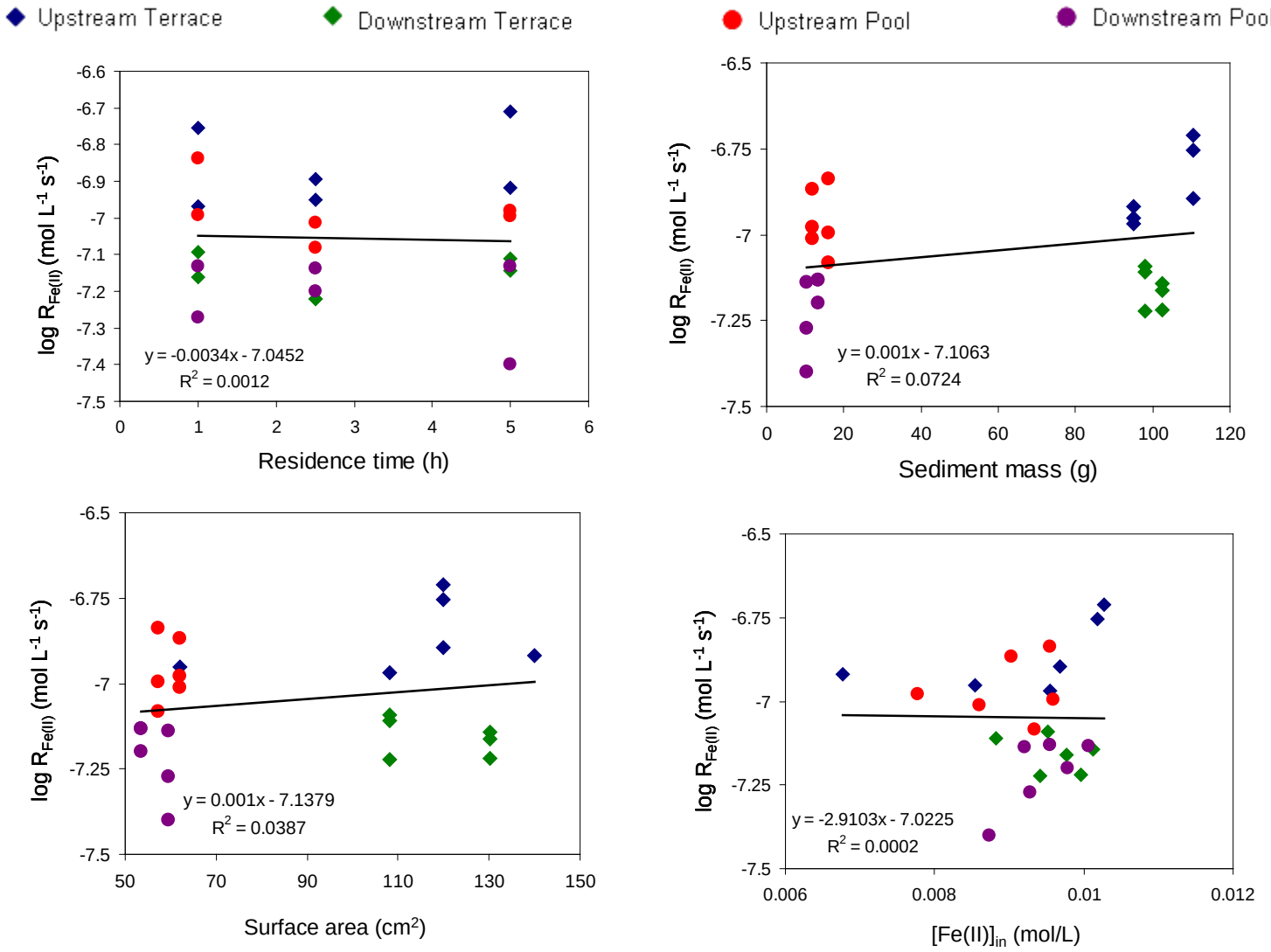

Figure B-2: Fe(II) oxidation rates (mol L^{-1} s^{-1}) were not correlated to residence time, sediment mass, surface area, or influent [Fe(II)].

Table B-2: Tabulated data for Figure B-2.

	Rate (mol L^{-1} s^{-1})		Sediment mass (g)		Sediment surface-area (cm^2)		$[Fe(II)]_{in}$ (mol L^{-1})	
	average	SD	average	SD	average	SD	average	SD
UT - A	1.94E-07	4.37E-08	110.48	2.67	120.03	6.22	0.0103	0.0004
UT- B	1.21E-07	3.37E-08	94.97	2.38	140.06	140.06	0.0068	0.0000
UP - A	1.01E-07	4.07E-08	15.99	12.24	57.36	4.54	0.0096	0.0000
UP - B	1.05E-07	2.26E-08	11.79	5.15	62.13	14.68	0.0078	0.0000
DT - A	7.19E-08	2.96E-08	102.50	0.87	130.27	9.47	0.0101	0.0007
DT - B	7.76E-08	2.25E-08	98.15	2.62	108.23	15.16	0.0088	0.0000
DP - A	7.38E-08	1.48E-08	13.27	2.01	53.61	11.70	0.0101	0.0000
DP - B	3.99E-08	1.38E-08	10.32	1.87	59.42	21.23	0.0087	0.0000
UT - A	1.27E-07	1.46E-08	110.48	2.67	120.03	6.22	0.0097	0.0007
UT- B	1.12E-07	1.98E-08	94.97	2.38	62.13	62.13	0.0085	0.0000
UP - A	8.27E-08	2.27E-09	15.99	12.24	57.36	4.54	0.0093	0.0000
UP - B	9.71E-08	2.40E-08	11.79	5.15	62.13	14.68	0.0086	0.0000
DT - A	6.02E-08	2.28E-08	102.50	0.87	130.27	9.47	0.0100	0.0006
DT - B	6.01E-08	2.23E-08	98.15	2.62	108.23	15.16	0.0094	0.0000
DP - A	6.33E-08	2.84E-08	13.27	2.01	53.61	11.70	0.0098	0.0000
DP - B	7.28E-08	1.27E-08	10.32	1.87	59.42	21.23	0.0092	0.0000
UT - A	1.76E-07	2.03E-08	110.48	2.67	120.03	6.22	0.0102	0.0005
UT- B	1.08E-07	6.59E-08	94.97	2.38	108.23	108.23	0.0095	0.0000
UP - A	1.46E-07	7.30E-08	15.99	12.24	57.36	4.54	0.0095	0.0000
UP - B	1.36E-07	1.04E-07	11.79	5.15	62.13	14.68	0.0090	0.0000
DT - A	6.90E-08	1.82E-08	102.50	0.87	130.27	9.47	0.0098	0.0002
DT - B	8.09E-08	7.81E-08	98.15	2.62	108.23	15.16	0.0095	0.0000
DP - A	7.39E-08	4.63E-08	13.27	2.01	53.61	11.70	0.0096	0.0000
DP - B	5.35E-08	5.46E-08	10.32	1.87	59.42	21.23	0.0093	0.0000

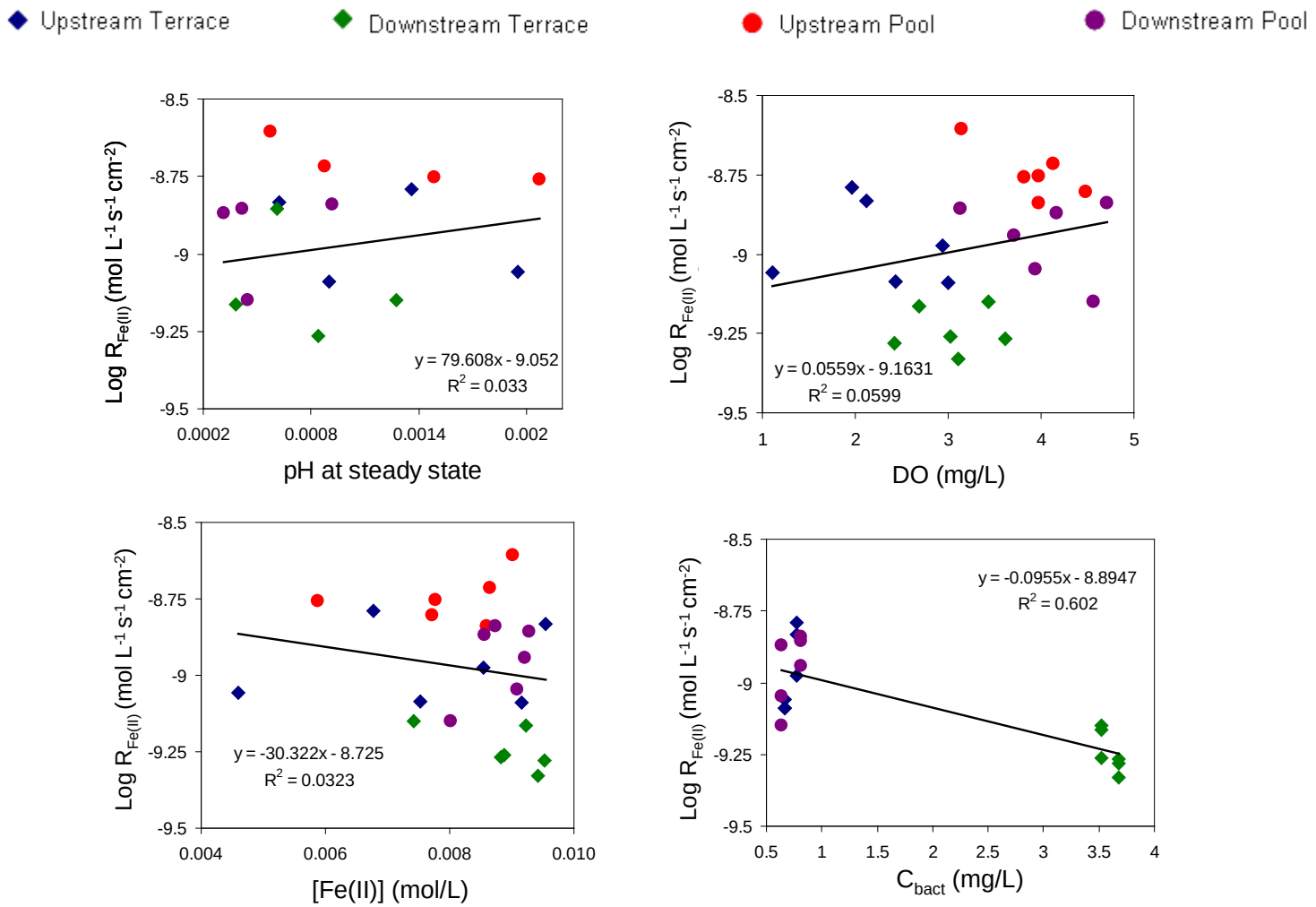

Figure B-3: Surface-area normalized Fe(II) oxidation rates (mol L^{-1} s^{-1} cm^{-2}) were not correlated to $[H^+]$, DO, [Fe(II)] or C_{bact} at steady state conditions.

Table B-3: Tabulated data for Figure B-3.

Sample	Rate (mol L^{-1} s^{-1} cm^{-2})		Fe (II) (mol/L)		$[H^+]$ (mol/L)		C_{bact} (mg/L)	DO (mg/L)		Residence time in individual reactor (h)
	average	SD	average	SD	average	SD		Average	SD	
UT - A	1.62E-09	3.32E-10	0.0068	0.0007	1.36E-03	1.90E-04	0.77	1.96	0.79	5
UT- B	8.75E-10	2.79E-10	0.0046	0.0003	1.95E-03	6.15E-05	0.66	1.11	0.22	5
UP - A	1.77E-09	6.81E-10	0.0078	0.0006	1.49E-03	0.00E+00	--	3.98	0.99	5
UP - B	1.74E-09	5.15E-10	0.0059	0.0005	2.07E-03	1.57E-04	--	3.82	0.34	5
DT - A	5.42E-10	1.88E-10	0.0088	0.0002	8.40E-04	7.48E-05	3.67	3.61	0.63	5
DT - B	7.08E-10	1.26E-10	0.0074	0.0003	1.28E-03	3.76E-05	3.52	3.44	0.14	5
DP - A	1.44E-09	4.67E-10	0.0087	0.0002	6.67E-04	7.64E-05	0.81	4.71	0.74	5
DP - B	7.07E-10	2.29E-10	0.0080	0.0004	9.21E-04	6.02E-05	0.63	4.57	0.79	5
UT - A	1.06E-09	1.25E-10	0.0085	0.0005	7.94E-04	1.18E-04	0.77	2.94	0.48	2.5
UT- B	8.18E-10	2.31E-10	0.0075	0.0006	1.24E-03	1.09E-04	0.66	2.43	0.10	2.5
UP - A	1.45E-09	1.46E-10	0.0086	0.0000	9.40E-04	1.78E-04	--	3.97	1.27	2.5
UP - B	1.57E-09	1.92E-10	0.0077	0.0002	1.39E-03	8.16E-05	--	4.48	0.05	2.5
DT - A	4.69E-10	2.00E-10	0.0094	0.0001	6.25E-04	4.74E-05	3.67	3.11	0.42	2.5
DT - B	5.48E-10	1.51E-10	0.0089	0.0002	9.74E-04	6.13E-05	3.52	3.02	0.25	2.5
DP - A	1.14E-09	3.19E-10	0.0092	0.0002	4.48E-04	6.09E-05	0.81	3.71	0.25	2.5
DP - B	1.35E-09	4.97E-10	0.0086	0.0002	6.98E-04	7.71E-05	0.63	4.17	0.40	2.5
UT - A	1.47E-09	1.40E-10	0.0095	0.0002	6.21E-04	4.92E-05	0.77	2.13	0.54	1
UT- B	8.15E-10	5.52E-10	0.0092	0.0002	9.03E-04	6.03E-05	0.66	3.00	1.27	1
UP - A	2.48E-09	1.09E-09	0.0090	0.0003	5.73E-04	1.58E-04	--	3.15	1.14	1
UP - B	1.92E-09	1.26E-09	0.0087	0.0002	8.78E-04	1.01E-04	--	4.13	0.47	1
DT - A	5.25E-10	1.07E-10	0.0095	0.0002	3.84E-04	2.54E-05	3.67	2.43	0.09	1
DT - B	6.88E-10	6.49E-10	0.0092	0.0002	6.13E-04	5.00E-01	3.52	2.69	0.23	1
DP - A	1.39E-09	8.16E-10	0.0093	0.0001	3.15E-04	4.31E-05	0.81	3.13	0.44	1
DP - B	8.97E-10	6.62E-10	0.0091	0.0001	4.15E-04	5.22E-05	0.63	3.94	0.40	1

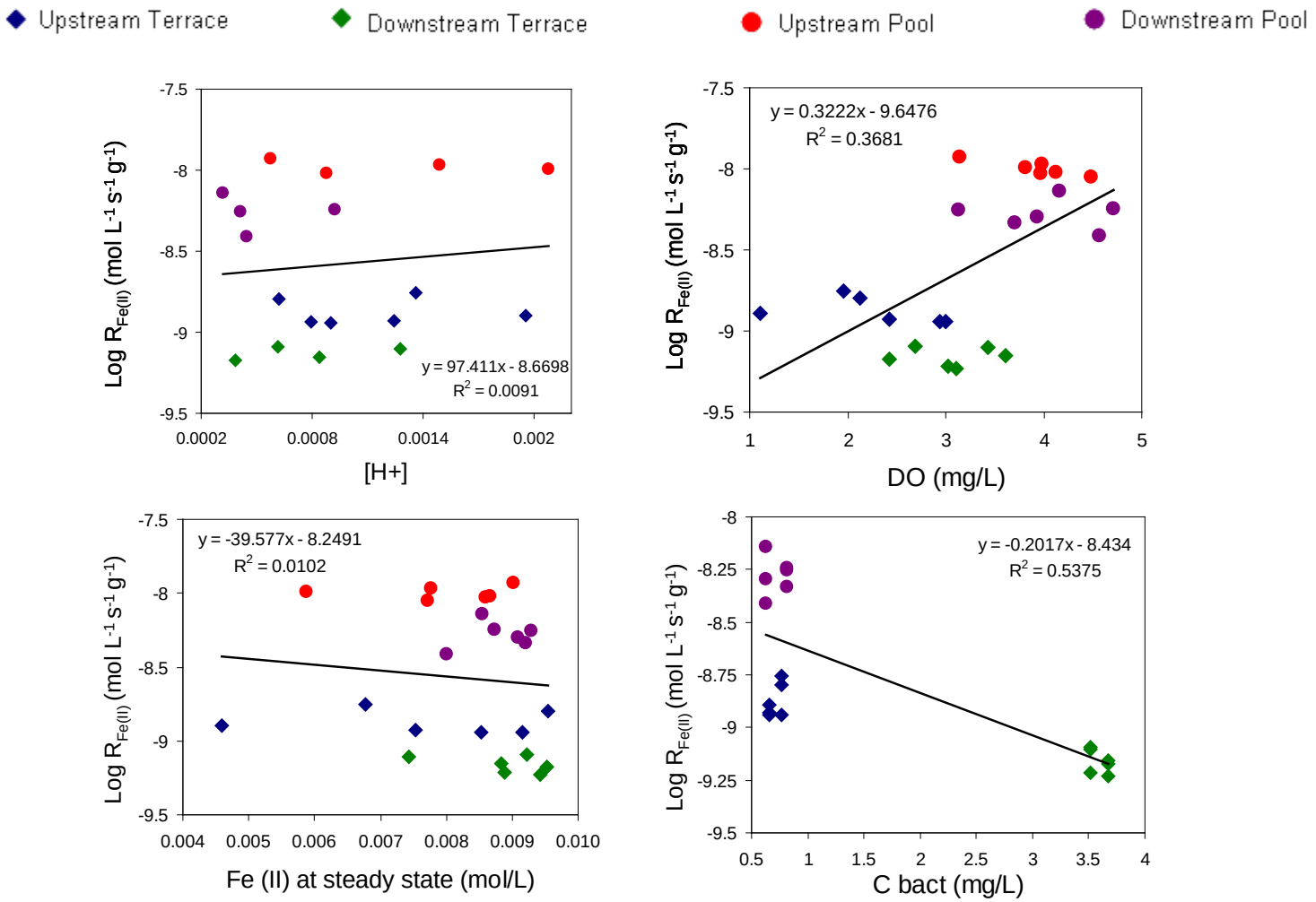

Figure B-4: Mass-normalized Fe(II) oxidation rates were not correlated to [H^+], [Fe(II)] at steady state conditions. A weak positive correlation was observed for DO and a weak negative correlation was observed for $C_{bact.}$

Table B-4: Tabulated data for Figure B-4.

Sample	Rate (mol L^{-1} s^{-1} g^{-1})		Fe (II) (mol/L)		$[H^+]$ (mol/L)		C_{bact} (mg/L)	DO (mg/L)		Residence time in individual reactor (h)
	average	SD	average	SD	average	SD		Average	SD	
UT - A	1.76E-09	4.19E-10	0.0068	0.0007	1.36E-03	1.90E-04	0.77	1.96	0.79	5
UT- B	1.27E-09	3.61E-10	0.0046	0.0003	1.95E-03	6.15E-05	0.66	1.11	0.22	5
UP - A	1.07E-08	8.84E-09	0.0078	0.0006	1.49E-03	0.00E+00	--	3.98	0.99	5
UP - B	1.02E-08	4.75E-09	0.0059	0.0005	2.07E-03	1.57E-04	--	3.82	0.34	5
DT - A	6.99E-10	2.83E-10	0.0088	0.0002	8.40E-04	7.48E-05	3.67	3.61	0.63	5
DT - B	7.87E-10	2.10E-10	0.0074	0.0003	1.28E-03	3.76E-05	3.52	3.44	0.14	5
DP - A	5.70E-09	1.56E-09	0.0087	0.0002	6.67E-04	7.64E-05	0.81	4.71	0.74	5
DP - B	3.87E-09	1.07E-09	0.0080	0.0004	9.21E-04	6.02E-05	0.63	4.57	0.79	5
UT - A	1.15E-09	1.40E-10	0.0085	0.0005	7.94E-04	1.18E-04	0.77	2.94	0.48	2.5
UT- B	1.18E-09	2.35E-10	0.0075	0.0006	1.24E-03	1.09E-04	0.66	2.43	0.10	2.5
UP - A	9.34E-09	7.26E-09	0.0086	0.0000	9.40E-04	1.78E-04	--	3.97	1.27	2.5
UP - B	8.92E-09	2.40E-09	0.0077	0.0002	1.39E-03	8.16E-05	--	4.48	0.05	2.5
DT - A	5.88E-10	2.26E-10	0.0094	0.0001	6.25E-04	4.74E-05	3.67	3.11	0.42	2.5
DT - B	6.09E-10	2.14E-10	0.0089	0.0002	9.74E-04	6.13E-05	3.52	3.02	0.25	2.5
DP - A	4.62E-09	1.52E-09	0.0092	0.0002	4.48E-04	6.09E-05	0.81	3.71	0.25	2.5
DP - B	7.23E-09	1.63E-09	0.0086	0.0002	6.98E-04	7.71E-05	0.63	4.17	0.40	2.5
UT - A	1.60E-09	2.09E-10	0.0095	0.0002	6.21E-04	4.92E-05	0.77	2.13	0.54	1
UT- B	1.15E-09	7.17E-10	0.0092	0.0002	9.03E-04	6.03E-05	0.66	3.00	1.27	1
UP - A	1.18E-08	5.53E-09	0.0090	0.0003	5.73E-04	1.58E-04	--	3.15	1.14	1
UP - B	9.54E-09	5.08E-09	0.0087	0.0002	8.78E-04	1.01E-04	--	4.13	0.47	1
DT - A	6.72E-10	1.72E-10	0.0095	0.0002	3.84E-04	2.54E-05	3.67	2.43	0.09	1
DT - B	8.10E-10	7.78E-10	0.0092	0.0002	6.13E-04	5.00E-01	3.52	2.69	0.23	1
DP - A	5.57E-09	3.27E-09	0.0093	0.0001	3.15E-04	4.31E-05	0.81	3.13	0.44	1
DP - B	5.05E-09	4.40E-09	0.0091	0.0001	4.15E-04	5.22E-05	0.63	3.94	0.40	1

Appendix C: Tabulated Data for Chapter 2

Table C-1: Data corresponding to Figure 2-3.

Site	Distance from source (m)	April 21,2009			June 1, 2009			July 6, 2009		
		pH	DO (µM)	Temperature (°C)	pH	DO (µM)	Temperature (°C)	pH	DO (µM)	Temperature (°C)
E	0.0	4.05	0.0	9.1	3.52	43.4	10.9	4.08	0.0	9.8
G	3.7	3.48	217.2	12.5	4.05	255.3	12.5		--	--
P1	7.0	3.37	185.0	13.3	3.52	331.9	10.9	3.59	302.5	13.5
T1	8.2	3.12	91.6	12.0	3.44	311.3	10.9	--	--	--
BP	10.4	3.41	264.1	14.2	--	--	--	--	--	--
BT	11.0	3.31	252.5	14.0	--	--	--	--	--	--
SPA	13.6	3.15	182.2	12.0	3.30	259.4	11.5	3.30	202.8	28.0
STA	14.3	3.01	195.9	14.5	3.25	260.6	19.4	--	--	--
LPA	26.8	2.98	184.1	16.8	3.04	177.8	22.0	--	--	--
LTA	27.7	2.93	188.8	15.7	2.97	241.3	21.3	--	--	--
SPB	50.6	2.78	193.4	17.1	2.85	210.3	23.3	2.81	145.9	22.0
STB	51.8	2.78	213.1	16.4	2.87	231.9	23.5	--	--	--
LPB	58.8	2.57	140.9	14.0	2.76	185.0	17.2	2.69	213.8	14.7
LTB	61.9	2.67	185.0	15.3	2.76	240.0	18.3	--	--	--
DS	119.2	--	--	--	--	--	--	2.46	209.4	21.8

Table C-2: Data corresponding to Figure 2-4.

Site	Distance from source (m)	April 21, 2009			June 12, 2009			July 6, 2009		
		Total Fe (mM)	Fe(III) (mM)	Fe(III)/Total Fe	Total Fe (mM)	Fe(III) (mM)	Fe(III)/Total Fe	Total Fe (mM)	Fe(III) (mM)	Fe(III)/Total Fe
E	0.0	9.57	0.35	0.04	9.25	0.00	0.00	9.52	0.00	0.00
G	3.7	9.24	0.00	0.00	--	--	--	--	--	--
P1	7.0	8.50	0.07	0.01	--	--	--	9.03	0.11	0.01
T1	8.2	9.22	0.52	0.06	--	--	--	8.73	0.57	0.07
BP	10.4	9.21	0.00	0.00	9.12	0.67	0.07	--	--	--
BT	11.0	7.34	0.00	0.00	--	--	--	--	--	--
SPA	13.6	9.09	1.54	0.17	8.72	1.54	0.18	8.70	0.92	0.11
STA	14.3	8.29	0.50	0.06	8.03	1.38	0.17	--	--	--
LPA	26.8	8.25	2.59	0.31	--	--	--	--	--	--
LTA	27.7	8.12	1.42	0.17	--	--	--	--	--	--
SPB	50.6	7.13	2.54	0.36	6.41	2.00	0.31	7.23	2.29	0.32
STB	51.8	7.60	3.30	0.43	--	--	--	--	--	--
LPB	58.8	6.09	1.97	0.32	6.49	2.90	0.45	6.69	3.10	0.46
LTB	61.9	5.44	1.65	0.30	--	--	--	--	--	--
DS	119.2	--	--	--	3.61	3.34	0.92	3.58	3.21	0.89

Table C-3: Data corresponding to Figure 2-6.

Site	Distance From Source (m)	Fe (mg/L)	Mn (mg/L)	Zn (mg/L)	Ni (mg/L)	Co (mg/L)	Al (mg/L)	Si (mg/L)
E	0.0	540	115	12	5.9	4.2	42	12
G	3.7	515	115	13	6.0	4.3	43	12
P1	7.0	515	115	13	6.0	4.3	43	12
T1	8.2	500	115	13	5.9	4.3	42	--
BP	10.4	515	115	13	5.9	4.3	43	12
BT	11.0	495	115	13	5.9	4.3	43	--
SPA	13.6	485	115	13	5.9	4.3	43	--
STA	14.3	480	120	13	6.0	4.3	43	--
LPA	26.8	455	115	13	6.0	4.3	43	12
LTA	27.7	445	120	13	6.0	4.3	43	13
SPB	50.6	415	115	13	6.0	4.3	44	14
STB	51.8	420	115	13	6.0	4.4	43	14
LPB	58.8	375	115	15	5.9	4.2	44	--
LTB	61.9	360	115	12	5.9	4.2	43	--

Table C-4: Tabulated data corresponding to Figure 2-10. Data in box at right hand side was not used in creating table.

Site name	E	P1	BP	SPA	LPA	SPB	LPB	LPB (10/09)	LTB (10/09)	LTA (4/09)
distance from source (m)	0	7	10	13.5	27	50.5	59	59	61	90
date collected	4/09	4/09	4/09	4/09	4/09	4/09	4/09	10/09	10/09	4/09
EUBMIX[a]	99.4 (±1.0)	99.8 (±0.6)	96.9 (±3.6)	97.6 (±2.4)	99.7 (±0.9)	99.0 (±2.6)	94.0 (±3.8)	83.7 (±5.0)	80.5 (±6.0)	98.6 (±1.4)
GAMBET[b]	34.1 (±4.1)	76.0 (±2.8)	75.5 (±11.9)	78.9 (±5.0)	92.1 (±7.8)	86.7 (±5.5)	77.0 (±6.8)	54.7 (±6.8)	53.7 (±4.9)	92.3 (±1.5)
GAM42a	2.2 (±2.0)	32.7 (±5.6)	6.3 (±3.4)	36.5 (±4.8)	79.8 (±7.7)	84.0 (±4.7)	71.8 (±9.5)	52.5 (±5.4)	50.8 (±7.2)	63.0 (±7.9)
BET42a[d]	31.9	43.3	69.2	42.4	12.3	*2.7*[c]	*5.2*[c]	*2.2*[c]	*2.9*[c]	29.3
THIO1	ND	ND	ND	ND	ND	2.3 (±3.2)	63.1 (±11.9)	47.2 (±6.0)	46.4 (±7.8)	ND

[a]EUBMIX is a combination of EUB338, EUB338(II), and EUB338(III)

[b]GAMBET is a combination of GAM42a and BET42a

[c]For italicized values, proportion GAMBET and GAM42a are not significantly different by Welch 2-sample T-test, therefore presence of betaproteobacteria cannot be confirmed

[d]BET42a data is calculated by subtracting GAM42a counts from GAMBET

ND = none detected

Table C-5: Data corresponding to Figure 2-12.

	Fe(II) mM					
Pore Volumes	No Sediment Control	"Live" Terrace Sediment Average	"Live" Terrace Sediment SD	Pore Volumes	Sterilized Control Average	Sterilized Control SD
0	9.65	9.61	1.53	0.05	8.82	0.22
1.2	11.16	6.33	0.73	0.75	9.00	0.08
1.55	11.22	5.21	0.77	2	9.51	0.23
2	11.01	4.72	0.66	4.45	10.19	0.12
3.85	11.20	4.57	0.03	7.225	10.28	0.01
5.95	10.60	4.62	0.55			

	Total Fe (mM)					
Pore Volumes	No Sediment Control	"Live" Terrace Sediment Average	"Live" Terrace Sediment SD	Pore Volumes	Sterilized Control Average	Sterilized Control SD
0	10.28	9.69	1.53	0.05	8.92	0.14
1.2	10.82	8.38	0.49	0.75	9.38	0.03
1.55	11.00			2	9.73	0.20
2	11.10	7.82	0.64	4.45	10.35	0.04
3.85	10.39	7.83	0.45	7.225	9.89	0.13
5.95	10.83	7.09	0.17			

	pH					
Pore Volumes	No Sediment Control	"Live" Terrace Sediment Average	"Live" Terrace Sediment SD	Pore Volumes	Sterilized Control Average	Sterilized Control SD
0	4.33	4.41	0.327	0.05	3.08	0.006
1.2	4.18	2.85	0.004	0.75	2.88	0.011
1.55	4.10	2.82	0.002	2	2.98	0.033
2	4.00	2.78	0.020	4.45	3.03	0.002
3.85	3.84	2.71	0.006	7.225	3.06	0.012
5.95	3.94	2.71	0.023			

	DO (µM)					
Pore Volumes	No Sediment Control	"Live" Terrace Sediment Average	"Live" Terrace Sediment SD	Pore Volumes	Sterilized Control Average	Sterilized Control SD
1.4	259.38	129.22	45.74	0.05	187.50	5.75
1.95	272.19	105.63	2.21	0.75	199.84	8.18
3.75	269.06	46.88	11.05	2	197.81	0.00
4.2	243.44	38.75	8.40	4.45	194.06	5.30
6	257.50	30.78	3.31	7.225	200.00	1.33

Table C-6: Data corresponding to Figure 2-13a.

	Fe(II) out/Fe(II) in			
	Cumulative Pore Volumes	UT Average	UT SD	No Sediment Control
10 hour	0	1.00	0.000	1.00
	1.2	0.60	0.068	1.05
	1.55	0.50	0.073	1.08
	2	0.46	0.052	1.00
	3.85	0.43	0.005	1.06
	5.95	0.47	0.057	1.12
5 hour	6.25	0.55	0.10	1.06
	7.15	0.68	0.06	1.08
	8.25	0.73	0.01	1.01
	10.55	0.78	0.02	1.02
	11.95	0.79	0.01	1.01
	25.05	0.77	0.04	1.00
2 hour	25.6	0.80	0.04	1.08
	26.725	0.84	0.01	1.03
	27.725	0.82	0.01	1.01
	29.475	0.90	0.03	1.02
	35.725	0.90	0.00	1.03

Table C-7: Data corresponding to Figure 2-13b.

	Fe(II) out/Fe(II) in			
	Cumulative Pore Volumes	DT Average	DT SD	No Sediment Control
10 hour	0	0.96	0.080	0.88
	1.275	0.75	0.056	1.00
	2.05	0.74	0.045	1.00
	4.15	0.77	0.009	1.01
	6.075	0.73	0.042	0.98
	8.25	0.75	0.002	1.04
	11.45	0.72	0.008	1.13
5 hour	11.625	0.82	0.038	1.09
	12.475	0.87	0.018	1.06
	14.775	0.88	0.049	1.02
	16.625	0.87	0.049	1.03
2 hour	20.375	0.91	0.010	1.04
	21.375	0.88	0.020	1.07
	22.625	0.93	0.018	1.11
	24.125	0.96	0.035	0.99

Table C-8: Data corresponding to Figure 2-13c**.**

	Fe(II) out/Fe(II) in			
	Cumulative Pore Volumes	UP Average	UP SD	No Sediment Control
10 hour	0	0.97	0.048	1.04
	0.775	0.74	0.030	1.01
	1.975	0.71	0.019	1.07
	2.725	0.69	0.064	1.05
	4.9	0.54	0.002	1.04
	6.925	0.61	0.041	1.09
	12.525	0.62	0.005	1.07
5 hour	14.25	0.80	0.050	0.98
	15.1	0.80	0.074	1.07
	16.05	0.83	0.067	1.05
	18.55	0.88	0.004	1.03
	19.7	0.84	0.025	0.99
	23.2	0.82	0.028	1.03
2 hour	24.3	0.97	0.016	0.96
	25.3	0.91	0.005	1.05
	27.675	0.90	0.023	1.02
	29.05	0.92	0.004	1.00

Table C-9: Data corresponding to Figure 2-13d.

	Fe(II) out/Fe(II) in			
	Cumulative Pore Volumes	DP Average	DP SD	No Sediment Control
10 hour	0.05	0.95	0.032	0.93
	0.8	0.89	0.027	1.04
	2	0.81	0.038	1.08
	4.725	0.80	0.015	1.01
	6.8	0.79	0.007	1.07
5 hour	7.375	0.86	0.085	1.12
	8.075	0.89	0.056	1.04
	8.875	0.87	0.023	1.08
	11.175	0.88	0.036	1.08
	16.95	0.90	0.039	1.07
2 hour	17.825	0.90	0.027	1.07
	18.825	0.94	0.006	1.01
	20.825	0.95	0.001	0.98
	26.325	0.96	0.027	1.00

Table C-10: Data corresponding to Figure 2-14.

Pore Volumes	Fe(II) (mM)				Dissolved Fe (mM)				pH			
	Sterile Upper Terrace		Sterile Upper Pool		Sterile Upper Terrace		Sterile Upper Pool		Sterile Upper Terrace		Sterile Upper Pool	
	average	SD	average	SD	average	SD	average	SD	average	SD	average	SD
0.05	8.82	0.22	8.92	0.40	8.92	0.14	9.09	0.03	3.080	0.006	3.224	0.088
0.75	9.00	0.08	9.48	0.44	9.38	0.03	9.30	0.19	2.880	0.011	3.129	0.026
2	9.51	0.23	9.83	0.27	9.73	0.20	10.10	0.23	2.983	0.033	3.217	0.014
4.45	10.19	0.12	10.10	0.01	10.35	0.04	10.00	0.34	3.034	0.002	3.313	0.031
7.225	10.28	0.01	10.43	0.08	9.89	0.13	9.80	0.28	3.058	0.012	3.362	0.035

Table C-11: Data corresponding to Figure 2-14.

Pore Volumes	DO (µM)			
	Sterile Upper Terrace		Sterile Upper Pool	
	average	SD	average	SD
0.25	187.50	5.75	203.59	6.41
0.775	199.84	8.18	214.22	7.73
2.35	197.81	0.00	212.81	7.95
4.475	194.06	5.30	204.53	7.73
7.275	200.00	1.33	214.84	5.08

Appendix D: Tabulated Data for Chapter 3

Table D-1: Tabulated data for Figure 3-2.

Lower Red Eyes (July 2009)			
Distance from source (m)	pH	DO (µM)	Fe(II) (mM)
0.0	4.08	0	9.65
7.0	3.59	302.5	8.92
8.2	--	--	8.16
13.6	3.30	202.81	7.78
50.6	2.81	145.94	4.94
58.8	2.69	213.75	3.58
119.2	2.46	209.38	0.38
Fridays-2 (July 2006)			
Distance from source (m)	pH	DO (µM)	Fe(II) (mM)
0.0	3.98	0.94	0.84
0.9	3.93	59.69	0.82
2.4	3.69	345.00	0.72
3.0	3.64	279.69	0.63
6.1	3.62	214.38	0.39
Hughes Borehole (August 2007)			
Distance from source (m)	pH	DO (µM)	Fe(II) (mM)
0.0	4.1	15.63	1.84
8.2	4.09	34.38	1.83
11.0	4.06	43.44	1.77
14.0	4.06	21.56	1.79
16.5	3.88	117.81	1.73
18.9	3.84	152.81	1.73
22.9	3.81	162.19	1.74
28.4	3.45	213.13	--
30.8	3.38	200.31	1.78

Table D-2: Tabulated data for Figure 3-9.

	pH										
	2.26	2.65	2.99	3.02	3.06	3.91[a]	3.99[b]	5.182	5.36	6.21	8.335
Al (ppm)	48	43	43	44	44	44	44	<.01	0.05	1.7	0.04
Co (ppm)	4.3	4.3	4.2	4.2	4.3	4.2	4.2	0.38	0.38	0.43	0.31
Cr (ppm)	0.05	0.04	0.03	0.03	0.03	0.03	0.03	0.01	0.02	0.02	0.01
Fe (ppm)	190	350	385	435	450	505	505	5.1	6.1	0.93	< 01
Mn (ppm)	110	110	110	110	110	110	110	37	37	41	33
Ni (ppm)	6.1	6	5.9	5.9	6	5.9	5.9	0.3	0.32	0.37	0.25
Si (ppm)	17	13	12	12	12	12	12	2.8	5.5	5.9	3.1
Zn (ppm)	13	13	13	13	13	13	13	0.16	0.16	0.3	0.15

[a]pH 3.91 corresponds to the intial conditions for the laboratory precipitation experiment
[b]pH 3.99 corresponds to the AMD emergence at Lower Red Eyes

Table D-3: Tabulated data for Figure 3-10.

pH	Goethite, {Fe^{3+}} (mg/L)	Schwertmannite, {Fe^{3+}} (mg/L)
2.0	2.53E+02	265867.92
2.5	3.62E-01	18913.26
3.0	1.41E-02	1149.54
3.5	1.91E-03	69.06
4.0	3.93E-04	5.93
4.5	1.05E-04	1.35
5.0	3.14E-05	0.59
5.5	9.99E-06	0.31
6.0	3.40E-06	0.17
6.5	1.34E-06	0.11
7.0	6.92E-07	0.10
7.5	4.94E-07	0.11
8.0	4.53E-07	0.17
8.5	5.09E-07	0.32
9.0	7.44E-07	0.78

Table D-4: Tabulated data for Figure 3-10.

Lower Red Eyes field data		Abiotic precipitation data	
pH	{Fe 3+} (mg/L)	pH	{Fe 3+}* (mg/L)
4.04	0	3.9095	505
3.53	7	5.182	5.1
3.45	18	5.36	6.1
3.24	74	6.21	0.93
2.98	128	8.335	0
2.82	138		
2.65	148		
2.40	199		

*Total Fe was assumed to be equal to Fe^{3+} for abiotic precipitation
Activity coefficients assumed to be 1

Table D-5: Chemical equations used to construct Figure 3-10.

Chemical Equation	Log K	Source
$H_2SO_4 = H^+ + HSO_4^-$	3.0	Cravotta, 2008b
$HSO_4^- = H^+ + SO_4^{2-}$	-1.99	Cravotta, 2008b
$Fe^{3+} + H_2O = Fe(OH)^{2+} + H^+$	-2.19	Cravotta, 2008b
$Fe^{3+} + 2\ H_2O = Fe(OH)_2^+ + 2\ H^+$	-5.67	Cravotta, 2008b
$Fe^{3+} + 3\ H_2O = Fe(OH)_{3(amorphous)} + 3\ H^+$	-12.56	Cravotta, 2008b
$Fe^{3+} + 4\ H_2O = Fe(OH)_4^- + 4\ H^+$	-21.6	Cravotta, 2008b
$Fe^{3+} + HSO4^- = FeHSO_4^{2+}$	2.48	Cravotta, 2008b
$Fe^{3+} + SO_4^{2-} = FeSO_4^+$	4.04	Cravotta, 2008b
$FeOOH_{(Goethite)} + 3\ H^+ = Fe^{3+} + 2H_2O$	1.4	Bigham et al. 1996
$Fe_8O_8(OH)_{(8-2x)}(SO_4)_{x\ (Schwertmannite)} + (24-2x)\ H^+ = 8\ Fe^{3+}$	18	Bigham et al. 1996

[a]Schwertmannite solubility determined assuming x = 1.75 (Cravotta, 2008)